UNIVERSIDADE DE SÃO PAULO
ESCOLA POLITÉCNICA
DEPARTAMENTO DE ENGENHARIA METALÚRGICA E DE MATERIAIS

VITORIA HONORATO FRANCO DE MENEZES

Use of voltammetry of microparticles (VMP) for the identification of metallic elements present in corrosion products and pigments

São Paulo
2023

VITORIA HONORATO FRANCO DE MENEZES

Use of voltammetry of microparticles (VMP) for the identification of metallic elements present in corrosion products and pigments

Corrected Version

Dissertation presented to Escola Politécnica, Universidade de São Paulo, to obtain the title of Master of Science.

Area of Concentration: Metallurgical Engineering and Materials

Advisor: Prof. Dr. Hercílio Gomes de Melo

SÃO PAULO
2023

Este exemplar foi revisado e corrigido em relação à versão original, sob responsabilidade única do autor e com a anuência de seu orientador.

São Paulo, 15 de Outubro de 2023

Assinatura do autor: Vitoria H. F. de Menezes

Assinatura do orientador: _____

Catalogação-na-publicação

de Menezes, Vitoria Honorato Franco
Use of voltammetry of microparticles (VMP) for the identification of metallic elements present in corrosion products and pigments / V. H. F. de Menezes -- versão corr. -- São Paulo, 2023.
131 p.

Dissertação (Mestrado) - Escola Politécnica da Universidade de São Paulo. Departamento de Engenharia Metalúrgica e de Materiais.

1.Voltammetry of microparticles 2.Pigments 3.Corrosion products 4.Metal identification 5.Cultural heritage I.Universidade de São Paulo. Escola Politécnica. Departamento de Engenharia Metalúrgica e de Materiais II.t.

ACKNOWLEDGEMENTS

This study was financed in part by the Coordenação de Aperfeiçoamento de Pessoal de Nível Superior -Brasil (CAPES) -Finance Code 001.

First, I am extremely grateful to my supervisor, Professor Dr. Hercilio Gomes de Melo, who helped me and enabled me to work in such a special project.

I am also deeply grateful to Professor Dr. Virginia Costa for all the help, suggestions and for introducing me to the voltammetry of microparticles technique.

I would like to thank Professor Dr. Rômulo Augusto Ando for the assistance with Raman spectroscopy and for allowing me to use his spectrometer for the characterization of the samples.

I would also like to thank Dr. Vitor Leite Martins for helping me with the characterization and measurements.

I am deeply thankful to Professor Dr. Márcia de Almeida Rizzutto, who agreed to share with me the pigment samples that made this work so much more complete.

I also want to thank all my colegues from LPE, specially Livio, Matheus, Oscar, Sandra and Wilmar for helping me with the samples.

On a more personal note, I want to thank my parents for all their support.

I also would like to thank my friends and family.

I specially want to thank Ana Carolina and Caroline Yumi, whose help and support was so important during this work that I promised each of them would get a full page in this section (but I hope this will be enough to show how grateful I am).

I also want to give a special thank you to Leandro (who was also promised a full page in this section) for everything, for always being there for me and helping me in so many ways.

RESUMO

A voltametria de micropartículas (VMP) é uma técnica eletroquímica de análise de sólidos que requer pequenas quantidades de material. Por ser considerada não invasiva (ou microinvasiva), dispor de equipamentos portáteis, apresentar baixo custo e fácil interpretação de resultados, tem sido utilizada pela ciência da conservação e aplicada em análises de objetos do patrimônio cultural. Observa-se na literatura, porém, a falta de um procedimento padrão para análise de amostras, com uma grande variedade de técnicas voltamétricas e eletrólitos. Assim, o objetivo desse trabalho é contribuir para a criação de uma base de dados para análise de metais por VMP a partir de amostras de composições conhecidas, e utilizar essa base de dados como referência para identificar a presença de íons metálicos em pigmentos utilizados em obras de arte e em produtos de corrosão. Para isso, inicialmente, foram selecionadas algumas amostras metálicas (prata, cobre, ferro, estanho, chumbo, zinco e tungstênio), que foram analisadas por MEV-EDS (microscopia eletrônica de varredura com análise por energia dispersiva de raios-X para determinação da composição elementar), e eletrólitos comumente utilizados na literatura para ensaios de VMP (ácido oxálico, ácido clorídrico, ácido sulfúrico, cloreto de potássio, hidróxido de sódio e solução tampão de acetato de sódio). A partir dos resultados de VMP utilizando voltametria cíclica e de onda quadrada verificou-se que a solução tampão de acetato de sódio seria a mais adequada para realizar os ensaios com os compostos (pigmentos e produtos de corrosão), pois foi a única que permitiu a identificação de picos anódicos para todos os metais escolhidos. Após esses resultados iniciais foram realizados ensaios de VMP em produtos de corrosão formados em duas peças metálicas anteriormente expostas a condições não controladas, e em pigmentos selecionados a partir de uma coleção de propriedade da Pinacoteca de São Paulo e fornecidos pela Professora Dra. Márcia de Almeida Rizzutto. Os resultados obtidos mostraram que através da coleta de pequenas quantidades de amostra, necessárias para a realização dos ensaios de VMP, foi possível identificar os picos de oxidação associados aos elementos metálicos presentes nas diferentes amostras, cuja presença nos referidos materiais foi confirmada por análises por MEV-EDS e espectroscopia Raman. A representação dos picos obtidos nas medidas voltamétricas em unidades arbitrárias se revelou uma boa metodologia para análise dos

resultados, permitindo uma comparação clara entre os picos obtidos a partir dos diferentes materiais ensaiados com aqueles determinados para as amostras metálicas de referência, os quais mostraram boa concordância, confirmando que a VMP pode ser utilizada de modo efetivo para a finalidade inicialmente proposta no projeto. O desenvolvimento do projeto também demonstrou que mudanças nas condições de realização dos ensaios de VMP (tipo de técnica e parâmetros de controle experimentais) podem ser essenciais para revelar aspectos importantes dos processos eletroquímicos interfaciais.

Palavras-chave: Voltametria de micropartículas, pigmentos, produtos de corrosão, identificação de metais, patrimônio cultural.

ABSTRACT

Voltammetry of microparticles (VMP) is an electrochemical analytical technique for the analysis of solids that requires small amounts of material. Due to it being considered non-invasive (or microinvasive), having portable equipment, being of low cost and presenting results that are easy to interpret, it has been used by conservation science and applied to the analyzes of cultural heritage objects. However, the literature presents a lack of standard procedures for samples analyzes, with a wide variety of voltammetric techniques and electrolytes being employed. So, the aim of the present work was to contribute to the creation of a database for VMP experiments based on samples of known composition, and to use it as a reference to identify the presence of metallic ions in pigments used in works of art and in corrosion products. For this, initially, some metallic samples were selected (silver, copper, iron, tin, lead, zinc and tungsten), which were analyzed by SEM-EDS (scanning electron microscopy coupled to X-ray energy dispersive spectroscopy for elementary composition analysis), as well as electrolytes commonly used in the literature for VMP experiments (oxalic acid, hydrochloric acid, sulfuric acid, potassium chloride, sodium hydroxide and sodium acetate buffer solution). From the results of VMP using cyclic and square wave voltammetry, it was verified that the sodium acetate buffer solution would be the most adequate to carry out the tests with the compounds (pigments and corrosion products), since it was the only electrolyte that allowed the identification of anodic peaks for all chosen metals. After these initial results, VMP tests were carried out on corrosion products formed on two metallic pieces previously exposed to uncontrolled conditions, and on pigments selected from a collection owned by *Pinacoteca de São Paulo* and provided by Professor Dr. Márcia de Almeida Rizzutto. The results showed that sampling only small amounts of powder allowed the identification of oxidation peaks associated with the metallic elements present in the different compounds, whose presence in the referred materials was confirmed by SEM-EDS analysis and Raman spectroscopy. The representation of the peaks obtained in the voltammetric measurements in arbitrary units proved to be a good methodology for presenting the results, allowing a clear comparison between the peaks obtained from the different tested materials with those from the metallic reference samples, which were in good agreement, confirming that VMP can be used effectively for the purpose initially

proposed in the project. The development of the project also demonstrated that changes in the conditions for carrying out the VMP assays (type of technique and experimental parameters control) can be essential to reveal important features of the interfacial electrochemical processes.

Keywords: Voltammetry of Microparticles, pigments, corrosion products, metal identification, cultural heritage.

LIST OF FIGURES

LIST OF TABLES

Summary

1. INTRODUCTION

Cultural heritage represents the history and culture of a people, developed by a community and passed down from generation to generation. It can be divided into tangible goods (sites, buildings, monuments, objects, works of art, historical and archaeological artifacts) and intangible goods (culture, beliefs, rites, traditions, customs, practices, values); the combination of these elements is responsible for characterizing a society [1]. Its conservation is important for the preservation of culture and for the connection of peoples with their ancestors, in addition to the preservation and perpetuation of their history.

Through careful examination associated with analytical studies of the objects that are part of this heritage, it is possible to obtain a diagnosis of their state of conservation, as well as to evaluate the compounds and techniques used and possible interventions already carried out in the original work. Considering that they are significant to history and culture, unique and irreplaceable, objects of cultural heritage ideally should not be sampled, let alone sacrificed. Thus, techniques used in analytical studies must be non-destructive, or based on sampling of small amounts of material that do not affect the appearance and/or structure of the artifact. Considering their fragility, the portability of the instrumentation and the possibility of carrying out measurements *in situ* are extremely important so that artifacts are not exposed to conditions different from the usual ones for long periods of time.

Detailed characterizations usually rely on techniques available at conservation institutes, such as X-ray diffraction, Raman spectroscopy and X-ray fluorescence. Despite being widely used in the area of conservation of historical heritage [2], they can present certain disadvantages, such as *in-situ* low resolution, and the need for sampling or moving the work to the place of analysis, which results in the demand for more accessible and easy-to-apply techniques.

For conservation science, the analysis of pigments is important because they are compounds, organic or inorganic, used in paintings, ceramics and manuscripts. Inorganic pigments can contain one or more metallic elements in their composition, which can undergo electrochemical reactions and, therefore, electroanalytical techniques can be used as an analytical tool for their identification. Electroanalysis can be considered as a non-invasive or micro-

invasive analytical technique, as it is possible to obtain satisfactory results using only small amounts of sample. This makes it interesting for applications in the field of conservation.

Among the electroanalytical techniques, voltammetry of microparticles (VMP) is a method that fulfills several of the necessary requirements for the study of cultural heritage objects. It is an accessible, non-invasive, portable, low-cost technique that requires small amounts of sample (less than a few micrograms). The VMP technique can provide information on the composition and oxidation state of electroactive species, and can be applied to the identification of organic and inorganic pigments, ceramic materials, metals, among others. However, even with all these advantages, it is still a reasonably new technique, used by only a few research groups. Moreover, the literature reports a wide variety of methodologies, which makes it difficult to compare the results. Thus, it is still necessary to develop a standard procedure that will allow the creation of a reliable database for this technique.

2. OBJECTIVES

General

The present work has the main goal of using VMP as a tool to identify metallic elements present in complex compounds like pigments used in works of art and corrosion products formed in metallic materials.

Specific

In order to do so, specific goals were settled:

- Creating a reference database using selected metallic samples of known composition (determined by means of Energy Dispersive X-ray Spectroscopy (EDS));
- Considering the chosen metallic materials, determining the most suitable voltammetric procedure for the identification of the metals' samples, as well as the best electrolyte solution, using as parameters the number of metallic elements identified by the chosen electrolyte and the peak resolution obtained in the anodic (positive going) voltammetric scan;
- Using the same experimental conditions previously determined, perform VMP experiments with corrosion products and pigments and compare the results with the created database to evaluate the usefulness of VMP as a tool for the main objective established in this work.

3. LITERATURE REVIEW

3.1. The importance and the challenges of analyzing cultural heritage objects

Cultural heritage objects, usually denominated as artifacts, are unique and can be defined as significant goods produced by historical and artistic traditions or the manifestations of a people's cultural dynamic [1]. The characterization of these objects is essential for the conservation and restoration of the culture and memory of the mankind. Conservation science takes the importance of these items into consideration and intends to study and contribute to the preservation of artifacts from the most varied origins and periods, from archaeological and historical sites to contemporary art, all of which are considered part of the cultural heritage [2].

The study of a work of art allows one to know not only its historical and artistic characteristics, but also its chemical and physical properties. And so, the first step for this study is to carry out an investigation that provides detailed and objective information about the artifact. Conservation science has a great demand for data, seeking analytical methods that provide information such as dating, characterization of artistic techniques and technologies used for the production of materials and pieces, authentication, identification of the state of conservation and detection of previously performed treatments [2]. The lack of knowledge about the object can lead to its damage or loss of important elements during the process of restoration. Therefore, a meticulous examination must be carried out in advance, and only after obtaining information about the object it is possible to decide the best form of protection or intervention for each specific case.

The analysis of artifacts presents some special difficulties. First, the analytical techniques applied must be, ideally, non-destructive (or at least, they need to require as little sampling as possible). This is important, so the appearance and structure of the object will not be affected [2]. Besides, the chosen technique should not require the removal of the object from its place of exposure for long periods, considering that it can be fragile [2]. It is also important to note that conservation science requires multiple analytical inputs that cannot be provided by a single technique. For instance, the evaluation of a painting

consists of colorimetric analyses, microscopy analysis to identify different layers and chemical and mineralogical analysis to determine the compositions of base coats, binders, pigments, protective layers and eventually an alteration product and/or later interventions. It is also necessary to monitor the presence of biological agents and the effect of the environment on the object [2]. Therefore, in order to obtain a complete characterization of an artifact, a wide variety of analytical techniques must be combined, each providing relevant information about a specific issue.

Among the main techniques used for the identification of pigments we can list [3]:

a) optical microscopy: mainly used at low magnification as it provides a good overview of the artifact surface;
b) scanning electron microscopy (SEM), coupled with an energy dispersive X-ray spectrometer (EDS): provides important information about the physical nature and elemental composition of the surface of solids;
c) X-ray diffraction (XRD): allows the identification of the different crystalline phases;
d) spectroscopic techniques, especially Fourier transform infrared spectroscopy (FTIR): qualitative analysis of organic substances, providing information about functional groups.

The instrumental analysis techniques currently used in the characterization of paintings are divided into non-invasive (such as spectroscopic techniques and X-ray fluorescence) and micro-invasive (such as optical and electron microscopy, infrared and Raman spectroscopy).

3.2. Raman spectroscopy

Raman spectroscopy is a widely used technique due to its non-destructive nature and its speed of analysis [4]. It studies molecular and crystal lattice vibrations [5], and so, it can give information about particles of organic or inorganic nature in any physical form, such as gases, liquids, solutions, and crystalline or amorphous solids due to its sensitivity to composition, bonding, and crystalline structure of the sample material [4,5]. This technique has been successfully used in the identification of oil paintings, medieval manuscripts,

archaeological objects, wall paintings and dyes. It can also be used for investigating degradation processes [4].

In this technique, a monochromatic photon beam with frequency v_0 is focused on the sample. Most of the radiation will either be absorbed, reflected or transmitted by the sample [5], but some of it can interact with the molecules resulting in transitions between vibrational energy levels (as shown in Figure 1). The molecules in the sample affected by the photon will transition to a “virtual” excited state, which is highly unstable, and will decay almost immediately back to the ground state. This will result in radiation scattering, which can happen in three different ways: elastically (through a phenomenon called Rayleigh scattering [5] or radiation [6], where the emission of the photon presents the same energy as the incident photon (hv_0)) and inelastically (generating frequency-shifted “Raman” photons) at energies both below ($hv_0 – hv_M$) (Stokes Raman scattering) and above ($hv_0 + hv_M$) (Anti-Stokes Raman scattering) the Rayleigh photons. Elastic scattering gives no information about the vibrational energy levels of the sample. When looking at inelastic scattering, however, the energy differences hv_M and $–hv_M$ compared to the excitation energy hv_0 are related to an energy loss (or gain) when the molecule returns to a higher or lower vibrational level. The vibrational energy levels are probed indirectly by Raman spectroscopy, and the spectrum can be considered a compound’s fingerprint [5,6].

Figure 1 - Diagram of transitions between vibrational energy levels corresponding to the processes of IR absorption/emission, and Rayleigh and Raman scattering.

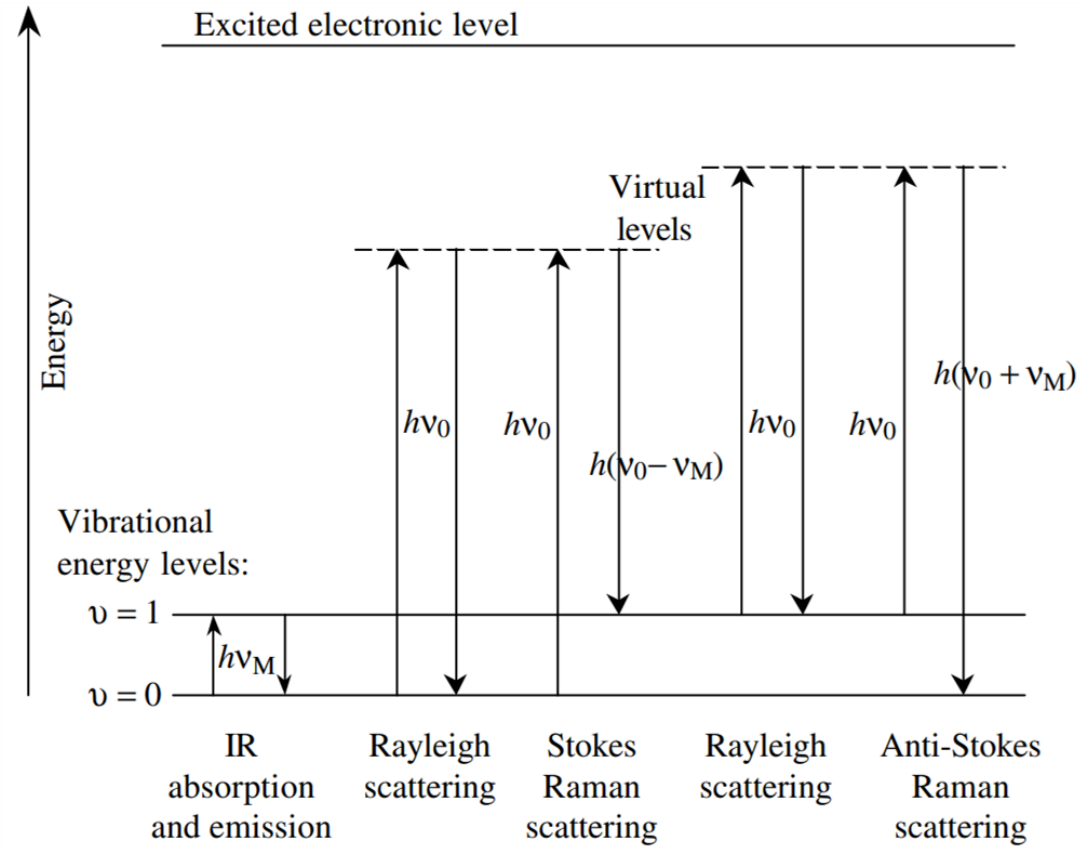

Source: Keresztury (2006) [7]

However, Raman spectroscopy has some setbacks, like its difficulty in analyzing materials that present fluorescence (either natural or from fluorophores that have become incorporated into artifacts from handling, burial, or other processes [5]). Different procedures, however, such as the use of extremely long or extremely short wavelength lasers or spectral manipulation, have already been developed to avoid fluorescence problems [5]. Also, nearly all pure metals cannot be identified through Raman spectroscopy, meaning that the technique cannot be applied in the analysis of some archaeological samples [5].

Many conservation science works have used this technique. Bellot-Gurlet *et al.* [8] applied Raman spectroscopy to the analysis of archaeological iron artifacts in different corrosion environments (such as aerated soil or indoor atmosphere), observing the conservation state of the samples through the identification of the compounds present in the layers of corrosion products. Buse *et al.* [9] used different historical recipes to create medieval copper pigments and, through Raman spectroscopy, created a database with the spectra for the

different groups of copper green pigments, as well as their degradation products. Schulte *et al.* [10] used Raman spectroscopy to identify more than 20 organic synthetic pigments used in artifacts from the 20th century.

3.3. Electrochemical techniques and solid state electroanalysis

Within the scope of characterization, electrochemical methods can be used as a complementary methodology to obtain chemical, mineralogical, and compositional information on samples of works of art and archaeological artifacts [2]. An alternative proposal is based on solid state voltammetric analysis, a less known and less developed area of electroanalysis (most usually focused on the analysis of solutions).

Electrochemical techniques are based on the correlation between electrical and chemical effects [11]. One major part of the studies in this area focus on the changes observed in the oxidation state caused by the passing of an electric current, as well as the electric energy produced by electrochemical reactions taking place at an interface [11].

An electrochemical experiment requires an electrochemical cell, consisting of conductive electrodes immersed in a conductive solution (electrolyte). The electrode surface inside the cell acts as an interface between an ionic (solution) and an electronic (electrode) conductor [11]. Considering dynamic techniques (that is, when the current passing through the system is not zero) [12] with a controlled potential, the potential applied to the electrode acts as a driving force to induce the analyte to gain or lose electrons (through reduction or oxidation reactions), causing energy absorption or electron transfer in the form of a measurable current [13].

By the end of 1980, electroanalytical studies (and especially voltammetric techniques) of organic and inorganic species in solution was a more well developed field in comparison to the analysis of the electrochemical behavior of solid species [14]. Solid state electroanalysis has always been considered challenging, due to difficulties in the preparation of samples as well as several other issues observed during the experiments: solids with low electrical conductivity could not be used as electrodes [14], electrodes made of conductive materials could act as an almost infinite reservoir for electrochemical dissolution, resulting in high currents and high ohmic drops (which may lead to difficulties for

voltammograms interpretation) [14], several solid materials could form passive films on their surfaces (and this can also lead to difficulties in interpretation) [14], and voltammograms of solid materials can be much more complex than those observed for dissolved species [14].

Besides, the development of solid state electroanalytical chemistry (SSEAC) was discouraged by a great number of studies showing that the experimental results depended on the sample surface, its crystallographic orientation, chemical or electrochemical pre-treatment, adsorption of contaminants and other aspects. This resulted in a general belief that information about solids could only be obtained from carefully prepared surfaces, following procedures that, most often than not, could only be achieved through preparation in specialized laboratories [15]. Due to its complicated nature, both from a theoretical and experimental point of view, SSEAC studies only developed some time after the analyses of solutions [15].

Despite all this, solid state reactions can give much information about a sample:

- elemental composition (qualitative and quantitative): electroactive species of a solid compound can be determined qualitatively, and their relative quantities allow them to be quantified [16];
- redox state of the electroactive elements: identification and relative quantification of the redox state (for instance, Fe(II) and Fe(III) in clays and ceramics) [12,16];
- composition of phases: a phase mixture can be distinguished from a single-phase solid solution, and phase mixtures can be analyzed quantitatively [16];
- kinetics and thermodynamics of the reactions of solids, which can be related to the composition, structure and chemical bonds of the sample [17,18].

Another main advantage of electroanalytical methods is that equipments usually cost less than the instruments used in other analytical techniques [12].

SSEAC only involves systems at which the analyzed material is a solid that either works as an electrode or is deposited on an electrode. The systems that can be studied include [16]:

- inorganic solid compounds (usually oxides, sulfides, halides, metal complexes, polyoxometalates, minerals) including doped materials and solid solutions;
- metals and solid alloys, semiconductors;
- organic solid compounds, including natural products or mixtures of products;
- micro and mesoporous materials with or without additional electroactive ions or molecules (functional zeolites, silica, silicate);
- organometallic structures and related materials exhibiting high permeability to ion transfer, usually called ionic sponges.

This includes, for instance, the analysis of minerals or pigments, as well as the quantification in samples containing a mixture of minerals or pigments combined with binders. It can also identify and quantify elements present in a single phase, which allows to identify impurities of certain exogenous elements in a mineral, dopants in semiconductors, among others [16].

SSEAC makes it possible to treat data through different parameters. In voltammetric techniques peak potential and peak current are typically used for identification, but other parameters may be used in order to differentiate species with similar electrochemical responses. These parameters characterize the voltammetric curves through peak width, peak separation and starting peak potential, including Tafel slopes and ordinates [16]. Sadly, SSEAC cannot give absolute information about the structure of the sample, like X-ray diffraction, and all information needs to be compared with a database collected from graphs of pure phases, or in the case of solid solutions, based on the thermodynamic rules of phase mixing [16,17].

3.3.1. Voltammetric techniques

Voltammetric techniques are among the most sensitive in SSEAC, enabling the determination of components that can be electrochemically oxidized or reduced. They can be used for determining electroactive inorganic elements and organic substances in quantities as small as nanograms or picograms, with fast analysis that can be done in just a few seconds [13]. In these methods, a potentiostat is used to apply a controlled potential to the sample through a conducting electrode (called “working electrode”) and the current flowing through

the electrode is measured. The potential, which works as a driving force for electrochemical reactions, varies within a specific range. If the oxidation or reduction potential for a component of the sample falls within this range, a variation of current will be observed [13]. The potential at which this occurs allows the identification of the component, and the amount of current produced is proportional to the concentration of the component in the specific phase. This is shown by the Randles-Savecik equation (Equation 1) at 25 °C [11].

$$i_p = (2{,}69 \times 10^5) n^{3/2} A D_o^{1/2} C_O^* v^{1/2} \qquad \text{Equation 1[11]}$$

With:

i_p: peak current (A);

n: number of electrons per mol;

A: electrode area (cm^2);

D_O: diffusion coefficient ($cm^2\ s^{-1}$);

C_O^*: concentration ($mol\ cm^{-3}$);

v: scan rate ($V\ s^{-1}$).

Apart from the working electrode, the electrochemical cell requires an auxiliary electrode and a reference electrode, positioned as close as possible to the former electrode. If the working electrode functions as a cathode, then the auxiliary electrode will work as anode and vice-versa. The potentiostat measures the potential in the pair reference/working electrode by means of a circuit in which the passage of current is practically zero. Since the potential at the reference electrode is constant, the circuit can precisely measure the potential at the working electrode, without needing to correct the effects of ohmic drop through the electrolyte [13].

Among the voltammetric analyses, cyclic voltammetry is one of the most used in SSEAC. In this technique, a linear sweep is performed to a certain potential and, after reversing the direction of the sweep, it returns to the initial potential while the current is recorded [13,17]. The potential is varied in a way similar to an isosceles triangle (like the schematic representation in Figure 2). The sweep can start either in cathodic or anodic direction.

Figure 2 - Variation of the potential applied to the working electrode in cyclic voltammetry in function of time.

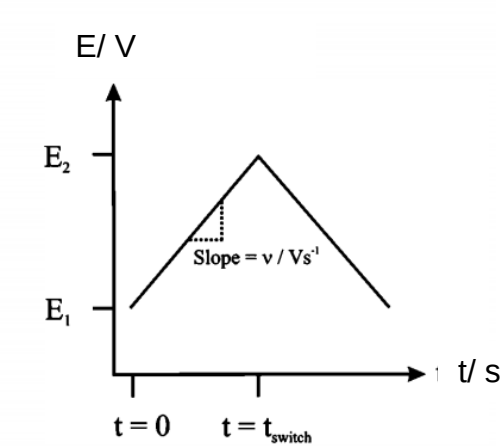

Source: Compton e Banks (2018) [19]

The current in the working electrode is recorded during the sweep, and, if an electrochemical reaction occurs at a given potential, there is a current increase. As an example, Figure 3 displays a typical voltammogram when a reversible redox reaction takes place at the electrode surface.

Figure 3 – Current variation during cyclic voltammetry for a reversible redox reaction.

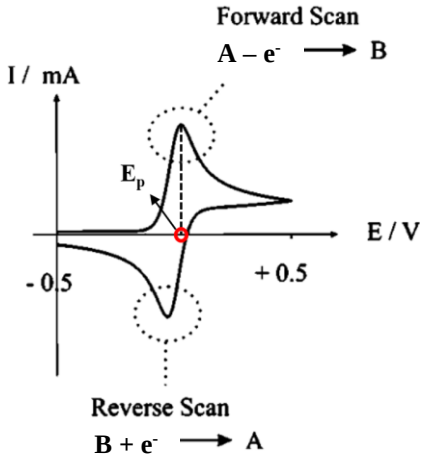

Source: Adapted from Compton e Banks (2018) [19]

Information can be obtained on the potential region at which the redox process takes place, the reversibility and type of process, reaction kinetics, transition intermediates and the nature of the reaction products [17]. The data obtained from cyclic voltammetry in solid state, however, are more complicated

and harder to interpret quantitatively than what is obtained from voltammetric analysis in solution [17].

The peak potential (*Ep*), although characteristic to each type of redox species in analysis, can be affected by experimental conditions such as scan rate, size of the particles of the sample and uniformity of phases [17].

Another widely used technique is square wave voltammetry. It is a pulse technique that can be used to improve the separation of overlapping redox processes [17], and presents lower time of analysis when compared to other pulse techniques (like differential pulse voltammetry) [11,13], being, in general, the best choice among pulse techniques. It presents some advantages to cyclic voltammetry, like the reduction of the background current and the analysis of systems containing lower concentrations of analyte [11]. The results obtained with cyclic voltammetry, however, are easier to interpret in chemical terms [11]. Figure 4 presents the variation of the potential in function of time, and the main parameters of square wave voltammetry.

Figure 4 - Schematic representation of a square wave voltammetry experiment.

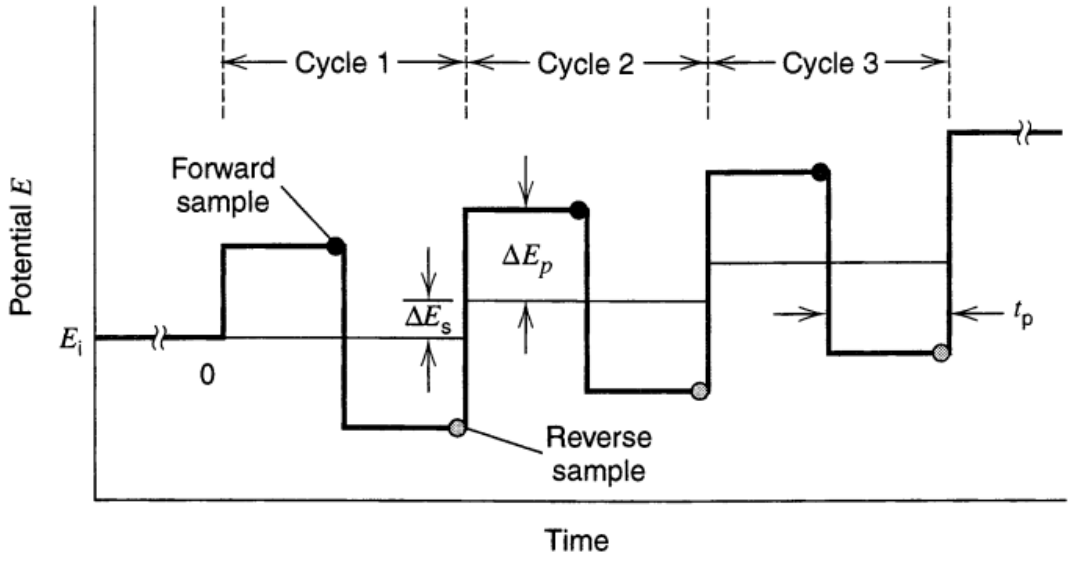

Source: Bard (2001)[11]

The bold line represents the potential applied to the working electrode, and the lighter line marks the base on which the square wave is superimposed. It is characterized by a pulse height (ΔE_p), measured from the base of the staircase, and by the pulse width (t_p) (which can be represented in terms of frequency $f = 1/(2t_p)$). The base of the staircase shifts by ΔE_s at the beginning of each cycle.

The current is measured twice per cycle, at the end of the pulse, with a forward current sample (i_f) (represented by the black dot in Figure 4) and a reverse sample current (i_r) (the white dot in Figure 4). The differential current Δi is calculated as i_f-i_r [11], reducing the contribution of the capacitive current to the signal.

Two experimental problems must be solved in order to study the electrochemistry of solid compounds. The first one is that they can generate or consume a great amount of electric charge because the electrochemically active species are concentrated in a small volume. This is the opposite to what is observed in diluted solutions, and the resulting high current can lead to an unwanted ohmic drop and a bad signal resolution. The second problem is the possibility of low conductivity. In this case, it is not easy to apply a potential difference through the material's interface with the electrolyte. For a technique to be able to solve these two problems it must work with small amounts of the solid compound and bring it as close as possible to the electric field [15].

Until 1989 there were two possible ways to prepare the solid samples for electrochemical analysis. The first one was using the sample as working electrode. Although this method had the advantage of providing better characterization of the surfaces, it could present problems when the material goes through anodic dissolution, not always presenting distinct signals. This problem can be avoided with the second method of sample preparation, where the sample is pulverized and then added to a carbon paste electrode. This procedure, however, is complex and time-consuming, and thus not applicable in recurrent analyses [18].

In 1989 a technique presented by Scholz, Nitschke and Henrion [18] evaded these two problems. In this technique, microparticles of a solid compound (less than 1 µg) are transferred to an electrode by abrasion [15,18,20]. An important characteristic of this technique is the possibility of reproducible measurements with the immobilized particles, which reflects the electrochemistry of the bulk of the microparticles [15]. This technique was initially called abrasive stripping voltammetry (AbrSV) and then, voltammetry of immobilized microparticles (VMP) [20].

3.4. Voltammetry of immobilized microparticles (VMP)

The introduction of VMP in 1989, and the recent developments of voltammetric methods based on the immobilization of microquantities of solids on the electrode surface, provided a quick way to obtain useful analytical information about a solid compound through electrochemical measurements, helping to expand the field of applications of solid state electrochemistry [16]. In principle, every insoluble solid sample with elements that can undergo electrochemical reactions can be analyzed by VMP [20]. Along with experimental research, the theoretical model of the electrochemical processes of solid particles has been developed.

VMP is an electrochemical technique with easy implementation, considered non-invasive or micro-invasive as it requires sample amounts in the order of micrograms [2]. These features make it an interesting tool for analyzing works of cultural heritage, as will be detailed later. It has expanded the possibilities of electroanalysis of solids, thanks to its wide applicability, ease of electrode and sample preparation, besides enabling a quick analysis without the need for pre-treatment [17,20]. It can be used for qualitative and semi-quantitative analysis, and it can give information on the kinetics of redox reactions [20]. VMP can be considered interesting also due to its versatility and low cost (including portable options) [21]. Several studies have been carried out in the characterization of metallic components of artifacts [22], corrosion products [23] and phenomena of alteration of pigments [2].

The initial name of the technique, abrasive stripping voltammetry, refers to the way in which the sample is deposited on the surface of the electrode by an abrasive process. The term “stripping” is justified because in most cases the solid compound is removed from the electrode surface through voltammetric measurements [14]. However, many electrochemical reactions of immobilized microparticles were studied afterwards, and no dissolution process was observed. Thus, the term most used to refer to the technique became voltammetry of immobilized microparticles (VIMP or VMP) [15].

The application of VMP is based on the fact that, according to Faraday's first law of electrolysis (Equation 2), very small amounts of a solid sample (between 10^{-10} and 10^{-12} moles) are sufficient to generate measurable currents [14,20].

$$w = \frac{itM}{nF}$$ Equation 2[24]

Where:

w: sample mass (g);

i: generated current (A);

t: time (s);

M: molar mass (g mol^{-1});

n: number of electrons involved in the redox reaction;

F: Faraday constant (s A mol^{-1}).

It can be observed that, for instance, 10^{-10} moles of silver (approximately 10^{-8} g) can provide a current increase of 1 μA when silver is oxidized anodically for 10 seconds [14]. The initial idea of the technique is to transfer small amounts of the analyzed material simply by abrasion, touching the electrode on the surface of the sample [14]. In the case of a powdered sample, one of the options of immobilization on the active surface would be to apply a slight pressure with the working electrode on a glass support where the substance of interest is collected [3].

VMP solves two experimental problems in the study of solid state electrochemistry, as it requires small amounts of solid sample and brings the sample as close as possible to the electric field. It overcomes the limitations presented by other electroanalytical methods, such as the extremely complicated procedures for electrode preparation, the high currents of voltammograms when the working electrode is the sample itself, and the dilution of the solid sample with an inert substance [25].

Different types of electrodes have been developed for application in solid state electrochemistry since the beginning of studies in the area. In many cases, the studied component is present in the electrode, mixed with graphite powder, in the so-called compact electrodes and carbon paste electrodes. Many researchers used this type of electrode to study the electrochemistry of solids [26–29]. However, their preparation is complex and time-consuming [18]. In VMP, the sample is not added to the working electrode, but immobilized on its surface.

Several electrodes were tested for the immobilization of solid particles, but the initial choice of graphite electrodes impregnated with paraffin (PIGE - Paraffin Impregnated Graphite Electrode), made from graphite billets of different sizes, was the one that provided the best results [15,20].

Graphite has become the most used electrode in VMP due to its chemical inertness, wide potential window, low price and ease of processing. In addition, PIGE proved to be quite suitable for fixing small amounts of solid particles on the electrode surface [20]. If the graphite has no external insulating coating, it is necessary to pay attention to the effective active area of the electrode in contact with the solution so that the measurements are reproducible. As graphite is microporous, penetration of the electrolyte into the graphite may occur, resulting in a high background current [15,20]. Furthermore, electrolyte penetration can lead to electrode contamination[15]. These problems are circumvented by impregnating graphite with paraffin.

VMP was developed for the study of solid materials, regardless of their physical and chemical properties [15]. Thus, it can be applied in the analysis of metals, metallic alloys, superconductors, minerals, oxides, organic compounds, pigments, soil and rock samples, and drugs [15,20,30]. It is highly sensitive in detecting species with low electrical conductivity, as well as samples that are weakly magnetic, with amorphous phases, or that are micro or nanocrystalline [30]. In addition, VMP can expand the perception of the relationship between structure and reactivity of solid compounds, making electrochemistry a versatile tool for the characterization of solids [15].

Compounds and solid materials must meet only two requirements to be analyzed by VMP: insolubility in the electrolyte and electroactivity. There are no restrictions on electronic conductivity, and even insulators can be studied, as the electrochemical reaction at the three-phase interface compound/electrode/solution can generate sufficient charge to produce measurable currents [20].

3.4.1. Mechanisms

The vast majority of configurations in classical electrochemistry exhibit electrodes with well-defined two-phase interfaces. In VMP, the electrode is always a multiphase system, consisting in the simplest case of a liquid phase and

two solid phases [15]. These are called “three-phase electrodes”, since the three phases are together [20]. One of the phases is the solid support (working electrode), which holds the immobilized particles of the solid sample and works as a conductor. The second solid phase is the sample itself. The third phase is the electrolyte solution, necessary for the exchange of ions that follows every electrochemical reaction, guaranteeing the neutrality of charges in the phases [15].

The electronic conductivity of the sample determines the potential difference between the solid phase and the electrolyte solution. If the conductivity is very high, the potential difference will be equal to that existing between the working electrode and the solution. In this case, the reaction can occur on the entire surface of the sample particles, at the reagent/electrolyte interface (if there is no other impediment). This will happen for metal particles and alloys. If the conductivity is very low, however, a direct electronic transfer from the graphite to the solid reagent can only occur at the limit where the three phases (electrode, sample and electrolyte) are in contact with each other (Figure 5), so that the electronic transfer between electrode and sample occurs simultaneously to the ionic transfer between solid sample and electrolyte solution [14,15]. In Figure 5, the arrows represent ionic and electron transfers occurring simultaneously.

Figure 5 - Schematic drawing of the three-phase system, with the electrode/compound/solution interface.

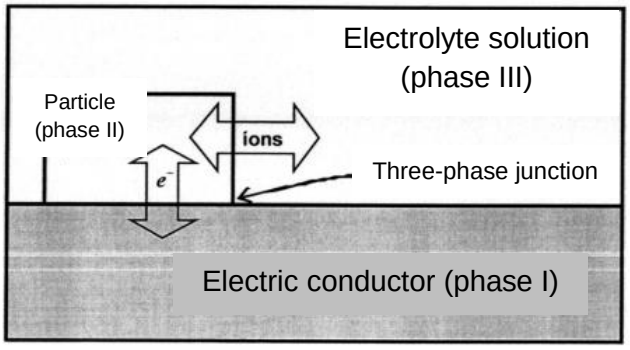

Source: Adapted from de Carvalho, Hilgemann, Spengler, do Nascimento and Bohrer (2010) [20]

Although the possible applications of VMP are diverse, in all of them the electrode with immobilized electroactive particles presents transfers of electrons

and ions occurring simultaneously [20]. Considering that the sample particle contains neutral molecules and ions with negative and positive charges in the same amount, the exchange of electrons between the electrode and the sample must be accompanied by the exchange of ions between the sample and the solution, to guarantee the electroneutrality of the particle. The redox reaction starts at the boundary between the three phases, and progresses across the surface and into the body of the crystal [15,20]. The theoretical treatment of the simplified model of the three-phase boundary (Figure 5), which exists when the sample crystal is incorporated into the surface of a solid electrode, allows the following assumptions:

- the boundary of the three phases is always the starting point of the reaction, regardless of particle geometry or conductivity [15];
- the reaction will be limited to the surface if diffusion of ions through the crystal is impossible or too slow [15];
- normally, the net current is the sum of the surface current and the current in the bulk [15];
- if surface and bulk reactions occur at similar rates, the reaction expands beyond the three-phase boundary [15];
- the surface current will be negligible in cases where the bulk reaction is dominant [15].

Unlike other voltammetric applications, only the circular end of the working electrode comes in contact with the electrolyte in VMP, ensuring that redox reactions occur only at the junction of the three phases [20]. The greatest difficulty in interpreting the mechanisms arises from the great variety in electrode reactions, including the possible formation of additional solid phases through the direct conversion of one phase into another, resulting in the variation in the number of solid phases during the electrochemical reaction. And so, instead of well-defined interfaces, it is possible to have a continuous transformation from one phase to another, with the formation of mixed phases. This transformation does not always proceed along a continuous series of mixed phases in the crystal, which only happens when the initial and product phase systems exhibit a miscibility gap. When mixed crystals do not exist, there is a range of immiscibility of the solid phases, which can lead to a separation of the cathode and anode

peaks in cyclic voltammetry because there is no “solution pathway” through which the reaction can proceed [15].

The possible reactions of immobilized particles in the three-phase system are seen in Figure 6 [20], namely: (1) reduction of an insoluble metallic salt to a metal (like silver chloride (AgCl) to silver (Ag), releasing chloride ions (Cl^-) that diffuse to the electrolyte); (2) oxidation of a metallic salt with the release of metal ions; (3) oxidation of the metal and formation of an insoluble metallic compound (this reaction can proceed via a supersaturated solution of MX metal halides, as in the case of the oxidation of silver to silver bromide (AgBr) and silver iodide (AgI)); (4) anodic oxidative dissolution of a metallic particle; (5) electrochemical insertion of a particle, when ions are exchanged between the solid particle and the electrolyte solution, and electrons are exchanged between the particle and the electrode; (6) electrochemical reaction confined to the surface layer; (7) electrochemical reaction via dissolution of an already existing solid particle; and (8) complete electrochemical dissolution of a particle resulting from its oxidation or reduction [20].

Figure 6 - Scheme of possible electrochemical reactions of solid particles at the three-phase boundary.

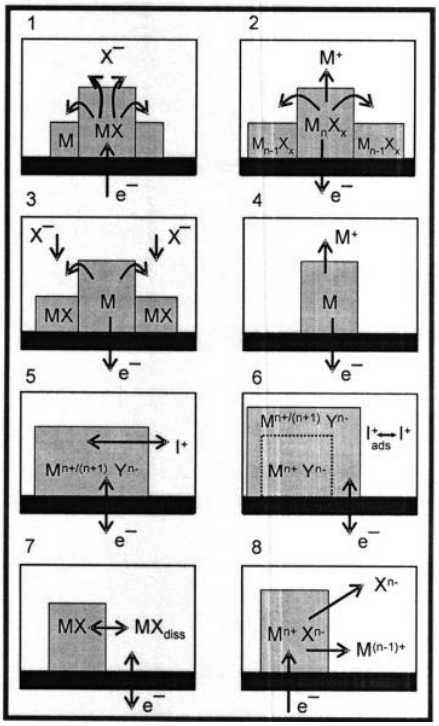

Source: de Carvalho, Hilgemann, Spengler, do Nascimento and Bohrer (2010)[20]

3.4.2. Advantages and disadvantages of VMP

At first, it seems that a major disadvantage of VMP is that the amount of sample deposited on macroscopic electrodes cannot be controlled [14,17]. Studies carried out with the technique, however, show that this does not prevent the extraction of quantitative information, through the currents and potentials of the obtained peaks [14].

Another problem for theoretical treatment is the morphology of particles distribution on the electrode surface. Due to the immobilization processes, the deposited microcrystals have a certain size distribution and may present a preferential orientation, exposing different faces to the solution and to the electrode. Thus, polycrystallinity can decisively influence the electrochemical properties [15]. However, the deposition of isolated particles on microelectrodes has already been performed using a micromanipulator [31], allowing to precise the amount of sample deposited and removing the influence of defective sample geometries on the electrode [17].

One more obstacle related to the distribution of particles in the electrode is observed in the identification of minerals. A mineral can be identified based on characteristic peak potentials, specific signals under fixed chemical and electrochemical conditions (electrolyte, electrode conditioning, electrochemical parameters). However, the peak potential and peak profile also depend on the shape, size and distribution of the microparticles deposited on the electrode. The degree of hydration and the crystallinity of the solid can also affect the voltammetric response. Therefore, it is important to use different analytical strategies in the electrochemical identification of solid analytes (or analytes in solids), using shape-dependent parameters, in addition to peak potential, for identification [16].

Electrochemical experiments for determining a given analyte can be affected by interfering species (whose analytical signal distorts or overlaps the analyte signal) and matrix effects (species affecting the analyte signal by complexation or adsorption), but some analytical strategies can be used to get the wanted information [16]. Strategies include, in addition to varying electrochemical conditions (technique, parameters such as speed rate in cyclic voltammetry or frequency in square wave voltammetry) the sequential use of

different electrolytes or the application of constant polarization before electrochemical measurements. The combination of these strategies allows identifying different compounds with similar responses [16].

Compared to commonly used atomic techniques such as X-ray fluorescence (XRF), VMP has the advantage of allowing identification of minerals and assessment of oxidation states. However, VMP cannot provide information about some elements, in particular ultra-trace elements. Compared to molecular techniques such as infrared and Raman spectroscopy, VMP offers the advantage of making it possible to determine minor components in the presence of substrates, such as calcareous supports in frescoes, exhibiting signals of considerably higher intensity (compared to infrared spectroscopy) without the disadvantage of being hindered by significant fluorescence (compared to Raman spectroscopy) [21].

Finely particulate samples (including nanocrystals and amorphous phases) are very advantageous for electrochemical analysis due to their high reactivity. In techniques such as X-ray diffraction (XRD), long-range ordering in solids is required, and therefore virtually no significant signals can be obtained in amorphous phases. This also complicates quantitative XRD analysis of crystalline analytes in an amorphous matrix. In many cases, voltammetry can detect both phase composition and elemental composition, which could only be achieved by combining two different techniques (such as XRD and electron microprobe analysis) [17].

The abrasion method is the least laborious technique for preparing a solid for electrochemical measurements and is suitable for compact and powdered samples. Microparticles from solid samples can be directly deposited on the surface of an appropriate electrode without the need for additives, such as the binders needed for composite electrodes. Despite providing information about the solid state redox process, experiments based on thick film deposits have disadvantages such as high currents and resistance effects. In contrast, the VMP procedure requires only sample traces to be deposited [17].

3.4.3. Identification of metals and alloys

Among the applications of VMP, the simplest one is the identification of metals. Pure metals can be unequivocaly identified by their anodic peaks, as

demonstrated by Scholz *et al.* [32] for copper, cadmium, tin, lead and antimony. Knowing the potential of the anodic peaks of each pure metal, it becomes possible to identify the metals present in unknown samples, using the same experimental parameters. VMP is widely used for the identification of metallic objects of cultural heritage, especially silver, copper, lead and gold, as well as their alloys (particularly bronze). Alloys are one of the most interesting parts of this application, and the analysis of the results can provide qualitative identification and quantitative determination of the alloy constituents, qualitative identification of the alloy by its voltammetric fingerprint, and identification of corrosion processes [11].

According to Cepriá *et al.* [33], VMP proves to be efficient in the analysis of brass, and can be applied in the quality control of the alloy or in the characterization of artifacts, pipes, heat exchangers and other engineering pieces. The work also demonstrated that the technique enables the differentiation of the α and β phases of brass. Another of the main copper alloys, bronze, was analyzed by Elia *et al.* [34], who compared the voltammograms obtained with standard copper, lead, tin, and copper-lead-zinc alloys and were able to identify the constituents of two bronze archeological objects and their corrosion products.

Cepriá *et al.* [25] analyzed silver, copper and alloys containing these two metals with different compositions, verifying the change in peak potentials as the composition of the alloy varied. In this work, two earrings and a pendant were also analyzed, and by comparing the voltammograms obtained with those observed for the patterns of metals and alloys, it was possible to identify the composition of the jewels, with one earring presenting an alloy richer in silver than the other earring and pendant (alloys with higher copper content).

Ottenwelter and Costa [22] verified the efficiency of the technique in identifying not only the main metallic alloys of archaeological artifacts, but also the metals used in the coating of the pieces, analyzing iron alloys coated with tin-lead solder and with the presence of silver, and copper alloy with the presence of tin and antimony. They verified that the technique allowed selective and local analysis, and running voltammograms on several areas of the samples resulted in the identification of the different metals present in the surface.

When the sample is covered with corrosion products, the identification of these compounds might be achieved through the analysis of the cathodic peaks,

which allow the differentiation of the formed compounds [35–37]. After applying a negative potential and reducing the species found in the corrosion product, it is possible to identify the metal that makes up the sample with an analysis of the anodic peaks, observed in a scan in the positive direction [38]. Costa *et al.* [38] carried out the analysis of two Roman fibulae showing greenish areas, indicating probable copper corrosion (and therefore leading to assume that the fibulae were made of bronze or brass) with grayish regions of some other alloy applied for decoration. Through VMP, it was observed that the anodic peak obtained for the metal in the grayish region corresponded to silver. In the greenish regions, the presence of copper, tin and lead was detected.

Fabrizi *et al.*[39] used a combination of non-destructive techniques (XRD, SEM, micro-Raman and VMP) in the analysis of medieval Roman silver coins, and the voltammetric analysis allowed to identify the presence of copper and silver compounds in the patinas. VMP was also used by Di Fazio *et al.* [40] in the analysis of Roman coins made with silver and copper alloys, identifying differences in the composition of the patinas and in the corrosion process.

Doménech-Carbó and Bernabeu-Aubán [41] used VMP in the analysis of copper artifacts from the archaeological site of La Vital (Gandia, Spain), which holds evidence of the beginning of copper metallurgy in the Iberian peninsula. The variation in the intensity of the current response of the copper corrosion products was considered as an indication for the different forms of manufacture, and the samples were grouped accordingly. Using this same principle, Domenéch-Carbó *et al.* [42], Di Turo *et al.* [23] and Di Fazio *et al* [43] grouped silver, brass and bronze coins from different archaeological sites in Europe, according to their coinage, based on the composition of the patina.

There are different electrolytes and voltammetric techniques used in the identification of metals and their alloys by VMP. Table 1 shows a compilation of the voltammetric techniques used to identify the metals investigated in this work, while Table 2 shows the electrolytes. Considering that different electrolytes were used in the literature, in the present investigation, all the solutions presented in Table 2 were tested in order to choose the one that would allow the identification of electrochemical processes in the highest number of metallic samples.

Table 1 - Voltammetric techniques used in the identification of metals and their references.

	Cyclic voltammetry	Square wave voltammetry	Differential pulse voltammetry
Silver	[22,44]	[42,45–48]	[25,49]
Copper	[3,22,44,50]	[33,34,52–55,37,42,43,45,47,48,50,51]	[25,32]
Iron	[56,57]	[58–60]	
Zinc	[3,44]	[43]	
Tin	[3,22,44]	[34,47]	[32,49]
Lead	[3,22,44,57]	[34,36,37,42,47,51,52,54,55,61]	[32]

Source: The author.

Table 2 - Electrolytes used in the identification of metals and their references.

	Oxalic acid (OA)	HCl	KCl	NaOH	Acetate buffer (HAc/NaAc)	H_2SO
Silver	[22,25,38,44,49]	[44,46]	[44]		[42,45–48]	[62]
Copper	[3,22,25,32,33,38,44]	[33,44,56]	[44]	[3,34,44]	[33,37,53–55,61,42,43,45,47,48,50–52]	[40,63]
Iron	[60]	[56,58–60]	[57]			[64–66]
Zinc	[3,38,44]	[44]	[44]	[3,44]	[43]	
Tin	[3,22,32,34,38,44,49]			[3,34,44]	[47]	[67]
Lead	[3,22,32,34,38,44]	[44]	[44,57]	[3,44]	[36,37,42,47,51,52,54,55,61,68]	[36,66]

Source: The author.

3.4.4. Identification of pigments

The identification of organic dyes and pigments used in paintings and fabrics plays an essential role in the fields of archaeometry, conservation and restoration of artifacts [20]. VMP can be applied in their analysis, especially in the study of the nature of pigments. Such a study can provide useful information about the preparation technique and the type of colors and materials used in a given historical era or location, or it can help to determine the historical period and provenance of a work that has not yet been characterized, through comparison with historical registers. It is also possible to diagnose more recent interventions in the works, with the addition and mixture of more modern pigments and/or with different composition than the original work. Finally, the study of possible processes of alteration and degradation of the pigments over time can

provide important information on the state of conservation of the work, and on the possible need for a restoration intervention [69].

VMP can help to identify inorganic pigments, organic dyes and pigment species in ceramic materials, as well as their alteration products. In more favorable situations there is only one (or just a few) electroactive species and, even in the second case, different species may present different electrochemical responses. In these cases, peak potentials and shape-dependent voltammetric parameters can be used to characterize different species [2]. Inorganic pigments with different metallic ions represent typical cases of clearly discernible voltammograms. One example is the electrochemical analysis of vermilion (HgS) and minium (Pb_3O_4), two red pigments used in medieval paintings. They present different electrochemical signals, corresponding to the reduction of the metallic salt to the metal and to the oxidation of the different metals [2]. In cases where a pigment presents two different metallic ions, such as lead-tin yellow, different peaks for the oxidation of each metal can be observed [21], resulting in a voltammetric pattern that works like a fingerprint for that specific pigment.

The differentiation of pigments of the same metal must be done through the analysis of their cathodic scanning, and the identification of pigments within the same family requires the use of other parameters such as half-width potentials and onset potentials [2]. For instance, Doménech-Carbó *et al.* [2] found that the voltammetric profiles for different commercial azurite pigments were essentially identical, and that the distinction between azurite and other copper pigments required the analysis of shape-dependent parameters.

The electrochemical response varies slightly with the particle size of the material and the type of supporting electrolyte, with the average particle size affecting the peak potential and particle distribution affecting the peak width [70]. A cooperative work between different universities showed that iron oxide pigments can be successfully differentiated using VMP and, despite the variation encountered when comparing the voltammograms from different laboratories, the results were very similar [70].

A complication that appears in several paint samples is due to the presence of binding media accompanying pigment particles. Proteins and amino acids present in the composition of the binders can form complexes with metallic cations, and this complexation interferes with the chromatographic determination

in paint samples. However, VMP allows the identification of the compounds due to the redox activity of the chromophores of the organic dyes and pigments present in the sample [20]. If necessary, it is possible to use chemical strategies, such as changing the composition of the electrolyte, changing the pH and/or adding a complexing agent to the electrolyte. The complexant can change the voltammetric response of selected analytes, increasing the difference between one compound and another or, eventually, blocking or promoting some voltammetric signals [2].

4. METHODOLOGY

4.1. Samples

The samples analyzed in this work were divided in three categories:

- Commercial samples of metals and alloys donated by different laboratories, namely: silver (Figure 7a), copper (Figure 7b), cast iron (Figure 7c), zinc (Figure 7d), tin (Figure 7e), lead with antimony (Figure 7f), lead with aluminum (Figure 7g), tungsten (Figure 7h). Their composition was determined by Energy Dispersive X-ray Spectroscopy (EDS), as presented in section 5.3.1.

Figure 7 - Commercial samples of silver (a), copper (b), cast iron (c), zinc (d), tin (e), lead with antimony (f), lead with aluminum (g) and tungsten (h). Scales bars represent 1 cm at full scale.

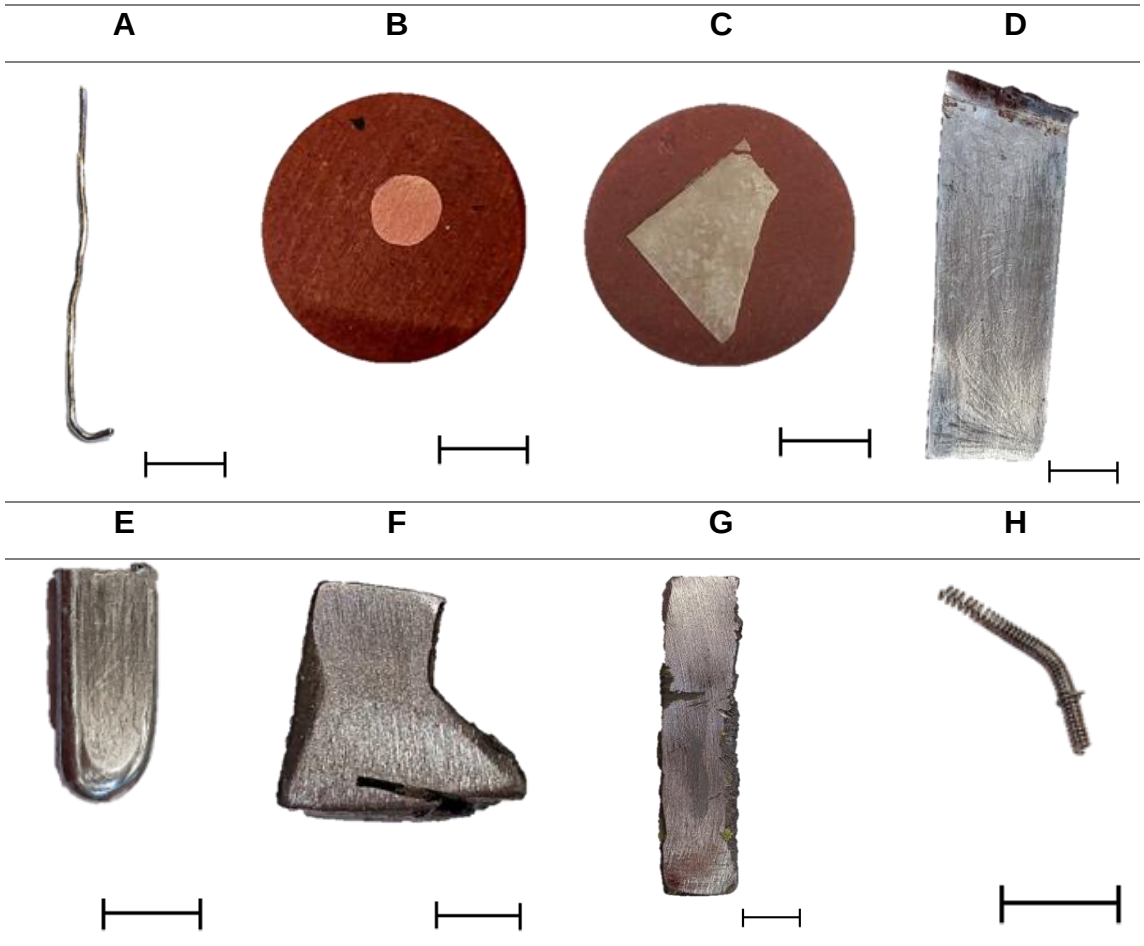

Source: The author.

- Two samples of metals, denominated “Green sample” (Figure 8a) and “Brown sample” (Figure 8b), of unknown provenance and covered with a

thick layer of corrosion products. These were collected on a beach as detached pieces of metal.

Figure 8 - Metallic samples called “Green sample” (a) and “Brown sample” (b). Numbers indicate the regions from which samples were collected for the different analyzes. Scales bars represent 1 cm at full scale.

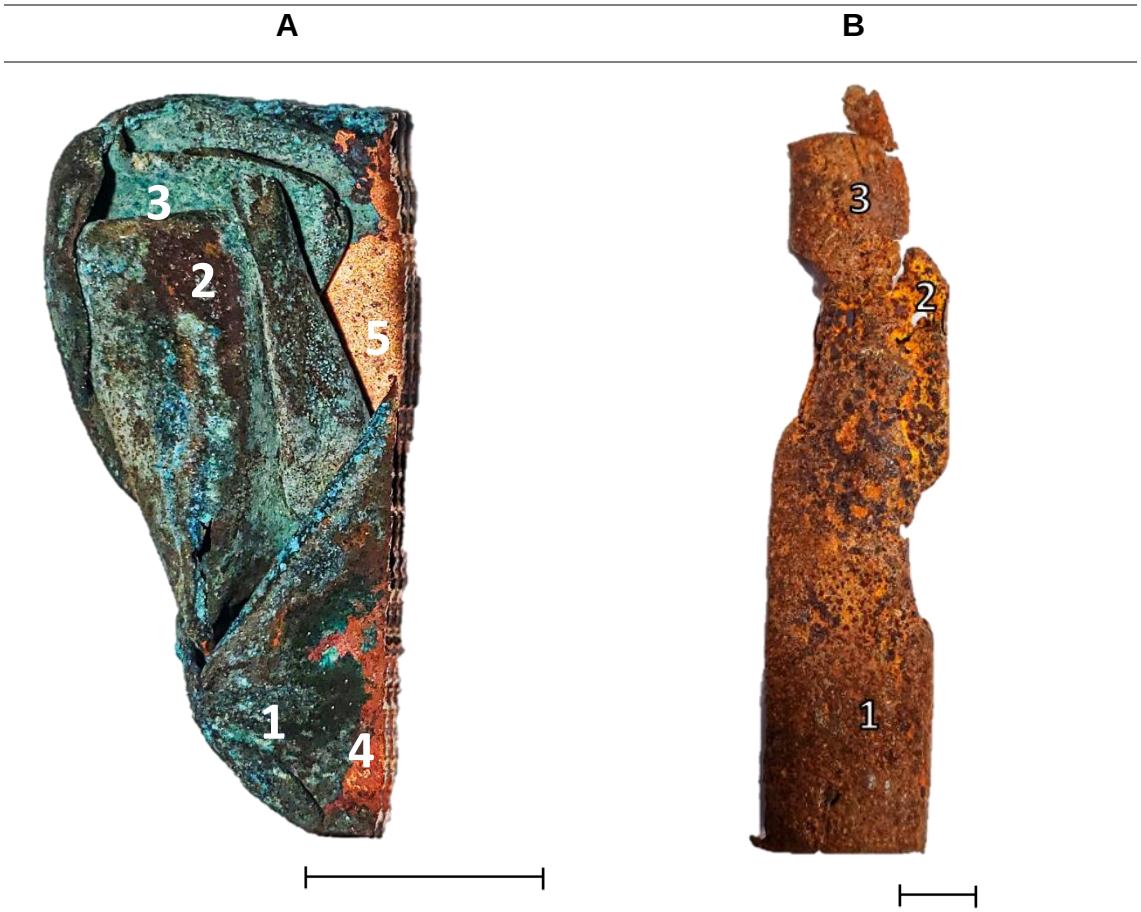

Source: The author.

- Five pigments (Pr09Pig03 (Figure 9a), Pr09Pig15 (Figure 9b), Pr11Pig03 (Figure 9c), Pr11Pig07 (Figure 9d), Pr11Pig11 (Figure 9e)) belonging to the collection of German artist Eleonore Koch, currently under the care of Pinacoteca de São Paulo. The designation of the pigments is based on the shelves (Pr) and position (Pig) in which they were stored.
- Three commercially available pigments (by Sennelier) under the denominations Green Earth (Figure 9f), Burnt Umber (Figure 9g) and Mars Yellow (Figure 9h). All the pigments were lent to us by Professor Dr. Márcia de Almeida Rizzutto from *Laboratório de Arqueometria e Ciências*

Aplicadas ao Patrimônio Cultural (LAPAC), in the Physics Institute of Universidade de São Paulo.

Figure 9 - Pigment samples Pr09Pig03 (a), Pr09Pig15 (b), Pr11Pig03 (c), Pr11Pig07 (d), Pr11Pig11 (e), Green Earth (f), Burnt Umber (g), Mars Yellow (h).

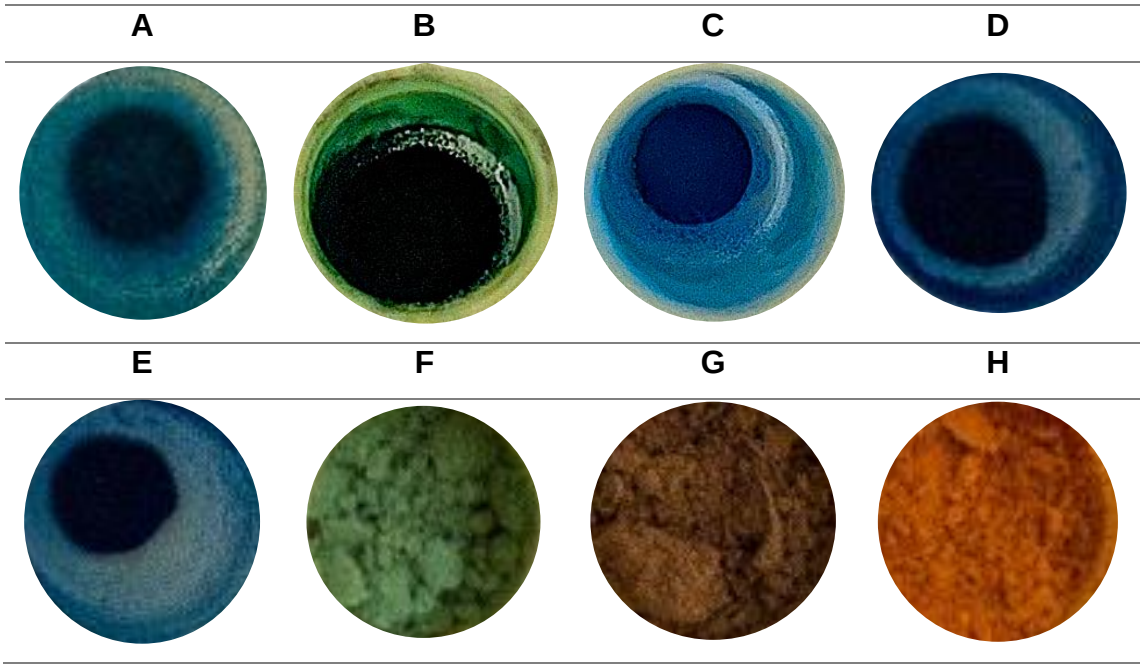

Source: The author.

4.2. Characterization techniques

All samples were characterized by Scanning Electron Microscopy (SEM) and their elemental compositions determined by Energy Dispersive X-Ray Spectroscopy (EDS) using a FEG - Inspect 50 scanning electron microscope, with secondary and backscattered electron detectors (EBSD – TEAM). Metallic samples like silver, zinc, tin, lead and tungsten were small enough and did not need any preparation, while copper and iron were cut from the original samples and embedded in Bakelite, sanded and polished. Their surfaces were cleaned with an alcohol swab prior to the introduction in the SEM chamber.

For the samples covered with corrosion products it was necessary to cut small representative pieces, and they did not receive any pre-treatment, whereas powder pigments were immobilized in carbon tape.

Corrosion products and pigments were also characterized by Raman Spectroscopy, performed with a Renishaw Invia Reflex, Raman Microscope at a

radiation wavelength of 532 nm (for the pigment samples) and 633 nm (for the corroded metal samples) from a diode LASER, with a power of 1 mW, focused with an Olympus 80x/0.75 objective. The spectra were obtained with an integration time of 20 seconds and 3 accumulations. A diffraction grating of 1800 lines/mm was used in the range of 100 to 3500 cm^{-1}. The analyses of the pigments were performed by placing the samples in a glass plate, whereas the “green sample” and “brown sample” were positioned directly on the Raman microscope base.

4.3. Preparation of the working electrode and immobilization of the microparticles

The graphite used to prepare the PIGEs are commercially available by Faber Castell, HB, with 2.0 mm diameter. First, using a closed vessel, paraffin (with a melting point between 70 °C and 80 °C) was melted in a water bath [15]. Graphite rods were then put inside the vessel, which was connected to a vacuum pump. Following, the vacuum pump was turned on until no gas bubbles evolved from the graphites surface, which happened after about 2 to 3 hours [14]. After re-establishing ambient pressure, the rods were removed from the vessel and left in filter paper until the paraffin cools and solidifies [15]. The lower end of the electrode, where the solid particles will be immobilized, was then carefully polished by gently making the movement of the infinity symbol (∞) in a smooth white paper [15].

The immobilization of the microparticles was achieved through an abrasive method, by gently rubbing the polished cross-section end of the PIGE to the surface of the sample, as described in the literature [14,15,20,71]. This procedure has the advantage of not altering the nature of the solid particles [15]. After immobilizing the microparticles, the electrode was inserted into the electrochemical cell.

After the experiments, the working electrode (PIGE) was cleaned and polished by gently rubbing its cross-section on smooth white paper, avoiding passing it at the same spot more than once (as multiple rubbing at the same place can lead to contamination of the electrode). However, when changing samples, the PIGE was rubbed on 1200 grit sandpaper and subsequently polished on white paper, as previously described.

The cleaning of the PIGE electrode was checked with voltammograms performed without samples (blank voltammograms), ensuring that the electrode was completely clean and increasing the reliability of the results.

In some cases, solid compounds may dissolve in the solution during the experiments, which will result in the contamination of the electrolyte. When this happens, the electrolyte must be replaced, however, it has been observed that this interference only occurs after a great number of experiments [15], which can be explained by the small amount of sample collected for each experiment.

4.4. Preparation of the electrochemical cell

The electrochemical cell, with approximately 200 mL, was composed by a three-electrode arrangement, as shown in Figure 10. The reference electrode (RE) was an Ag|AgCl (KCl sat.), the auxiliary electrode (CE) was a platinum plate and the working electrode (WE) was the PIGE with the immobilized particles in its extremity. A metallic pencil was used to give mechanical support for the PIGE, also providing electrical contact with the potentiostat.

Figure 10 - Electrochemical cell and its representation. The formed meniscus is indicated in the cell representation.

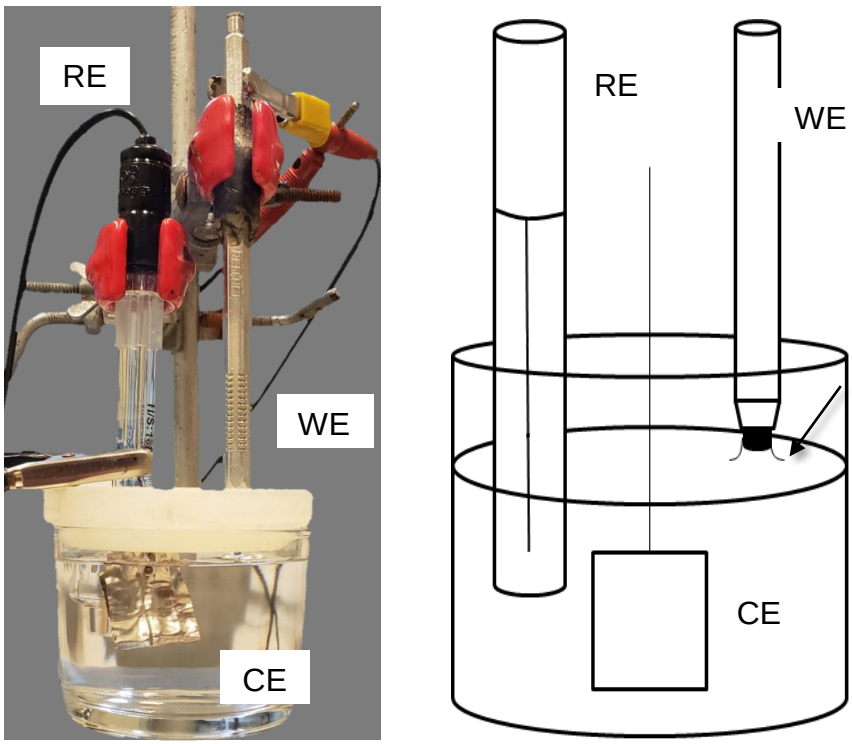

Source: The author.

For the mounting of the experiment, the electrochemical cell was placed on a Lab Jack and the PIGE dipped into the solution. Then, the cell is slightly lowered so that only the cross section of the graphite remains in contact with the solution, forming a meniscus between the tip of the PIGE and the electrolyte (indicated in the scheme of Figure 10). This procedure guarantees that the active electrode surface area is reproducible in all experiments [15]. It also reduces the capacitive background current and increases the signal to noise ratio [20].

4.5. Electrolytes

The chosen electrolytes are presented in Table 3, with the references from works that have previously used them in VMP analysis. Choosing a support electrolyte will depend on the nature of the studied compound. Mostly, for VMP measurements, aqueous solutions are used as electrolytes. However, organic solvents can also be used, as long as they have dielectric constants that allow the dissolution of salts in order to obtain the necessary conductivity [20]. The most important matter to observe when choosing an electrolyte, however, is the low solubility of the sample in the solution [20]. Usually, the same solution can be used for several measurements [15]. In order to determine the ideal potential window for each of these solutions, cyclic voltammetry was performed with the PIGE electrode without sample (blank experiment), using a scan rate of 100 mV s^{-1}.

Table 3 - Electrolytes, their concentrations and references.

Electrolyte	Concentration	Reference
Oxalic acid (OA)	0.1 mol L^{-1}	[3,22,34,38,44,49]
HCl	1%	[33,44,56]
KCl	0.1 mol L^{-1}	[44]
NaOH	0.1 mol L^{-1}	[3,34,44]
HAc/NaAc buffer	0.25 mol L^{-1}	[37,42,68,43,48,50–55]
H_2SO_4	0.5 mol L^{-1}	[36,63–67,72,73]

Source: The author.

4.6. Electrochemical experiments

The potentiostat used for the electrochemical experiments was an Autolab PGSTAT30. Initially, open circuit potential (OCP) was recorded during a stabilization period of 120 seconds, determined immediately after the cell adjustement, as previously described (4.4). In all the cases, the voltammograms started with a cathodic (negative going) scan, which was immediately followed by the anodic (positive going) scan. This procedure assures that most of the immobilized species would be reduced to their metallic state, allowing a better definition of the anodic (oxidation) peaks.

Unless otherwise stated, cyclic voltammograms were acquired with a scan rate of 100 mV s^{-1} (selected after an analysis of the effect of the scan rate on the peaks resolution, as presented in section 5.2). When necessary, square wave voltammetry (SQW) was performed with a potential increment of 4 mV, amplitude of 25 mV and frequency of 5 Hz, in agreement with parameters previously used in the literature [36,37,53,55,58,59,61,42,43,45,47,48,50–52].

All the voltammetric measurements were performed considering the potential window for each electrolyte. To determine this parameter for a particular electrolyte, a blank voltammetric experiment was performed; the electrolyte potential window corresponds to the potential range at which the current remains sufficiently low, so it does not interfere with the observation of the sample peaks. It usually corresponds to a potential range at which no faradaic reaction ascribed to the electrolyte occurs (mainly H_2 and O_2 evolution for the cathodic (negative going) and anodic (positive going) scans, respectively).

VMP experiments were performed in aerated conditions, and all voltammograms were repeated at least 3 times. Each experiment was carried out by immobilizing new particles in a PIGE cleaned tip according to the procedure described in section 4.3, and the reproducibility was confirmed through relative standard deviation (RSD), calculated using Equation 3.

$$RSD = \frac{standard\ deviation}{|arithmetic\ mean\ of\ the\ replicates|} 100\ \%$$ Equation 3[13]

Expected RSD for VMP measurements is between 3 % to 15 % [17,74], and all RSD values are presented in Appendix 1.

Considering that the amount of immobilized particles on the PIGE tip is small, and that the current response is proportional to the amount of sample, the current resultant from a VMP experiment may be only slightly higher than that registered in the blank experiment for a given electrolyte. Hence, the voltammograms were corrected with the electrolyte baseline (determined in the blank experiment), and only the peaks resulting from oxidation or reduction of the samples will be shown. Also, since it is difficult to control the amount of immobilized sample, VMP is not considered a quantitative technique; therefore, peak currents were normalized from 0 to 1 and are presented in arbitrary units (a.u.). All potentials are presented vs Ag|AgCl (KCl sat.).

5. RESULTS AND DISCUSSION

5.1. Determination of the potential window for the different electrolytes (blank voltammograms)

First, the potential window was determined for each of the chosen electrolytes using a PIGE with no immobilized particles (blank experiment). The voltammograms were acquired after 120 seconds of OCP stabilization. The chosen scan rate was 100 mV s^{-1}. The results for the different electrolytes and a table with the potential windows determined for each one of them are presented in Figure 11 and Table 4, respectively.

Figure 11 - Potential windows for the different electrolytes. Standalone PIGE (blank experiments). Cyclic voltammetry: 100 mV s^{-1}.

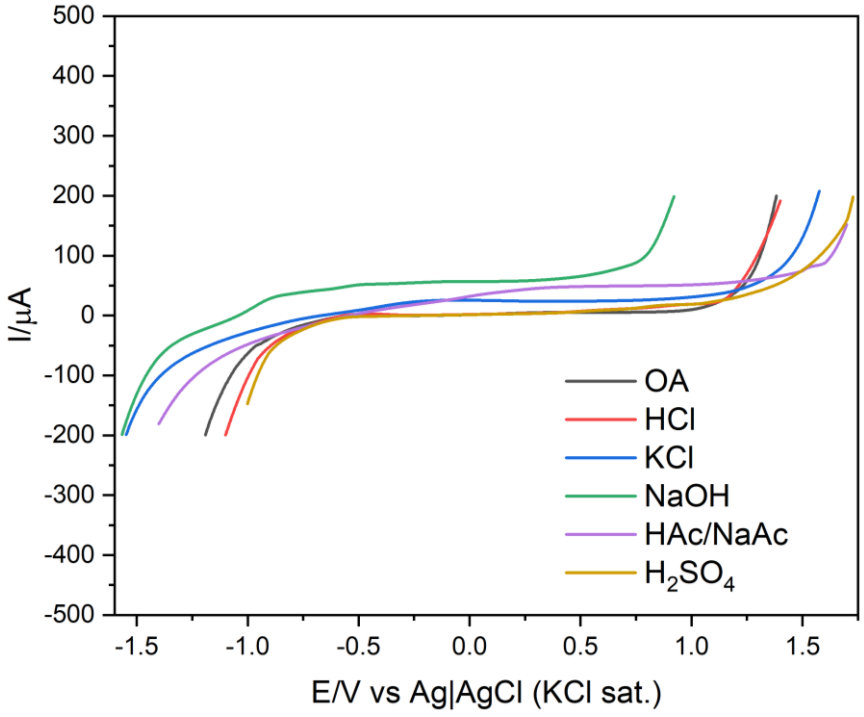

Source: The author.

Table 4 - Potential window for the different electrolytes. Standalone PIGE (blank experiments). Cyclic voltammetry: 100 mV s^{-1}.

Electrolyte	Potential window (V vs Ag|AgCl (KCl sat.)
OA (0.1 mol L^{-1})	-1.2 to +1.4
HCl (1.0 %)	-1.1 to +1.4
KCl (0.1 mol L^{-1})	-1.5 to +1.6
NaOH (0.1 mol L^{-1})	-1.6 to +0.9
HAc/NaAc (0.25 mol L^{-1})	-1.4 to +1.7
H_2SO_4 (0.5 mol L^{-1})	-1.0 to +1.7

Source: The author.

As previously described, the criterion adopted to determine the potential window was that the increase in current caused by the electrolyte reactions (oxygen and hydrogen evolution) should not be high enough to interfere with the observation of the oxidation peaks from the analyzed samples. The blank tests revealed that KCl and HAc/NaAc presented the widest potential windows: 3.1 V, with current increasing at similar potentials both in the negative (cathodic) and positive (anodic) going scan directions. HCl as well as H_2SO_4 showed reduced limits in the negative going scan, and, therefore, may not be ideal for analyzing active metals, as, for instance, zinc. NaOH, on the other hand, presented a reduced potential limit in the positive direction, which may hinder the analysis of nobler metals. Finally, the potential window determined for OA was 2.6 V, with current increasing at less negative and less positive potentials than KCl and HAc/NaAc in the negative and positive going scans, respectively.

5.2. Influence of the scan rate in the oxidation and reduction peaks

The next step for choosing the standard procedure was evaluating the effect of the scan rate on the intensity, position and shape of the current peaks. For this, a PIGE with silver sample was tested in a sodium acetate buffer solution (HAc/NaAc). This solution was selected because it is one of the most cited in VMP works found in the literature (as seen in Table 2). Figure 12(a) shows representative voltammograms for the entire potential window of this electrolyte obtained with the following scan rates: (5, 10, 25, 50, 100 and 200) mV s^{-1}; whereas Figure 12(b) presents the region of the voltammograms displaying the

relevant anodic and cathodic peaks. Figure 12(c) presents the voltammograms normalized and in arbitrary units.

Figure 12 - Cyclic voltammograms for silver in HAc/NaAc 0.25 mol L^{-1} at different scan rates: a) the entire potential window; b) region of the voltammograms with the relevant peaks; c) current intensity normalized and presented in arbitrary units.

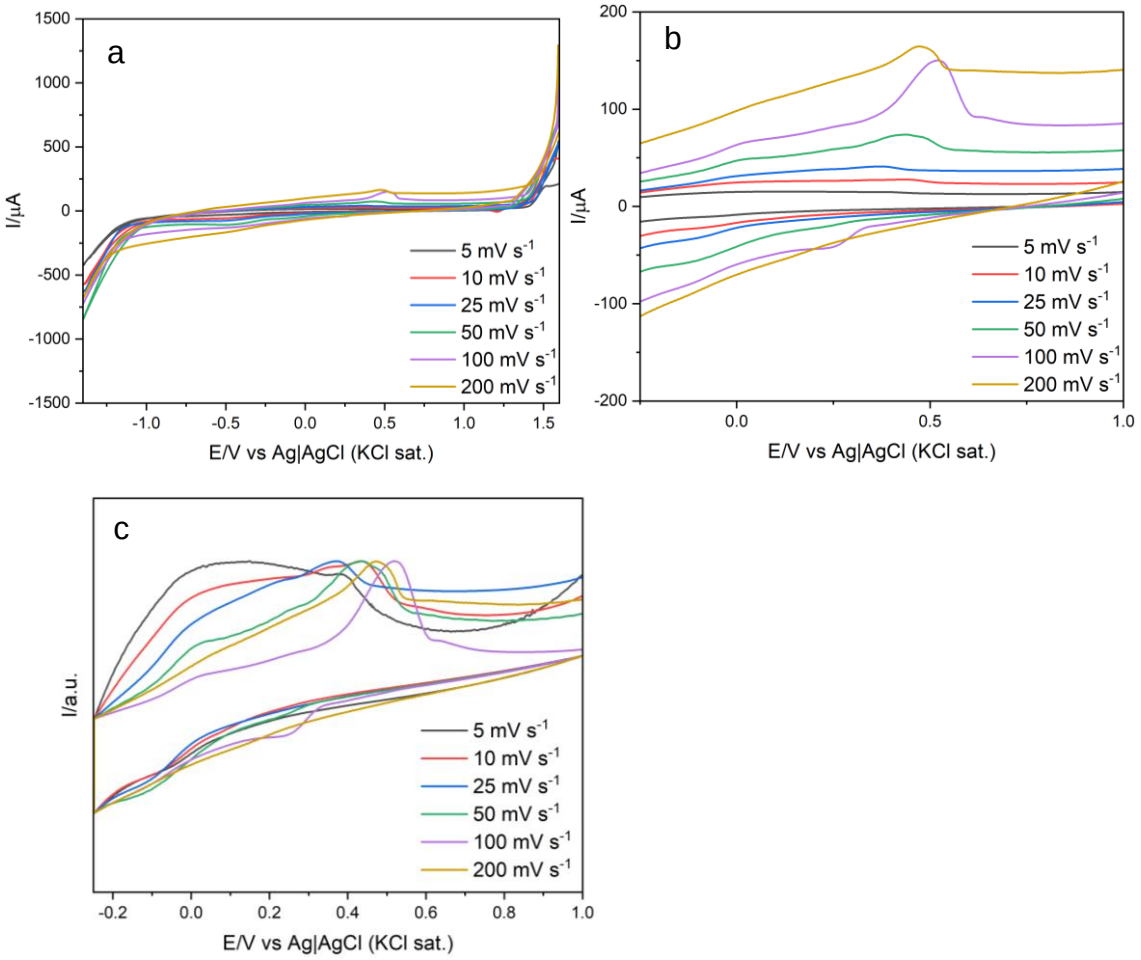

Source: The author.

The voltammograms reveal that the higher the scan rate, the higher the current response, resulting in improved peak resolution, which is an expected outcome for voltammetric analyses, as seen in the Randles-Sevcik equation (Equation 1). However, the current response is also proportional to the amount of sample, and the abrasion method for microparticle immobilization does not allow controlling the amount of sample collected at the PIGE cross-section [14,17]. Considering this latter feature, and the fact that the present work aims to use VMP as a tool for qualitative identification of samples containing metallic elements, the currents of the voltammograms were normalized and presented in

arbitrary units (a.u.), as demonstrated in Figure 12(c). Also, it is possible to observe that the peak potential shifts with different scan rates, which goes according to the literature [11,17,75].

The results in Figure 12 also show that voltammograms acquired at lower scan rates (5 mV s^{-1}, 10 mV s^{-1} and 25 mV s^{-1}) do not present good current resolution, making it difficult to identify the peak corresponding to silver oxidation. Conversely, the voltammogram at 200 mV s^{-1} presents a considerable contribution of the capacitive current, which also hinders the identification of the current peaks. Considering all these features, the best response was obtained with 100 mV s^{-1}, which presented more discernible oxidation and reduction peaks.

The same procedure was adopted for the cast iron sample, and the results are depicted in Figure 13. Just as observed for the silver sample, voltammograms obtained with lower scan rates (specially 5 mV s^{-1} and 10 mV s^{-1}) present low current response and lower peak resolution. Besides, the voltammogram obtained at 200 mV s^{-1} is also strongly influenced by the capacitive current. It is important to notice, however, that the number of peaks in the positive going scan changes with the scan rate. The peak close to -0.25 V becomes more noticeable when using a scan rate of 50 mV s^{-1} or higher, as well as the peak in +0.31 V. This shows that the scan rate can influence the analysis in many ways, like influencing the peaks shapes, influence of capacitive current and number of identifiable electrochemical processes. The reactions of the cast iron sample will be further explored in section 5.3.2.

Figure 13 - Cyclic voltammograms for cast iron in HAc/NaAc 0.25 mol L^{-1}.at different scan rates: a) the entire potential window; b) region of the voltammograms with the relevant peak; c) current intensity normalized and presented in arbitrary units.

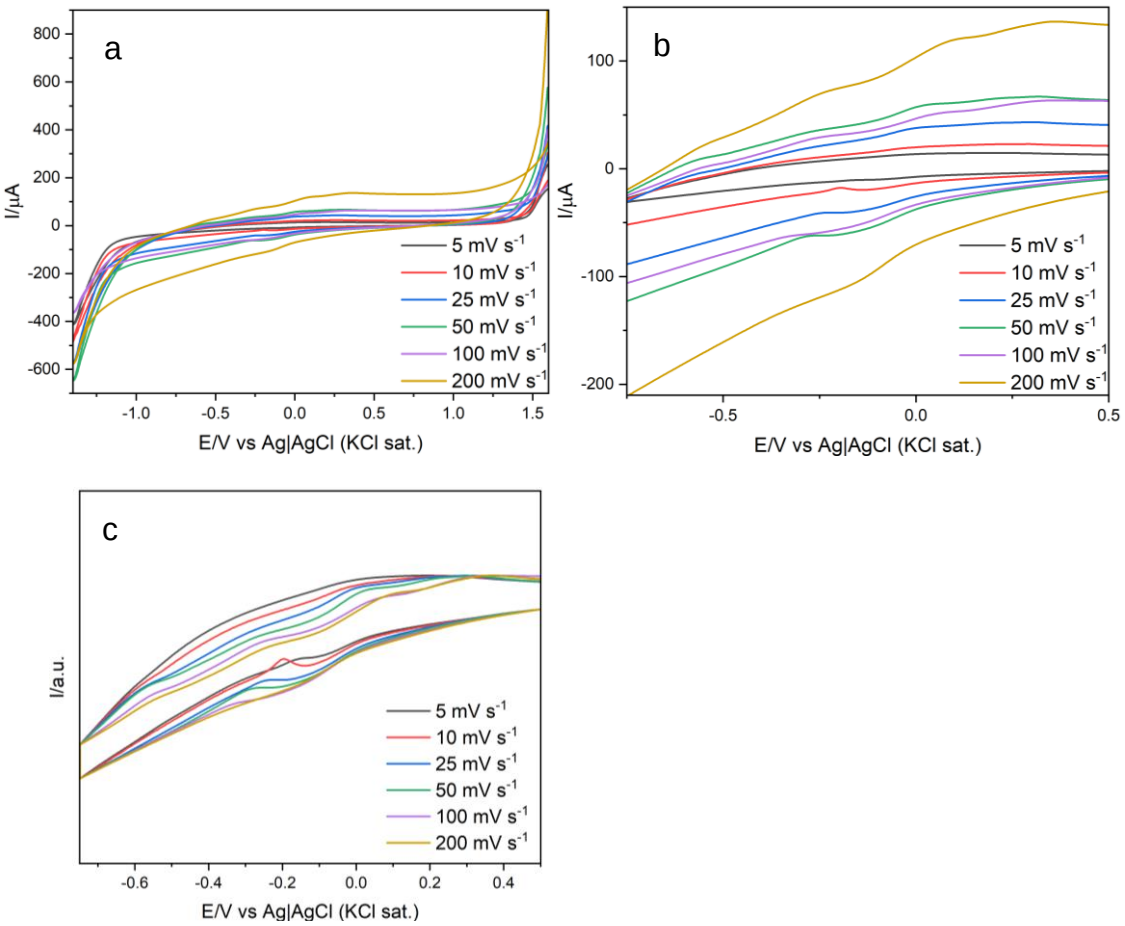

Source: The author.

The results presented in this section show that peaks resolution improves at higher scan rates; however, optimized conditions must be searched, according to the metal. In most of the experiments performed in the present investigation, the chosen scan rate was 100 mV s^{-1}, which showed, in most of the cases, to be a good compromise between good peak resolution and speed to perform the experiments; however, other value for this parameter can be adopted for better peak definition, which, when adopted, will be specified and justified.

5.3. Analysis of metals and alloys, and electrolyte selection

5.3.1. Characterization of metallic samples

The metallic samples used in this work came from different sources, and, therefore, determining their composition was the first step. With this goal, all of

them were submitted to SEM-EDS analysis. The micrographs can be seen in Figure 14 and a compilation of the EDS analyses results is presented in Table 5. Copper, zinc and tungsten consisted of pure metals. On the other hand, iron presented C and Si, and its micrograph shows that it is a cast iron sample, which, for the sake of simplicity, will be denominated as “iron” hereafter. Silver and the lead sample with aluminum contained less than 3% wt. of other species, while the lead sample with antimony is made of 94.4% wt. Pb and 5.6% wt. Sb.

Figure 14 - SEM imaging of metallic samples: a) silver, b) copper, c) cast iron, d) zinc, e) tin, f) lead with antimony, g) lead with aluminum and h) tungsten.

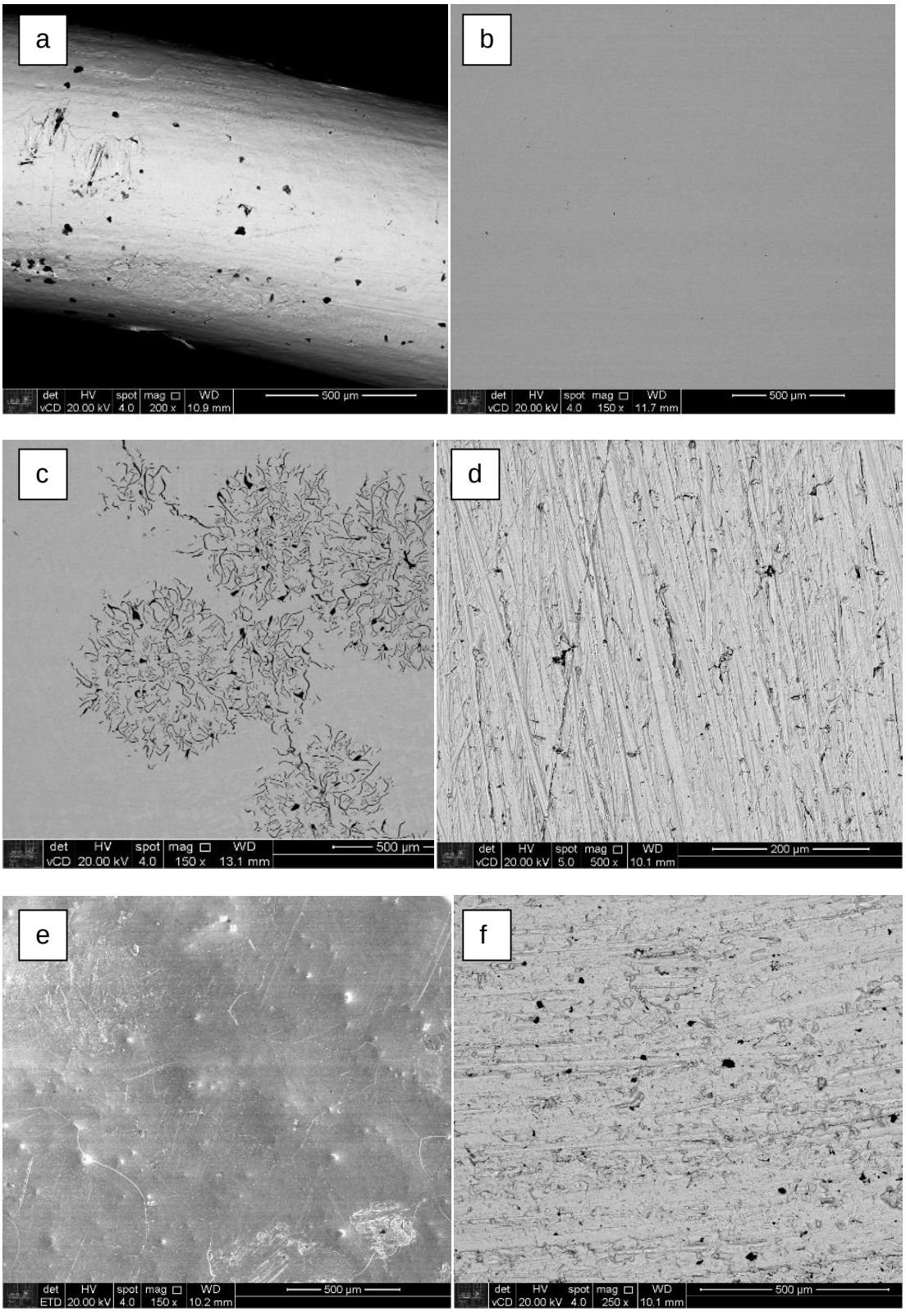

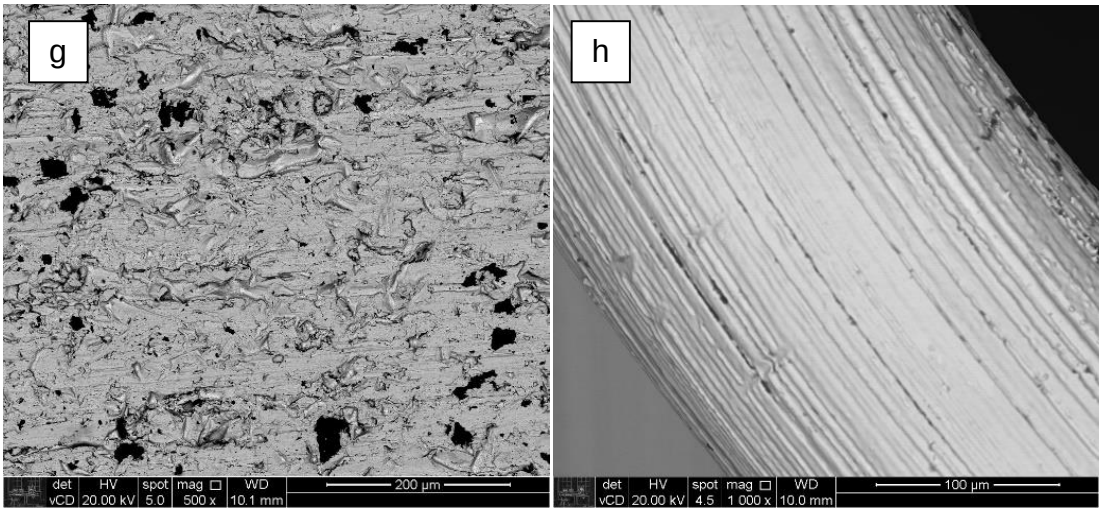

Source: The author.

Table 5 - EDS analyzes of the metallic samples.

Element	**Silver sample (% wt.)**
Ag	98.92
Al	0.70
Mg	0.38
Element	**Copper sample (% wt.)**
Cu	100.00
Element	**Cast iron sample (% wt.)**
Fe	87.80
C	11.90
Si	0.30
Element	**Zinc sample (% wt.)**
Zn	100.00
Element	**Tin sample (% wt.)**
Sn	98.71
Pb	1.29
Element	**Lead with antimony (% wt.)**
Pb	94.38
Sb	5.62
Element	**Lead with aluminium (% wt.)**
Pb	97.01
Al	2.99
Element	**Tungsten sample (% wt.)**
W	100.00

Source: The author.

5.3.2. VMP analysis of metallic samples and electrolyte selection

After SEM-EDS characterization, experiments were performed in order to choose the best electrolyte for the VMP analysis. All metals were tested in different solutions used in previous VMP studies, as shown in Table 2. The criteria for choosing the best electrolyte were peaks definition, the identification of the largest possible number of metals with the same electrolyte, as well as a better differentiation between the different analysed samples. Considering that the identification of metals is done through their oxidation peaks, in the present item, only the anodic scans will be shown. In all voltammograms current scales are presented in arbitrary units.

a) NaOH

The window displaying the relevant peaks observed during the VMP anodic scans in 0.1 mol L^{-1} NaOH for the set of metallic samples is shown in Figure 15 and the peaks potentials are displayed in Table 6. In this electrolyte, only three of the eight samples presented oxidation peaks. Although no studies have been found analyzing silver in NaOH solution, it has been observed that metallic silver will oxidize to Ag_2O in basic solutions at +0.38 V [76], via reaction exhibited in Equation 4.

$$Ag + 2OH^- \rightarrow Ag_2O + H_2O + 2e^-$$ Equation 4 [76]

Oxidation of copper is characterized by two peaks corresponding to the oxidation of metallic copper to Cu^+ and Cu^{2+} [34], which have been previously observed at -0.38 V and -0.18 V [34]. Oxidation of lead is usually characterized by two [3] or even more [34] peaks, due to the formation of Pb^{2+}, Pb^{4+} or of other intermediate oxides. However, in the experimental voltammograms, only one peak was observed, probably attributed to the oxidation of metallic lead to Pb^{2+}. This peak has been previously reported at -0.60 V [77].

Figure 15 - Anodic (positive going) scan window displaying the relevant peaks for the metallic samples in 0.1 mol L^{-1} NaOH. Cyclic voltammetry. Scan rate: 100 mV s^{-1}. A cathodic (negative going) scan was applied beforehand. Current in arbitrary units.

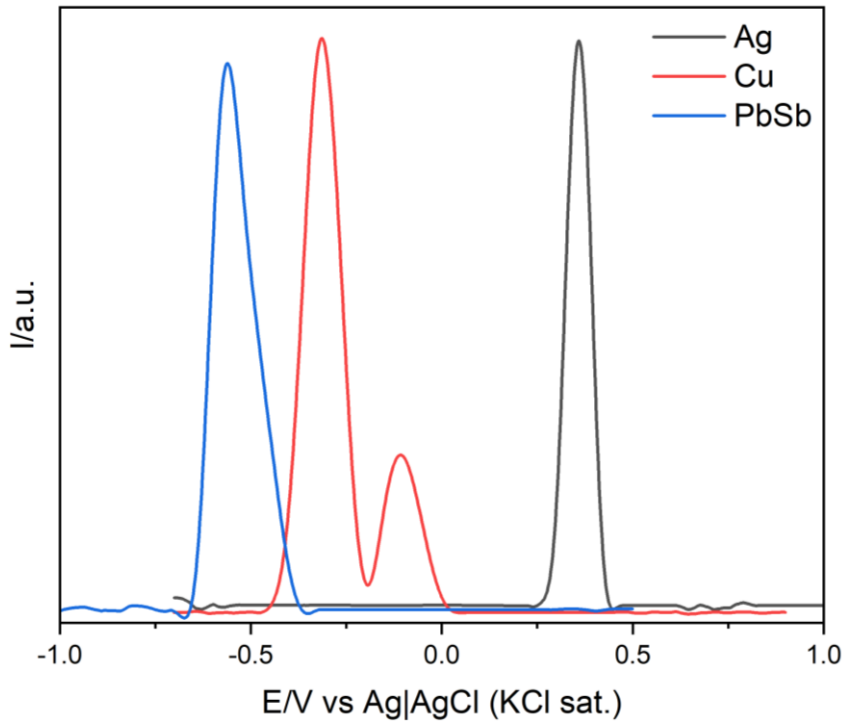

Source: The author.

Table 6 - Peaks potentials (*Ep*) for the metallic samples in 0.1 mol L^{-1} NaOH. Cyclic voltammetry. Scan rate: 100 mV s^{-1}.

Sample	E_p/V vs Ag|AgCl (KCl sat.)
Ag	+0.36
Cu	-0.32
	-0.11
PbSb	-0.56

Source: The author.

b) KCl

The samples were then studied in KCl 0.1 mol L^{-1}. The window displaying the relevant peaks observed during the VMP anodic scans is depicted in Figure 16, and the peaks potentials displayed in Table 7.

Figure 16 – Anodic (positive going) scan window displaying the relevant peaks for the metallic samples in 0.1 mol L^{-1} KCl. Cyclic voltammetry. Scan rate: 100 mV s^{-1}. A cathodic (negative going) scan was applied beforehand. Current in arbitrary units.

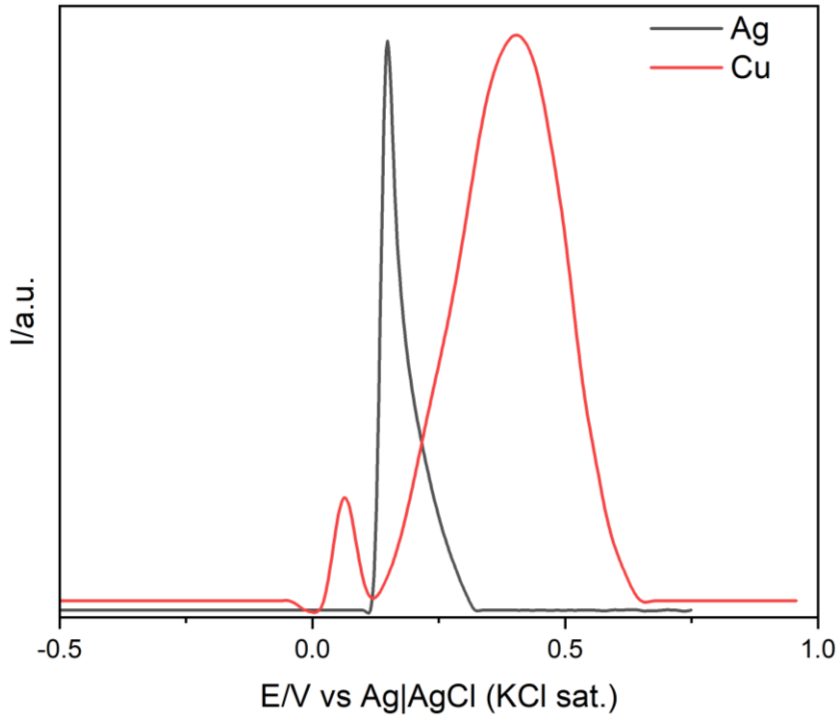

Source: The author.

Table 7 - Peaks potentials (*Ep*) for the metallic samples in 0.1 mol L^{-1} KCl. Cyclic voltammetry. Scan rate: 100 mV s^{-1}.

Sample	E_p/V vs Ag|AgCl (KCl sat.)
Ag	+0.15
Cu	+0.06
	+0.40

Source: The author.

Although it was possible to observe the electrochemical processes of the two lead samples (PbSb and PbAl) using cyclic voltammetry, the voltammograms were noisy and the peaks did not have good resolution. Using square wave voltammetry facilitated the observation of the two Pb oxidation peaks for both samples, and the anodic scan window for these samples is presented in Figure 17. The peaks potentials are shown in Table 8.

Figure 17 – Anodic (positive going) scan window displaying the relevant peaks for PbSb and PbAl samples. Square wave voltammetry in 0.1 mol L^{-1} KCl. Potential step increment 4 mV; square wave amplitude 25 mV; frequency 5 Hz. A cathodic (negative going) scan was applied beforehand. Current in arbitrary units.

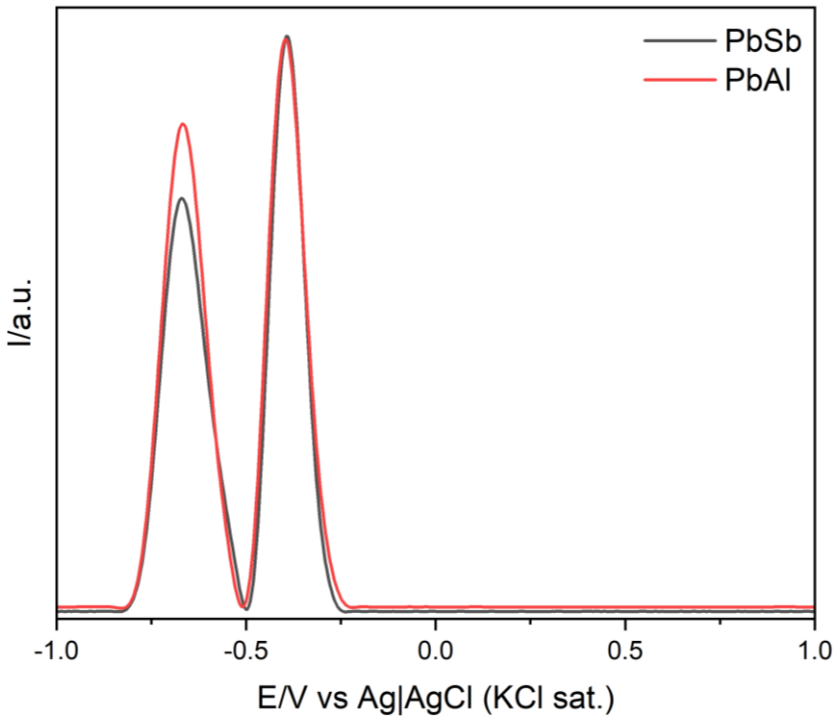

Source: The author.

Table 8 - Peaks potentials (*Ep*) for the metallic samples in 0.1 mol L^{-1} KCl using square wave voltammetry. Potential step increment 4 mV; square wave amplitude 25 mV; frequency 5 Hz.

Sample	E_p/V vs Ag|AgCl (KCl sat.)
PbSb	-0.67
	-0.39
PbAl	-0.67
	-0.39

Source: The author.

Although in our literature survey it was not possible to find works at which silver has been analyzed in KCl using VMP, it has been reported that silver will oxidize at +0.19 V and form silver chloride (Equation 5) [78].

$$Ag + Cl^- \rightarrow AgCl + e^- \qquad \text{Equation 5 [78]}$$

No works were found in the literature that analyze copper in KCl, but it has been observed that copper in neutral chlorine media presents two oxidation peaks. The first one, reported at approximately +0.14 V [79] or +0.12 V [80], can be attributed to the formation of CuCl (Equation 6); whereas, the second one,

observed at approximately +0.32 V [79] or +0.44 V [80] can either represent the formation of Cu^{2+} ions in solution (Equation 7) [79] or the oxidation of copper (I) oxide to copper (II) oxide (Equation 8) [80].

$Cu + Cl^{-} \rightarrow CuCl + e^{-}$ Equation 6 [79,80]

$CuCl_2^{-} \rightarrow Cu^{2+} + 2Cl^{-} + e^{-}$ Equation 7 [79]

$Cu_2O + H_2O \rightarrow 2CuO + 2H^{+} + 2e^{-}$ Equation 8 [80]

According to the literature, the oxidation of Pb^0 to Pb^{2+} in chlorine media occurs via two different pathways [57,75]. This has been reported as a result of different reduction processes, with the peak at more negative potentials being attributed to the oxidation of Pb^0 originated from metallic Pb, and the more positive peak attributed to the oxidation of Pb^0 originated from the reduction of PbO [57,75]. In 1 mol L^{-1} KCl, with cyclic voltammetry and with a scan rate of 50 mV s^{-1}, these peaks have been reported at -0.53 V and -0.40 V [57].

c) Oxalic acid (OA)

Next tested electrolyte was 0.1 mol L^{-1} OA. The window displaying the relevant peaks observed during the VMP anodic scans of cyclic voltammetry in this electrolyte is shown in Figure 18, and the peaks potentials are presented in Table 9. OA was a better electrolyte than NaOH and KCl, allowing the observation of the oxidation processes of five out of the eight samples. However, the electrochemical responses for lead and tin were too close to differentiate between them. Silver presented one oxidation peak, in agreement with previous studies analyzing silver in alloys. It has been observed at +0.45 V [22,25], and has been attributed to the formation of silver oxalate (Equation 9) [25]. The peak observed for copper is attributed to the oxidation of metallic copper to Cu(II) oxalate (Equation 9) [25] and has been previously reported at +0.04 V [25] or +0.11 V [34]. Tin also presented one peak ascribed to its oxidation to Sn(II) oxalate [34] (Equation 9), previously reported at -0.46 V [3,22].

$2Me + C_2O_4^{2-} \rightarrow Me_2C_2O_4 + 2\,e^{-}$ (Me = Ag, Cu or Sn) Equation 9 [25]

Lead samples also presented one oxidation peak, close and indistinguishable from tin oxidation peak. Some previous works have also reported just one peak for the oxidation of lead in oxalic acid, at -0.48 V [3] or -0.41 V [22]. Other works, however, reported two oxidation peaks, at -0.48 V and -0.40 V [34].

Figure 18 – Anodic (positive going) scan window displaying the relevant peaks for the metallic samples in 0.1 mol L^{-1} OA. Cyclic voltammetry. Scan rate: 100 mV s^{-1}. A cathodic (negative going) scan was applied beforehand. Current in arbitrary units.

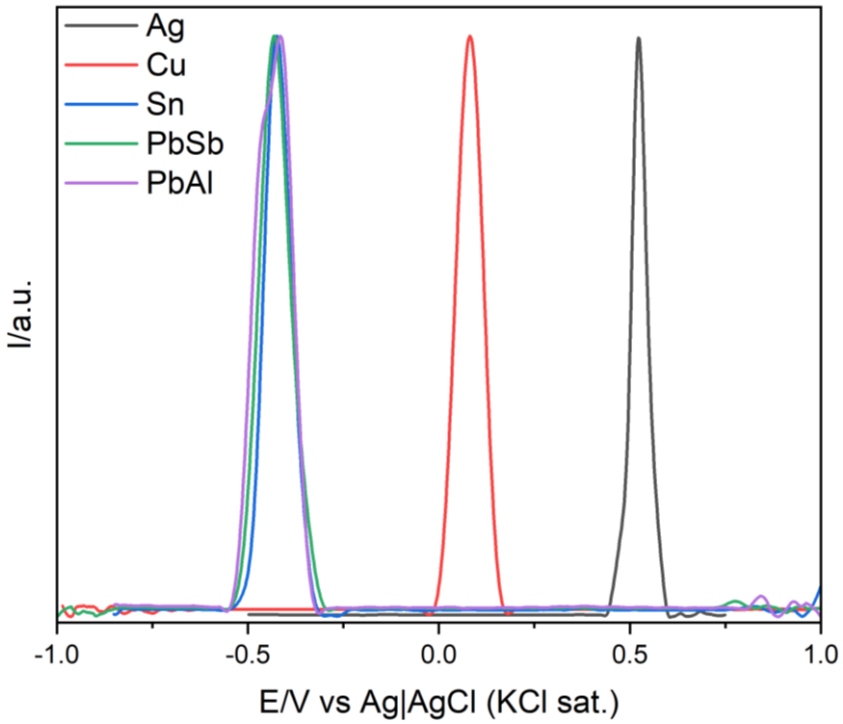

Source: The author.

Table 9 - Peaks potentials (*Ep*) for the metallic samples in 0.1 mol L^{-1} OA. Cyclic voltammetry. Scan rate: 100 mV s^{-1}.

Samples	E_p/V vs Ag|AgCl (KCl sat.)
Ag	+0.52
Cu	+0.08
Sn	-0.42
PbSb	-0.43
PbAl	-0.41

Source: The author.

d) H_2SO_4

Another tested electrolyte was 0.5 mol L^{-1} H_2SO_4. The window displaying the relevant peaks observed during the VMP anodic scans of cyclic voltammetry is presented in Figure 19, and the peaks potentials are displayed in Table 10.

Figure 19 – Anodic (positive going) scan window displaying the relevant peaks for the metallic samples in 0.5 mol L^{-1} H_2SO_4. Cyclic voltammetry. Scan rate: 100 mV s^{-1}. A cathodic (negative going) scan was applied beforehand. Current in arbitrary units.

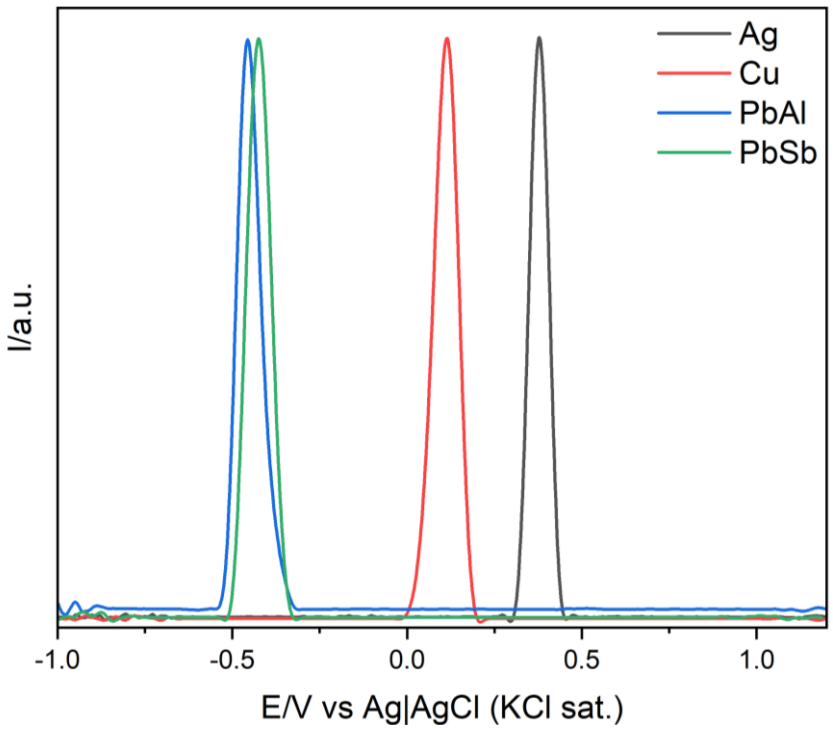

Source: The author.

Table 10 – Peaks potentials (*Ep*) for the metallic samples in 0.5 mol L^{-1} H_2SO_4. Cyclic voltammetry. Scan rate: 100 mV s^{-1}.

Samples	E_p/V vs Ag|AgCl
Ag	+0.38
Cu	+0.11
PbSb	-0.42
PbAl	-0.46

Source: The author.

When analyzing the metallic samples in this electrolyte, but using a more sensitive technique (square wave voltammetry), it became possible to observe the electrochemical response for tin as well. The anodic scan window of tin

compared to lead samples, both obtained with this technique, is depicted in Figure 20. The peaks potentials are displayed in Table 11.

Figure 20 – Anodic (positive going) scan window displaying the relevant peaks for the metallic samples. Square wave voltammetry in 0.5 mol L^{-1} H_2SO_4. Potential step increment 4 mV; square wave amplitude 25 mV; frequency 5 Hz. A cathodic (negative going) scan was applied beforehand. Current in arbitrary units.

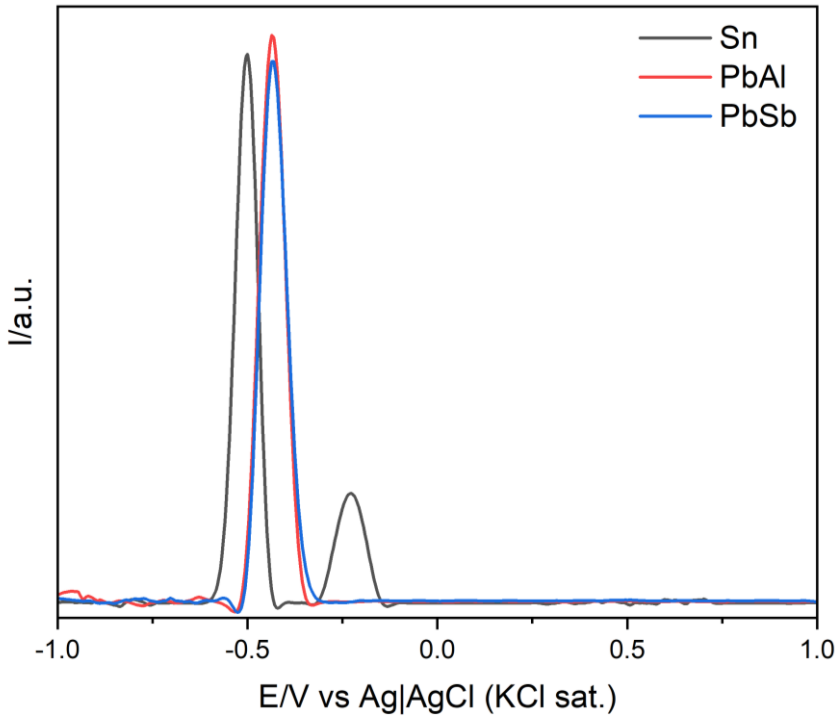

Source: The author.

Table 11 - Peaks potentials (*Ep*) for the metallic samples in 0.5 mol L^{-1} H_2SO_4 using square wave voltammetry. Potential step increment 4 mV; square wave amplitude 25 mV; frequency 5 Hz.

Samples	E_p/V vs Ag|AgCl (KCl sat.)
Sn	-0.50
	-0.23
PbSb	-0.43
PbAl	-0.43

Source: The author.

Although it was necessary to use a different technique, H_2SO_4 also allowed the identification of five out of eight metallic samples. The advantage in comparison with OA, however, was the differentiation of tin and lead. Silver presented one oxidation peak, previously reported at +0.44 V [62]. The oxidation of copper has been observed at +0.14 V [40]. When looking at previous works studying tin in H_2SO_4, it has been reported that stripping oxidation of metallic tin

to Sn^{2+} in solution occurs at -0.50 V [67], but the second peak observed at -0.23V, detected with square wave voltammetry, has not been previously reported in the literature. Our literature survey did not identify a report on the anodic behavior of lead in H_2SO_4; however, the peak potential is close to what is expected for the oxidation of Pb^0 to Pb^{2+} in acid media (-0.48 V [3] or -0.41 V [22] in oxalic acid, and -0.45 V [51], or -0.48 V [54] in sodium acetate buffer (pH 4.5)).

e) HCl

Next, the samples were analyzed in 1.0 % HCl. The window displaying the relevant peaks observed during the VMP anodic scans is presented in Figure 21. The peaks potentials are shown in Table 12. HCl presented the advantage of identifying five of the eight samples, like OA and H_2SO_4, and also differentiating tin and lead. In this case, however, only one technique was enough for differentiating them. Silver oxidation in HCl has been reported at +0.11 V [63]. The voltammogram for copper shows two oxidative processes. The first one is related to copper oxidation in HCl media (Equation 10), expected to occur at -0.02 V [81], while the second one is attributed to the oxidation of metallic copper to Cu^+, previously reported at +0.38 V [81].

$$Cu + 3\ Cl^- \rightarrow CuCl_3^- + 2\ e^-$$ Equation 10 [81]

The peak observed for tin can be attributed to the oxidation of Sn^{2+} to Sn^{4+}, previously reported at -0.34 V [82], which can indicate the formation of tin oxides which were not reduced during the cathodic scan. Lead sample presented two oxidation peaks. As it was discussed for the KCl solution, the oxidation of Pb^0 to Pb^{2+} in chlorine media occurs via two different pathways [57,75]. In 0.1 mol L^{-1} HCl, the two peaks have been reported at -0.42 V and -0.26 V [75].

Figure 21 – Anodic (positive going) scan window displaying the relevant peaks for the metallic samples in 1.0% HCl. Cyclic voltammetry. Scan rate: 100 mV s^{-1}. A cathodic (negative going) scan was applied beforehand. Current in arbitrary units.

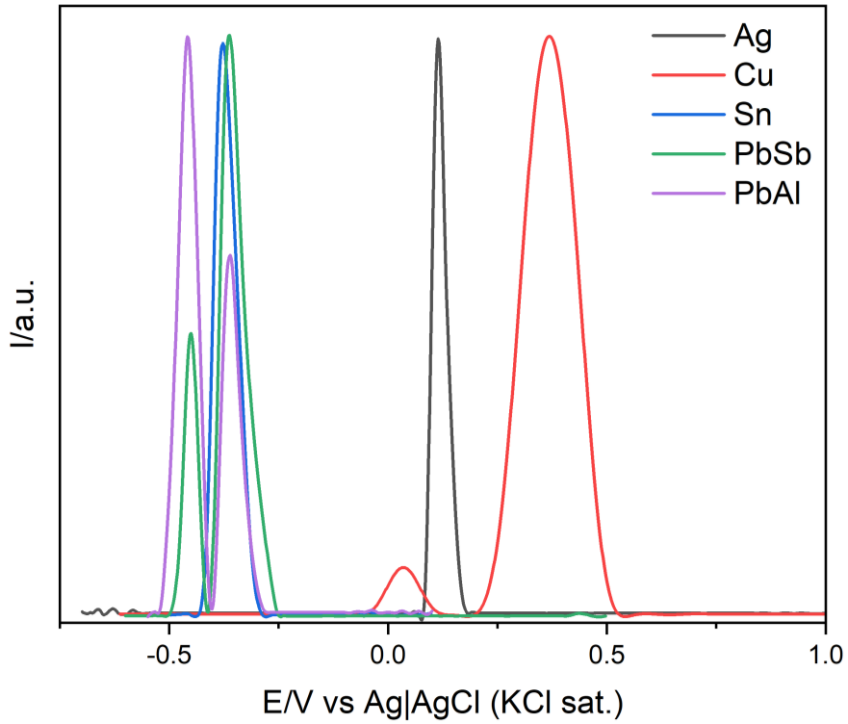

Source: The author.

Table 12 - Peaks potentials (*Ep*) for the metallic samples in 1.0% HCl. Cyclic voltammetry. Scan rate: 100 mV s^{-1}.

Sample	E_p/V vs Ag|AgCl (KCl sat.)
Ag	+0.11
Cu	+0.04
	+0.37
Sn	-0.38
PbSb	-0.45
	-0.36
PbAl	-0.46
	-0.36

Source: The author.

f) Sodium acetate buffer (HAc/NaAc)

Lastly, the samples were analyzed in 0.25 mol L^{-1} HAc/NaAc. The window displaying the relevant peaks observed during the VMP anodic scans with cyclic voltammetry is presented in Figure 22, with peaks potentials displayed in Table 13.

Figure 22 – Anodic (positive going) scan window displaying the relevant peaks for the metallic samples in 0.25 mol L^{-1} HAc/NaAc. Cyclic voltammetry. Scan rate: 100 mV s^{-1}. A cathodic (negative going) scan was applied beforehand. Current in arbitrary units.

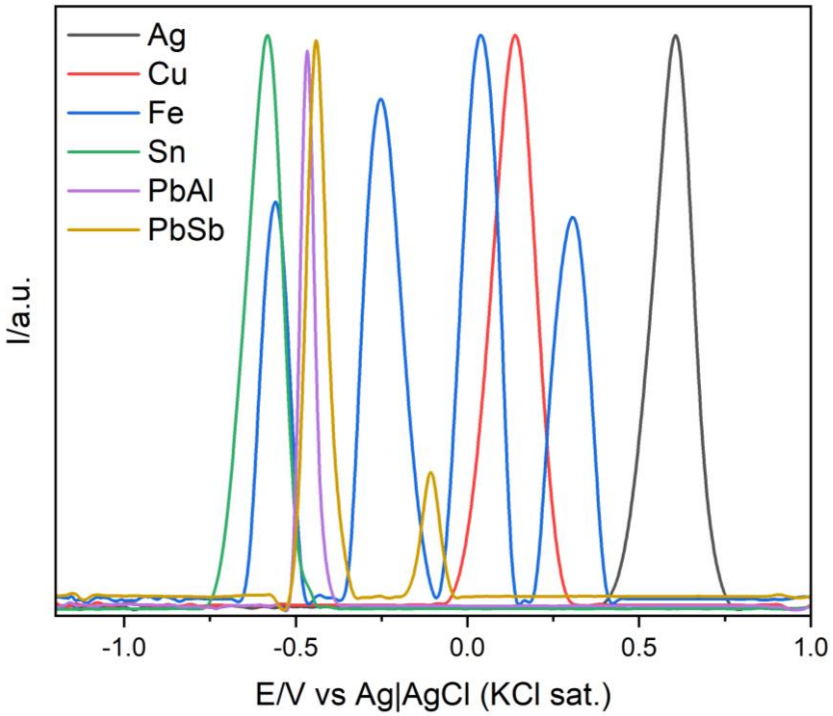

Source: The author.

Table 13 - Peaks potentials (*Ep*) for the metallic samples in 0.25 mol L^{-1} HAc/NaAc. Cyclic voltammetry. Scan rate: 100 mV s^{-1}.

Sample	E_p/V vs Ag|AgCl (KCl sat.)
Ag	+0.60
Cu	+0.14
Fe	-0.56
	-0.25
	+0.04
	+0.31
Sn	-0.58
PbSb	-0.44
	-0.12
PbAl	-0.47

Source: The author.

When using square wave voltammetry, oxidation of Zn and W were also observed. The anodic scan window of these samples is presented in Figure 23, and the peaks potentials are shown in Table 14.

Figure 23 - Anodic (positive going) scan window displaying the relevant peaks for the metallic samples. Square wave voltammetry in 0.25 mol L^{-1} HAc/NaAc. Potential step increment 4 mV; square wave amplitude 25 mV; frequency 5 Hz. A cathodic (negative going) scan was applied beforehand. Current in arbitrary units.

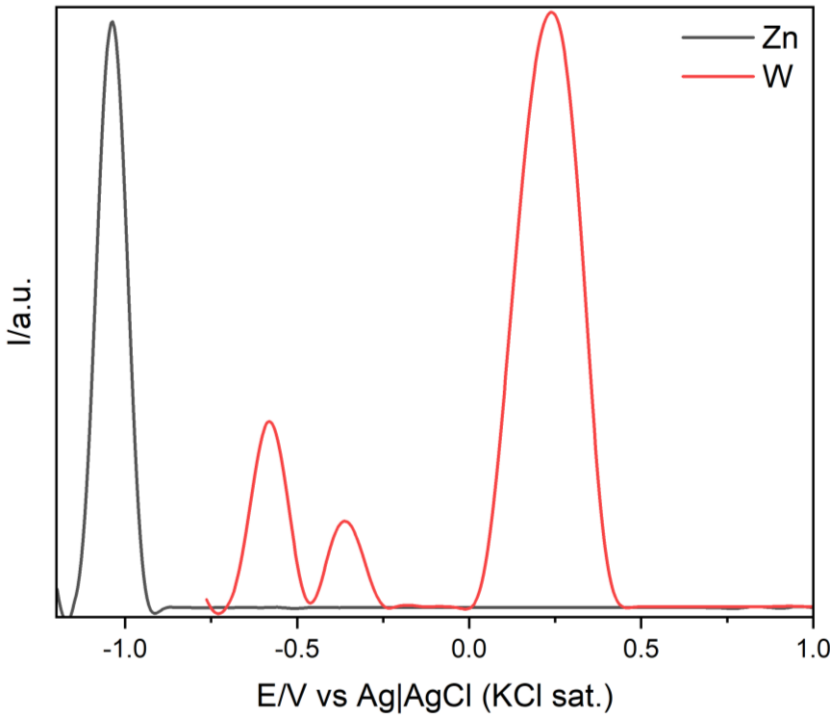

Source: The author.

Table 14 - Peaks potentials (*Ep*) for the metallic samples in 0.25 mol L^{-1} HAc/NaAc determined using square wave voltammetry. Potential step increment 4 mV; square wave amplitude 25 mV; frequency 5 Hz.

Sample	E_p/V vs Ag|AgCl (KCl sat.)
Zn	-1.04
W	-0.58
	-0.36
	+0.24

Source: The author.

HAc/NaAc allowed the identification of all metallic samples investigated in the present study as well as the differentiation between tin and lead. Hence, it was the best electrolyte and it was chosen for the next steps in this work. Silver presented one oxidation peak at +0.60 V, which is the standard potential for the oxidation of metallic silver to Ag^+ [83]. What has been reported in the literature, however, is that silver can present peak splitting at +0.20 V (attributed to the oxidation of silver to Ag(I)) [45] and +0.45 V (attributed to the oxidation of silver

to silver acetate) [45]. Other works show just one peak for the oxidation of silver, at +0.30 V [42], +0.44 V [84] or +0.50 V [85]. The oxidation of copper (+0.14 V), coincident with the standard potential for the pair Cu/Cu(II) [83], has been previously observed at +0.20 V [23,50] or 0.00 V [45,54,84]. Oxidation of iron produces four different peaks: -0.56 V, -0.25 V, +0.04 V and +0.31 V. The peak at -0.56 V can be attributed to the oxidation of metallic iron do Fe^{2+}, reported previously at -0.53 V [86], while the peak at +0.31 V can be attributed to the oxidation of Fe^{2+} to Fe^{3+}, reported in the literature at +0.32 V [86]. These two peaks can be used for the identification of the electrochemical processes of iron, but considering the complexity of iron oxidation process, with the possibility of forming different polymorphs, other anodic processes may occur. This is shown by the other two peaks observed, at -0.25 V and +0.04 V, attributed in the literature to the oxidative dissolution of iron compounds (and reported at -0.29 V and +0.09 V, respectively [86]).The oxidation of tin (-0.58 V), previously observed at -0.50 V, can be attributed to the oxidation of metallic tin to Sn^{2+} [47]. The oxidation of metallic lead to Pb^{2+} (here reported at -0.47 V and -0.44 V) has been observed at -0.35 V [36], -0.45 V [51], -0.48 V [54]. The peak at -0.12 V, observed for the PbSb sample, is tentatively attributed to the oxidation of antimony, since it has been previously reported at -0.20 V [54] in the same electrolyte . Finally, the oxidation peak for zinc (-1.04 V) was observed at a potential lower than those reported in the literature (-0.80 V [43] or -0.96 V [87]).

Even though no works were found analyzing tungsten in sodium acetate buffer, its electrochemical behavior has been widely analyzed (including in relation to solution pH). However, these analyses are often contradictory [88], and the electrochemistry of tungsten is hard to precise due to the different types of oxides formed, and the great variety of compounds given by these oxides [89]. The oxidation of metallic tungsten can either form passive oxides, which will then stop the metal from further oxidizing, or ions like WO_4^{2-}. The first peak (-0.58 V) can be attributed to the oxidation of metallic tungsten to tungsten (IV) oxide (Equation 11).

$$W + 2\ H_2O \rightarrow WO_2 + 4\ H^+ + 4\ e^-$$ Equation 11 [88]

Considering the electrolyte's pH, this reaction is expected to occur at -0.57 V [88] or -0.59 V [90]. The next peak (-0.36 V) can be ascribed to the oxidation of

WO_2 to tungsten (V) oxide (Equation 12), which should occur at -0.40 V [91]. The oxidation potentials for W (IV), W (V) and W (VI) are close [92], and the oxidation of WO_2 to ions WO_4^{2-} (Equation 13) can also occur in this potential range.

$$2\ WO_2 + H_2O \rightarrow W_2O_5 + 2\ H^+ + 2\ e^-$$ Equation 12 [88]

$$WO_2 + 2\ H_2O \rightarrow WO_4^{2-} + 4\ H^+ + 2\ e^-$$ Equation 13 [88]

The nobler peak (+0.24 V) occurs in a region where nonstoichiometric tungsten oxides will form WO_3, a stable oxide, which halts the oxidation of the sample [89,91].

g) Comparison between electrolytes

The peaks potentials of the samples in all the electrolytes, as well as the technique used to indentify them, are consolidated and presented in Table 15.

Table 15 - Peak potentials and techniques used to identify the samples in all tested electrolytes.

	Ag	Cu	Fe	Zn	Sn	PbSb	PbAl	W
NaOH (0.1 mol L^{-1})	+0.36 (CV)	-0.32, -0.11 (CV)				-0.56 (CV)		
KCl (0.1 mol L^{-1})	+0.15 (CV)	+0.06, +0.40 (CV)				-0.67, -0.39 (SWV)	-0.67, -0.39 (SWV)	
OA (0.1 mol L^{-1})	+0.52 (CV)	+0.08 (CV)			-0.42 (CV)	-0.43 (CV)	-0.41 (CV)	
H_2SO_4 (0.5 mol L^{-1})	+0.38 (CV)	+0.11 (CV)			-0.50, -0.23 (SWV)	-0.42 (CV)	-0.46 (CV)	
HCl (1%)	+0.11 (CV)	+0.04, +0.37 (CV)			-0.38 (CV)	-0.45, -0.36 (CV)	-0.46, -0.36 (CV)	
HAc/ NaAc (0.25 mol L^{-1})	+0.60 (CV)	+0.14 (CV)	-0.56, -0.25, +0.04, +0.31 (CV)	-1.04 (SWV)	-0.58 (CV)	-0.44, -0.12 (CV)	-0.47 (CV)	-0.58, -0.36, +0.24 (SWV)

Source: The author.

5.4. Analysis of metals covered with corrosion products

In order to evaluate the efficiency of VMP in the analysis of corrosion products and their respective metals, two metallic samples of unknown provenance covered with corrosion products were studied. As previously informed, they were found on a beach as detached pieces of metal, and there was no information about their previous exposure conditions. They were denominated “green sample” (Figure 8a in section 4.1.) and “brown sample” (Figure 8b in section 4.1.). With the intention of thoroughly investigating their whole surface, five points were selected for analysis in the green sample and three points in the brown sample, as indicated in Figure 8.

5.4.1. Green sample

Aiming to identify the composition of the green sample, a representative region was initially analyzed by SEM-EDS. Considering the size of the sample, a piece was cut out for the analysis, and, therefore, the micrograph cannot be associated with one of the regions shown in Figure 8a. The micrograph (Figure 24) shows that there are two characteristic regions: one covered with a thick corrosion product layer, while the other is relatively corrosion product free, which are identified, respectively, as A and B in the Figure. EDS analysis (Table 16) shows that region A contains mostly copper and oxides, with the presence of other elements such as Cl, Mg and Ca, while region B is mostly composed of metallic copper, with less than 7 % of Cl and O.

Figure 24 - SEM micrograph of the green sample, showing two different surface features: A and B.

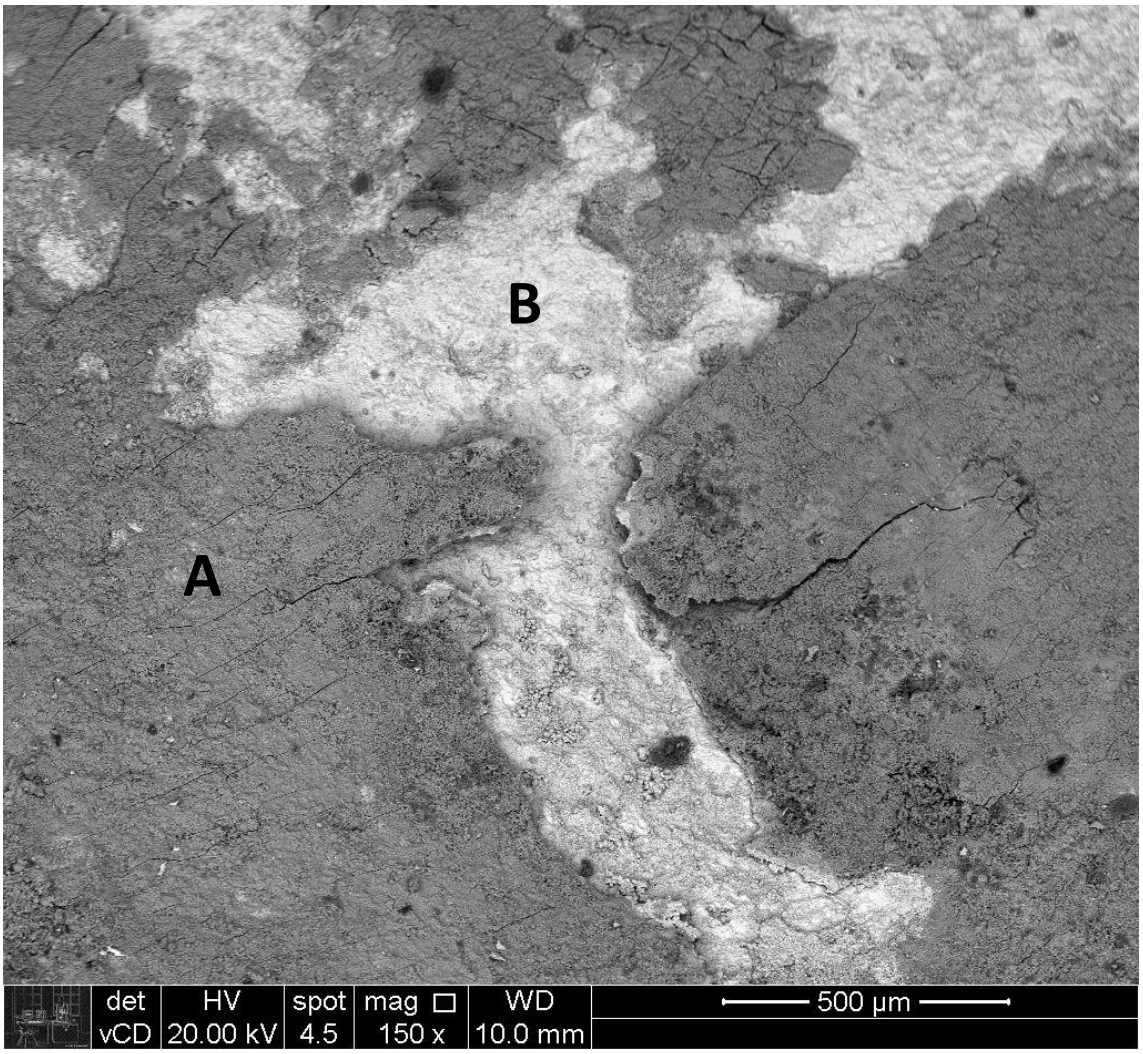

Source: The author.

Table 16 – EDS analysis of regions A and B of the green sample (wt. %).

Element	Region A (% wt.)	Region B (% wt.)
C	7.11	-
O	31.76	4.80
Si	0.72	-
Mg	1.56	-
Al	0.91	-
S	0.96	-
Cl	4.49	1.83
K	0.21	-
Fe	0.46	-
Cu	50.50	93.37

Source: The author.

Next, Raman spectroscopy was used to investigate the compounds present in the corrosion product layer. Spectra were collected at points 1 to 4 (presented in Figure 8a), and the results are presented in Figure 25. Point 5 represents an area where metallic copper is exposed, so the spectrum only showed fluorescence and, therefore, will not be presented. The exact composition of the corrosion product layer could not be determined, but some characteristic bands associated with Cu corrosion products were observed, which are indicated by the arrows. The spectrum of region 1 shows a band at 173 cm^{-1}, and the spectrum for region 4 presents a band at 133 cm^{-1}, both of them being attributed to OCuO bending and indicating the presence of copper oxides [93,94]. Spectrum of region 4 also shows a band at 533 cm^{-1} attributed to CuO stretching vibration [94], and at 614 cm^{-1} attributed to aqueous sulfate tetrahedral oxyanion vibration [95]. The band at 390 cm^{-1}, seen in the spectrum number 2, arises from CuCl stretching [95], and it could be related to the presence of atacamite. The band observed at 1069 cm^{-1}, in the spectrum number 3, represents sulfate symmetric stretching [95], which can be related to the presence of brochantite.

Figure 25 - Raman spectra of the green sample, with samples collected at a) region 1, b) region 2, c) region 3 and d) region 4 of Figure 8. Relevant peaks are indicated by arrows.

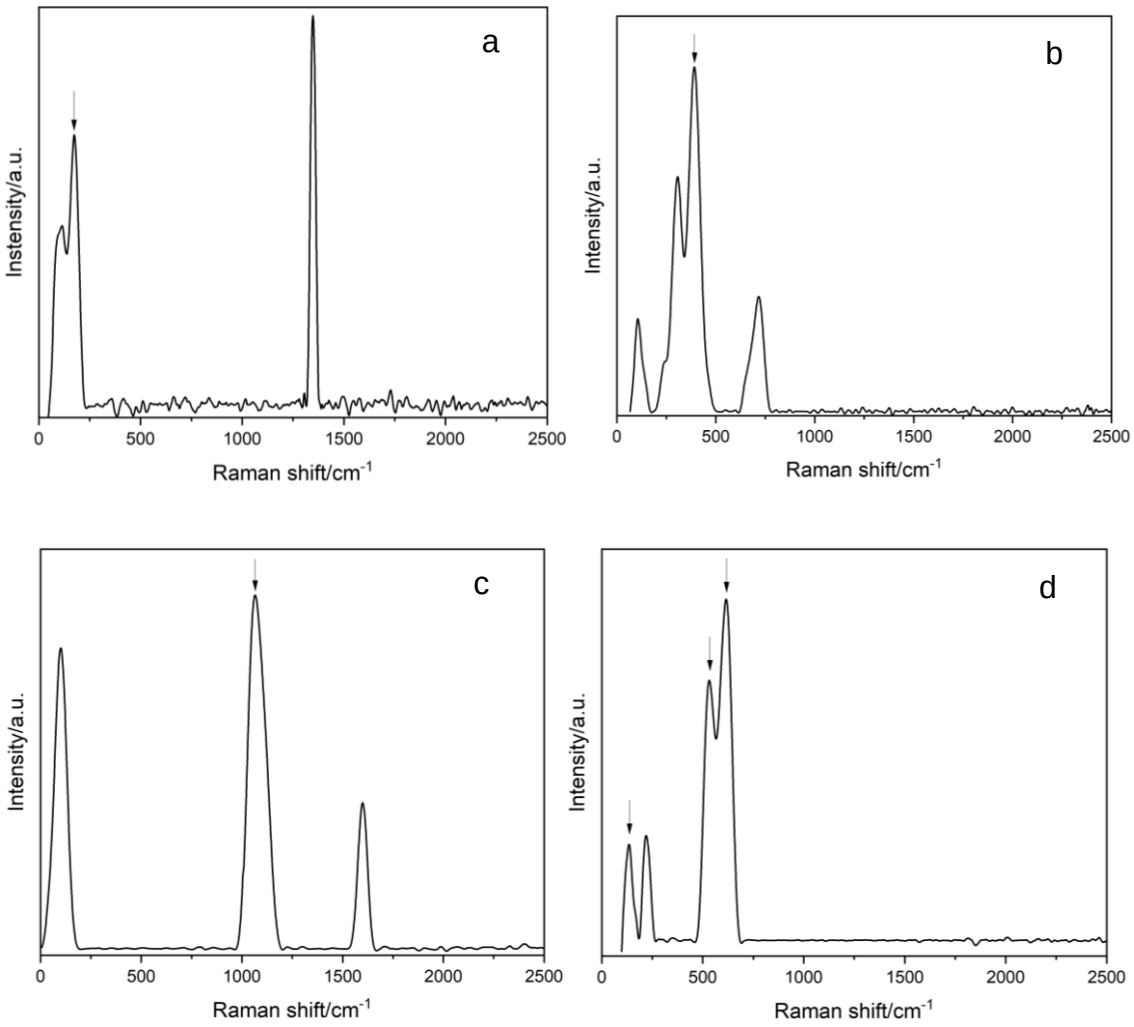

Source: The author.

For the electrochemical analysis, cyclic voltammetry was used. The scan started at +1.7 V, going in the negative direction until -1.4 V, and then returning to the starting potential. The window displaying the relevant peaks observed during the VMP cathodic (negative going) scans for the samples collected at the five points indicated in the green sample is shown in Figure 26, with the peaks potentials displayed in Table 17. Peak I, observed close to -0.15 V, can be attributed to the reduction of copper compounds like cuprite (Cu_2O) [23,45,53,96,97]. Peak II, close to -0.70 V, can be assigned to the reduction of compounds like tenorite (CuO). The reduction of cuprite and tenorite, respectively, are represented in Equations 14 and 15 [97].

$Cu_2O + 2H^+ + 2e^- \rightarrow 2\ Cu + H_2O$ Equation 14

$CuO + 2H^+ + 2e^- \rightarrow Cu + H_2O$ Equation 15

The presence of Cu_2O, indicated by the reduction process in peak I, suggests a layer of primary copper patina. This is the first layer of corrosion product formed when copper is exposed to ordinary atmospheric conditions [23,45,53,96–98]. If the metal is exposed to more corrosive environments, a secondary patina layer may be formed [23,97]. This layer is composed of minerals such as tenorite (CuO), malachite ($Cu_2CO_3(OH)_2$), brochantite ($Cu_4SO_4(OH)_6$) or atacamite ($Cu_2Cl(OH)_3$). The reduction of these minerals is indistinguishable from that of tenorite, taking place at similar potentials (represented by peak II) [23,97,98]. Tenorite is formed at the expense of cuprite in the primary layer, and competes with the formation of the other minerals [98], which result from the processes of hydrolysis and ion exchange [23].

Figure 26 - Cathodic (negative going) scan window displaying the relevant peaks for the samples collected at the five areas of the green sample indicated in Figure 8. Cyclic voltammetry in 0.25 mol L^{-1} HAc/NaAc buffer. Scan rate: 100 mV s^{-1}.

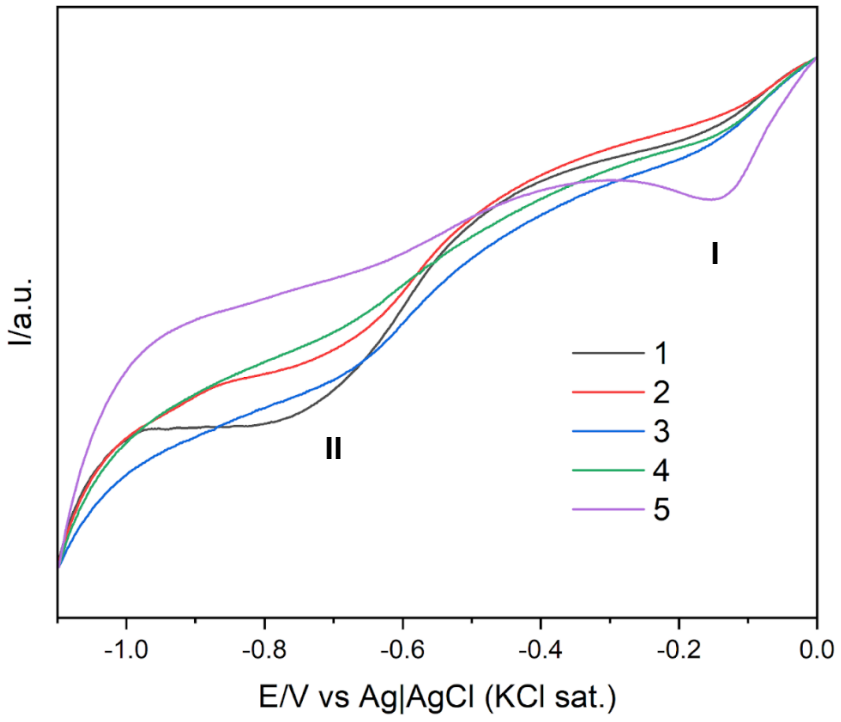

Source: The author.

Table 17 - Peaks potentials (*Ep*) identified in the cathodic (negative going) scans for the samples collected at the five areas of the green sample indicated in Figure 8. Cyclic voltammetry in 0.25 mol L^{-1} HAc/NaAc buffer. Scan rate: 100 mV s^{-1}.

Area	E_p/V vs Ag|AgCl (KCl sat.)
1	-0,19
	-0,75
2	-0,14
	-0,70
3	-0,17
	-0,68
4	-0,16
	-0,69
5	-0,14

Source: The author.

The window of the anodic (positive going) scans showing the single peak of the samples collected at the different regions of the green sample, compared to the scan of a pure copper sample, is shown in Figure 27, and peaks potentials assignments are shown in Table 18. The single peak observed around +0.10 V corresponds to the oxidative dissolution of metallic copper, which was formed in the previous reduction of the corrosion products [23,50,53].

Figure 27 – Anodic (positive going) scans window displaying the relevant peak for the samples collected at the five areas of the green sample indicated in Figure 8. Cyclic voltammetry in 0.25 mol L^{-1} HAc/NaAc buffer. Scan rate: 100 mV s^{-1}. After cathodic reduction of the corrosion products. As a reference the result obtained with a pure copper sample was also added.

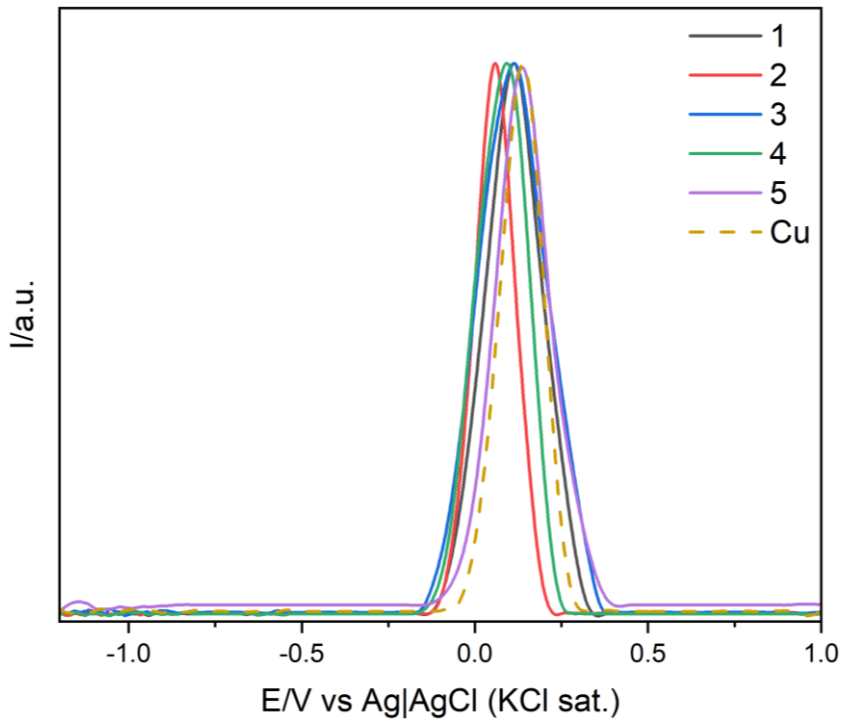

Source: The author.

Table 18 - Peaks potentials (*Ep*) identified in the anodic (positive going) scan for the samples collected at the five areas of the green sample indicated in Figure 8. Cyclic voltammetry in 0.25 mol L^{-1} HAc/NaAc buffer. Scan rate: 100 mV s^{-1}. As a reference the peak observed for a pure copper sample is also given.

Area	E_p/V vs Ag|AgCl (KCl sat.)
1	+0.11
2	+0.06
3	+0.11
4	+0.09
5	+0.14
Cu	+0.14

Source: The author.

5.4.2. Brown sample

The same characterization protocol applied to the green sample was adopted for the brown sample. A representative SEM micrograph is presented in Figure 28, showing corrosion products exhibiting two distinct morphologies, which were labeled as A and B. The results of the EDS analyses of these two regions are displayed in Table 19. They indicate that the corrosion products are

mostly composed of iron oxides with other minor elements such as C, Na and Cl. A is a chloride-richer zone, while B is primarily iron oxides.

Figure 28 - SEM micrograph of the brown sample, showing corrosion products with different morphologies. EDS analyses of A and B are displayed in Table 19.

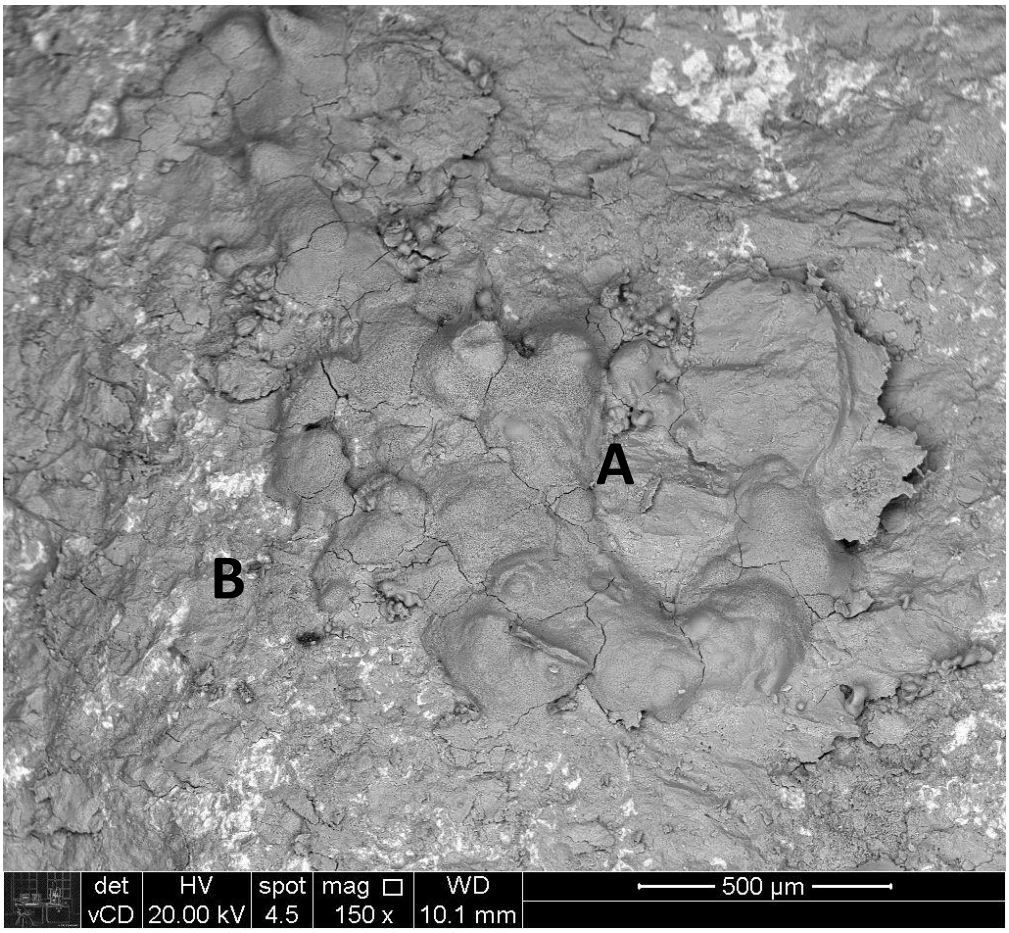

Source: The author.

Table 19 - EDS analysis of regions A and B of the brown sample (wt. %).

Element	Region A (% wt.)	Region B (% wt.)
C	3.56	4.79
O	39.58	22.53
Na	-	2.57
Mg	-	1.00
S	0.27	0.25
Cl	3.02	0.25
Fe	54.57	68.61

Source: The author.

Then, Raman spectroscopy was used to investigate the chemical composition of the corrosion product layer on the three regions of the brown sample identified in Figure 8(b). The spectra are presented in Figure 29. As for the green sample, it was not possible to determine the exact composition of the corrosion products; however, some peaks associated with iron compounds could be determined and are identified by arrows in each diagram. The peaks at 275 cm^{-1} and 380 cm^{-1} in the spectrum of region 1 (Figure 29(a)), can be associated with the presence of lepidocrocite (γ-FeOOH) [8]. The spectrum obtained for region 2 (Figure 29(b)) shows that the main corrosion product in this region is akaganeite (β-FeOOH), associated with the peaks at (308, 397 and 719) cm^{-1} [8]. In region 3 (Figure 29(c)), the main corrosion product is probably hematite (α-Fe_2O_3), identified by the peaks at (222, 282, 391 and 1290) cm^{-1} [8].

Figure 29 – Raman spectra of the brown sample obtained at: a) region 1, b) region 2 and c) region 3 indicated in Figure 8(b). Relevant peaks are indicated by arrows.

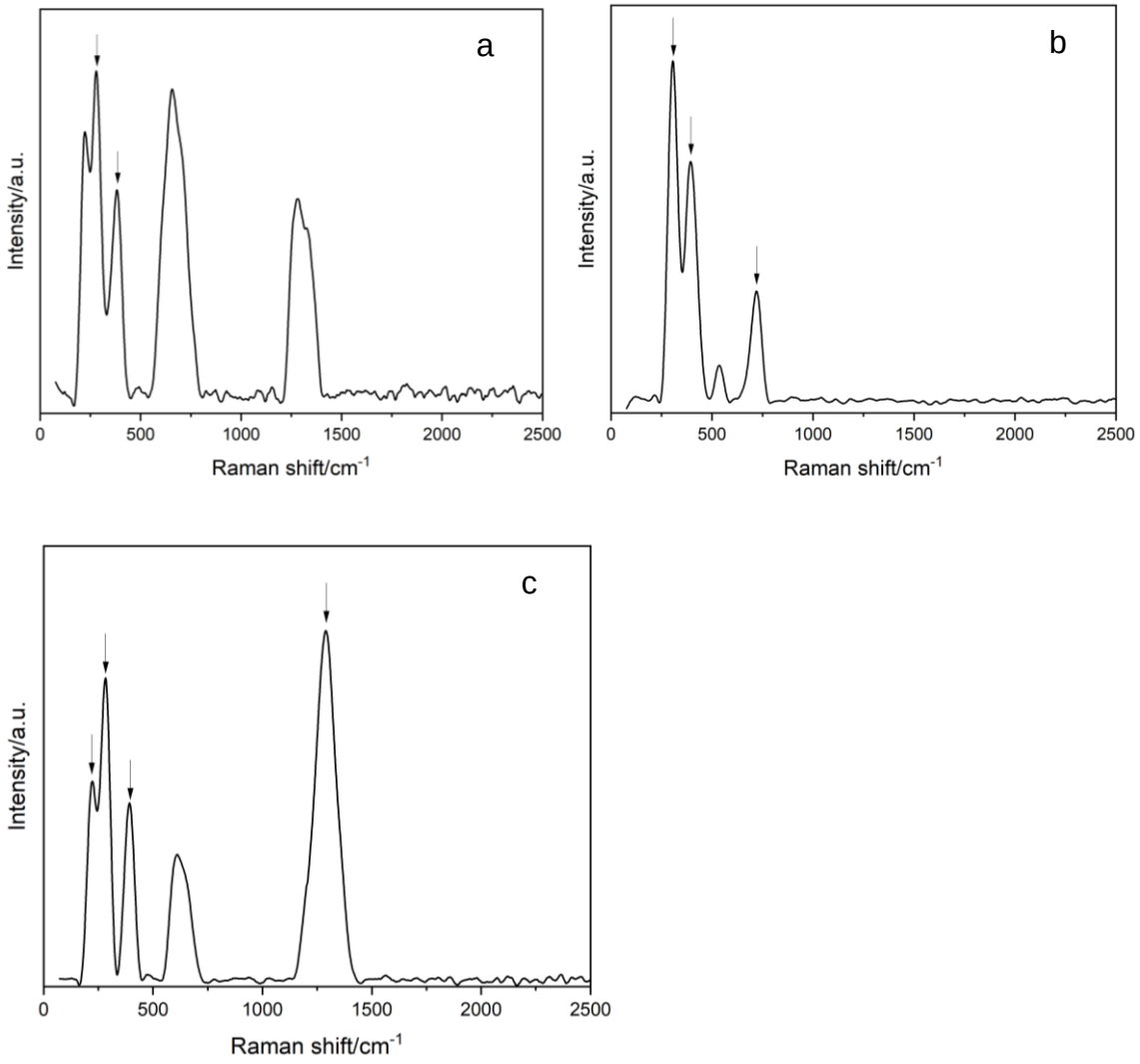

Source: The author.

The electrochemical window of the VMP cathodic (negative going) scans displaying the relevant peaks for the powder collected at the three different regions of the brown sample identified in Figure 8(b) is presented in Figure 30. The peaks potentials are presented in Table 20. The cathodic peaks for the three samples are broad, which can be a consequence of the heterogeneous composition of the corrosion products in each region [58]; moreover, their potential are similar, despite the fact that Raman spectra have indicated that a different iron compound is predominant in each analyzed region. Even though studies analyzing iron synthetic pigments in different laboratories have shown that VMP can be used to distinguish between poorly crystalline and well-

crystalline iron oxides [70], it has been previously reported that the identification of iron corrosion products is not straightforward due to the presence of complex mixtures of compounds, and the fact that peaks are observed at similar potentials, slightly changing with crystallinity and hydration [58]. According to the literature, reduction of solid species in solution, like hematite or goethite, to metallic iron can be observed through a cathodic peak close to -0.81 V [99], which is not far from the broad peak observed for the samples collected in the three different regions of the brown sample.

Figure 30 – Cathodic (negative going) scan window displaying the relevant peaks for the samples collected at the three areas of the brown sample indicated in Figure 8(b). Cyclic voltammetry in 0.25 mol L^{-1} HAc/NaAc buffer. Scan rate: 100 mV s^{-1}.

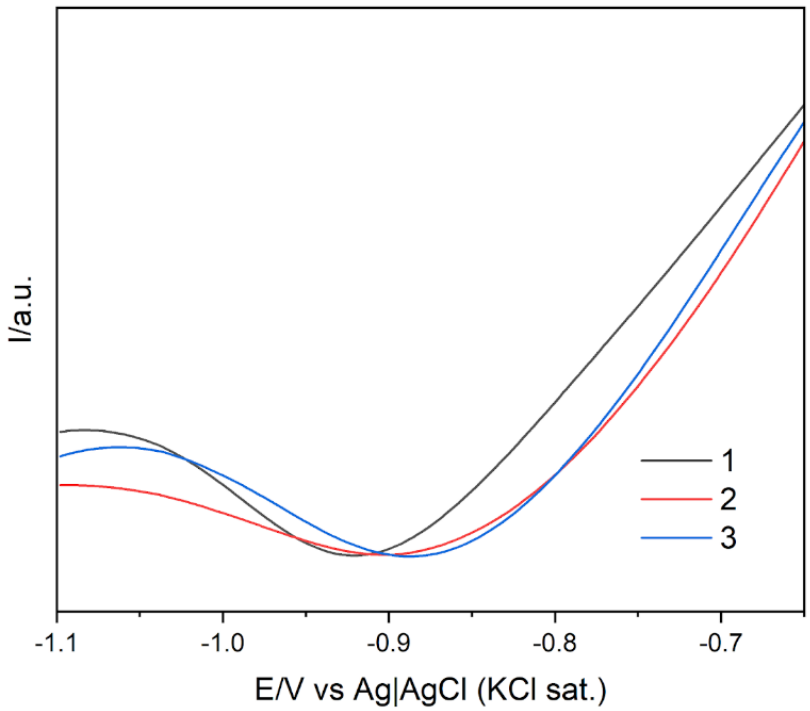

Source: The author.

Table 20 - Peaks potentials (*Ep*) identified in the cathodic (negative going) scans for the samples collected at the three areas of the brown sample indicated in Figure 8(b). Cyclic voltammetry in 0.25 mol L^{-1} HAc/NaAc buffer. Scan rate: 100 mV s^{-1}.

Area	E_p/V vs Ag|AgCl (KCl sat.)
1	-0.92
2	-0.89
3	-0.89

Source: The author.

Figure 31 depicts the window of the anodic scans displaying the relevant peaks obtained in the VMP analysis of the samples collected in the three regions

of the brown sample indicated in Figure 8(b), which are compared with the voltammetric profile of a sample collected from metallic iron. Table 21 summarizes the peaks potentials. Peaks I and IV, characteristic of iron oxidation and attributed to the oxidation of metallic iron to iron (II) and of iron (II) to iron (III), respectively (as discussed in section 5.3.2.), are observed for all samples in potentials close to those reported in the literature (-0.53 V and +0.32 V, respectively [86]). Peak III, attributed to the oxidation of iron compounds, is also observed in a potential close to what has been previously reported (+0.09 V [86]). Peak II, also associated with the oxidation of iron compounds (see previous discussion in section 5.3.2.), was not verified for the corrosion products samples.

Figure 31 – Anodic (positive going) scan window displaying the relevant peaks for the samples collected at the three areas of the brown sample indicated in Figure 8(b). Cyclic voltammetry in 0.25 mol L^{-1} HAc/NaAc buffer. Scan rate: 100 mV s^{-1}. The scan was carried out from -1.4 V to +1.7 V. After cathodic reduction of the corrosion products. As a reference the result obtained for a sample collected from metallic iron is also given.

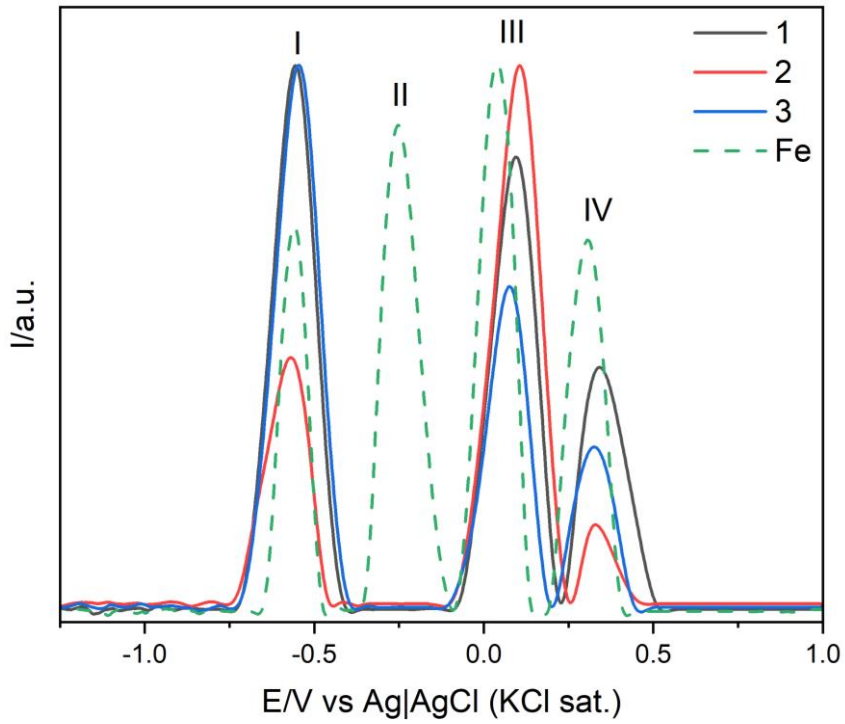

Source: The author.

Table 21 - Peaks potentials (*Ep*) identified in the anodic (positive going) scans for the samples collected at the three areas of the brown sample indicated in Figure 8(b). Cyclic voltammetry in 0.25 mol L^{-1} HAc/NaAc buffer. Scan rate: 100 mV s^{-1}. As a reference the peaks for a sample collected in metallic iron is also given.

Area	E_p/V vs Ag|AgCl (KCl sat.)
1	-0.55 (I)
	+0.09 (III)
	+0.34 (IV)
2	-0.57 (I)
	+0.11 (III)
	+0.33 (IV)
3	-0.54 (I)
	+0.08 (III)
	+0.33 (IV)
Fe	-0.56 (I)
	-0.25 (II)
	+0.04 (III)
	+0.31 (IV)

Source: The author.

5.5. Analysis of pigments

The pigments analyzed in this work were divided in two categories: commercially available pigments sold by Sennelier, namely: Green Earth, Burnt Umber and Mars Yellow, and pigments belonging to the collection of German artist Eleonore Koch, which is currently under the care of the "*Pinacoteca de São Paulo*". They were all donated from *Laboratório de Arqueometria e Ciências Aplicadas ao Patrimônio Cultural* (LAPAC), from the Physics Institute of *Universidade de São Paulo*. Independently of their origins, pigments were grouped according to the main metallic ion present in their composition.

5.5.1. Copper-based pigments

Three pigments from the *Pinacoteca* collection (Pr09Pig03, Pr11Pig07 and Pr11Pig11) were made of copper compounds. Initially, they were analyzed by SEM-EDS. SEM micrograph of Pr09Pig03 (Figure 32a) shows faceted geometric particles bigger than the other pigments, with a mean size of about 200 µm. EDS analysis (Table 22) shows that the pigment is composed of copper, oxygen and carbon. SEM imaging of Pr11Pig07 (Figure 32b) shows particles with irregular shapes, most of them smaller than 20 µm. According to the EDS analysis, they

are composed of copper, carbon and nitrogen. The particles of pigment Pr11Pig11 (Figure 32c) are similar to those observed for Pr11Pig07, and contain copper, carbon, nitrogen and oxygen (Table 22). The high amounts of C detected in the EDS analyzes can be attributed either to the presence of carbon-based compounds in the pigments composition or the carbon tape used for the immobilization of the samples.

Figure 32 - SEM micrograph of pigments: a) Pr09Pig03, b) Pr11Pig07 and c) Pr11Pig11.

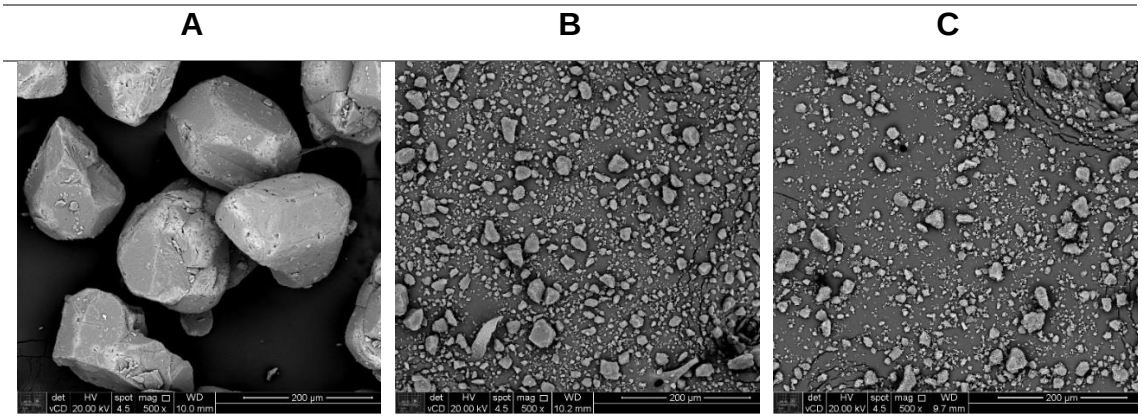

Source: The author.

Table 22 - EDS analyzes of pigments: Pr09Pig03, Pr11Pig07, Pr11Pig11 (wt. %).

Element	Pr09Pig03 (% wt.)	Pr11Pig07 (% wt.)	Pr11Pig11 (% wt.)
C	28.89	69.91	65.21
O	29.29	-	3.52
N	-	14.09	17.24
Cu	41.83	16.00	13.93

Source: The author.

Raman spectroscopy was performed for identifying the compounds present in each pigment. The spectrum for Pr09Pig03 (Figure 33a) shows typical acetate bands at (703, 943, 1418, 1440, 2941, 2981 and 3029) cm^{-1} and Cu-O stretches at (229 and 321) cm^{-1}, which can be attributed to copper acetate [9,100]. Pr11Pig07 and Pr11Pig11 spectrum (Figure 33b) show the same bands, indicating that they are made of the same compound. Bands at (680 and 746) cm^{-1} represent deformation vibrations of the phthalocyanine macrocycle, and the band at 232 cm^{-1} represents the bond between the metal ion and nitrogen [10]. These bands can be attributed to copper phthalocyanine [10,101].

Figure 33 - Raman spectra for a) Pr09Pig03, b) Pr11Pig07 and Pr11Pig11. Relevant peaks are indicated by the arrows.

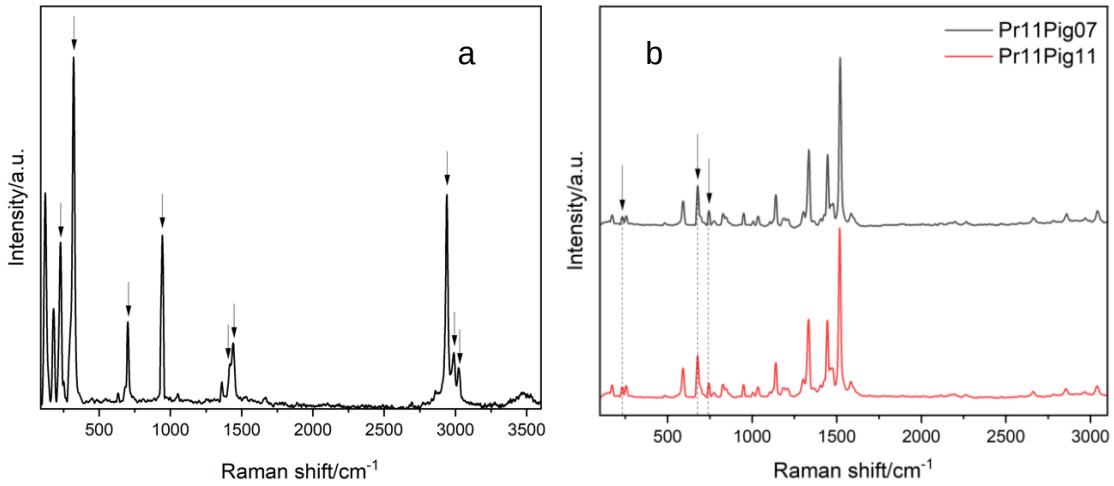

Source: The author.

For the voltammetric analysis the pigments were first reduced through a cathodic (negative going) scan from +1.7 V to -1.4 V. The scan window with the relevant peaks for the three samples is shown in Figure 34, and the peaks potentials are presented in Table 23. Pr09Pig03 shows two cathodic peaks: at -0.14 V (peak I) and at -0.32 V (peak II). Peak I represents the process of two-electron reduction of verdigris [50], shown in Equation 16.

$$\{Cu(Ac)_2\} + 2H^+ + 2e^- \rightarrow Cu + 2HAc \qquad \text{Equation 16}$$

Considering that the literature about the voltammetric behavior of verdigris did not show a second reduction peak (-0.32 V), it is suggested that peaks' separation could be related to the kinetics of the reduction reaction, *i.e.*, the chosen scan rate (100 mV s^{-1}) could be too fast to reduce all the Cu^{2+}. Therefore, the same experiment was repeated with lower scan rates ((50, 25 and 10) mV s^{-1}), and the potentials windows with the relevant peaks are shown in Figure 35. It was observed that, lowering the scan rate, the two peaks progressively merge into one, until, at 10 mV s^{-1}, only one peak was observed at -0.16 V. Pr11Pig07

and Pr11Pig11 present only one cathodic peak, attributed to the reduction of the phthalocyanine ring [102,103], which, nevertheless, were displaced from each other, appearing at -0.47 and -0.38, respectively.

Figure 34 - Potential window displaying the relevant peaks for pigments Pr09Pig03, Pr11Pig07 and Pr11Pig11 revealed in the cathodic (negative going) scans. Cyclic voltammetry in 0.25 mol L^{-1} HAc/NaAc buffer. Scan rate: 100 mV s^{-1}.

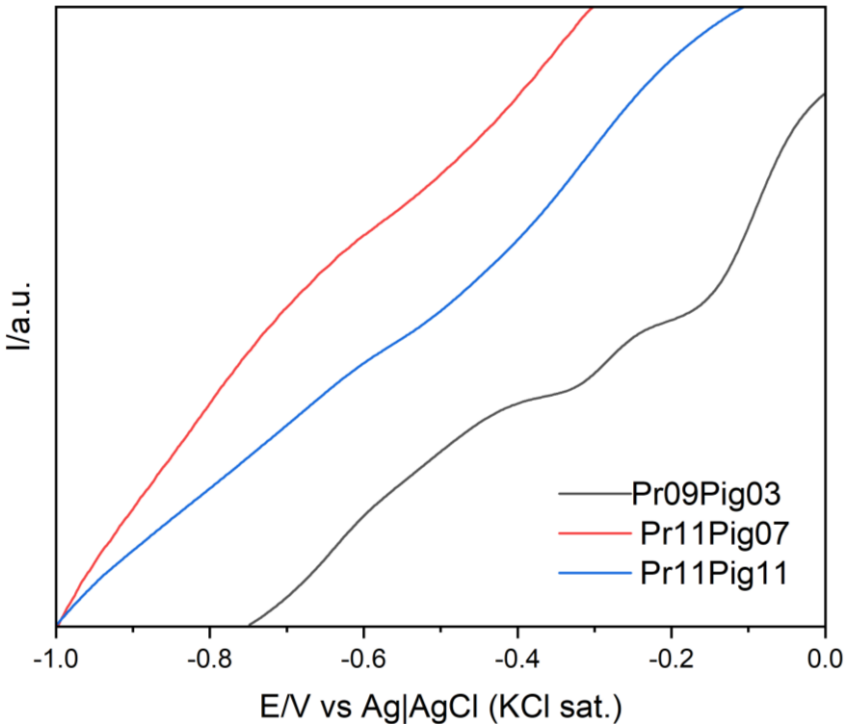

Source: The author.

Table 23 – Peaks potentials (*Ep*) identified in the cathodic (negative going) scans for pigments Pr09Pig03, Pr11Pig07 and Pr11Pig11. Cyclic voltammetry in 0.25 mol L^{-1} HAc/NaAc buffer. Scan rate: 100 mV s^{-1}.

Sample	E_p/V vs Ag|AgCl (KCl sat.)
Pr09Pig03	-0.14
	-0.32
Pr11Pig07	-0.47
Pr11Pig11	-0.38

Source: The author.

Figure 35 – Potential window displaying the relevant peaks for the cathodic (negative going) scans for pigment Pr09Pig03 at different rates. Cyclic voltammetry in 0.25 mol L^{-1} HAc/NaAc buffer.

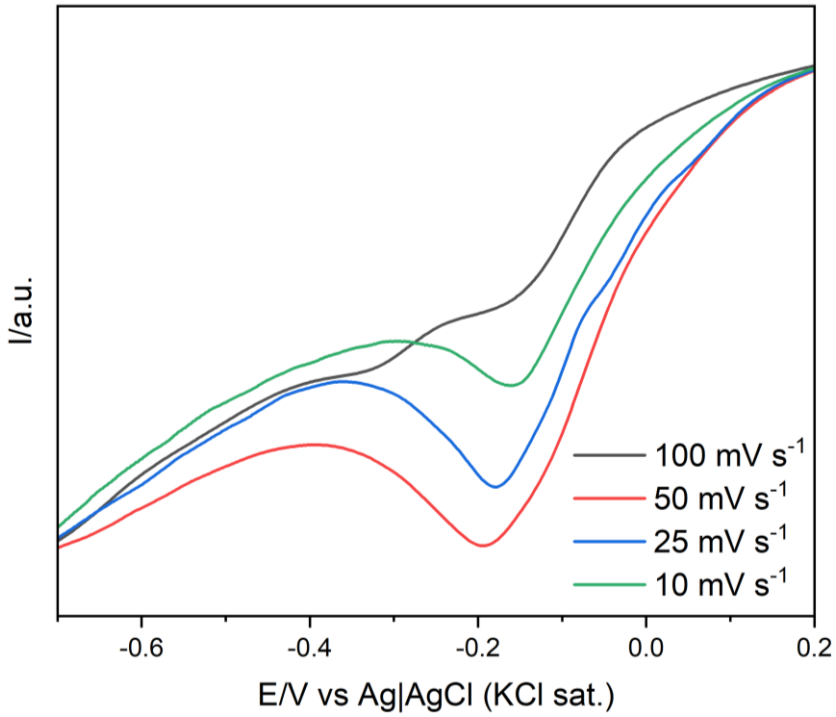

Source: The author.

After the cathodic scan, the scan direction was immediately reversed until reaching the starting potential (+1.7 V). The potential window displaying the relevant peaks for Pr09Pig03, Pr11Pig07 and Pr11Pig11 compared to a sample collected from metallic copper is depicted in Figure 36, and the peaks potentials are shown in Table 24. The anodic peak is attributed to the oxidative dissolution of metallic copper, formed in the previous reduction process [23,50,53].

Figure 36 - Potential window displaying the relevant peaks for pigments Pr09Pig03, Pr11Pig07 and Pr11Pig11 revealed in the anodic (positive going) scans. Cyclic voltammetry in 0.25 mol L^{-1} HAc/NaAc buffer. Scan rate: 100 mV s^{-1}. For comparison, the result of a scan for a sample collected from metallic copper is also presented.

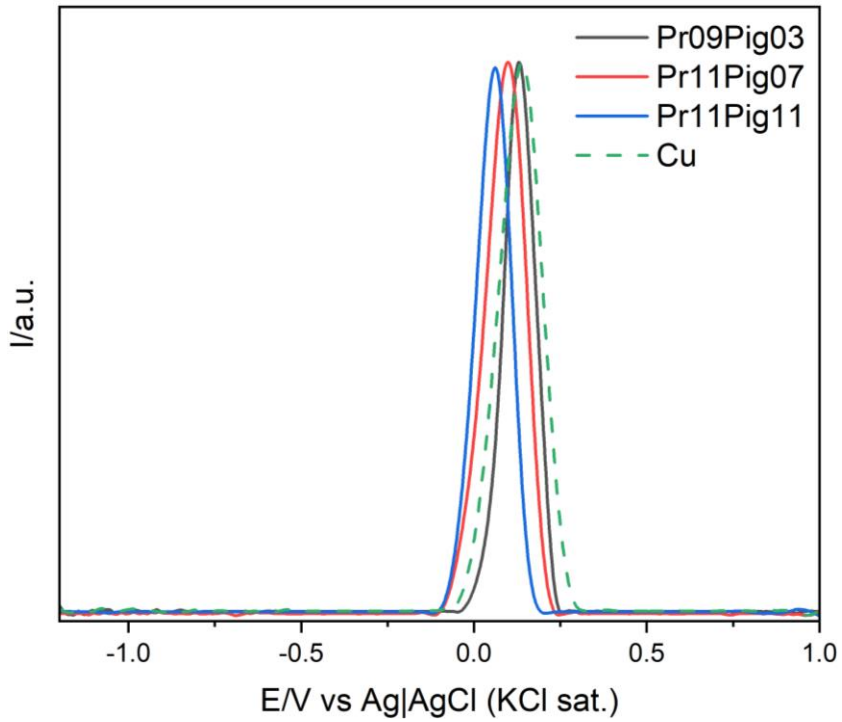

Source: The author.

Table 24 - Peaks potentials (*Ep*) identified in the anodic (positive going) scans for pigments Pr09Pig03, Pr11Pig07 and Pr11Pig11. The peak obtained from a sample collected from metallic copper is also presented. Cyclic voltammetry in 0.25 mol L^{-1} HAc/NaAc buffer. Scan rate: 100 mV s^{-1}.

Sample	E_p/V vs Ag|AgCl (KCl sat.)
Pr09Pig03	+0.13
Pr11Pig07	+0.10
Pr11Pig11	+0.06
Cu	+0.14

Source: The author.

5.5.2. Iron-based pigments

As for the copper-based pigments, the three pigments by Sennelier were initially characterized by SEM-EDS. SEM imaging of Green Earth (Figure 37a) shows small irregular particles with varying sizes, with all of them lower than 20 µm. According to EDS analysis, presented in Table 25, this pigment presents a

heterogeneous composition; besides Fe, C and O, it also presents Si, Al, Ca and S. This goes according to what is expected for Green Earth pigments, mostly represented by glauconites ($K(Fe,Al)_2(Si,Al)_4O_{10}(OH)_2$) and celadonites ($K(Mg,Fe,Al)_2(Si,Al)_4O_{10}(OH)_2$) [104–107]. The SEM micrograph of Burnt Umber (Figure 37b) shows small irregular particles with varying sizes, which, as for the Green Earth sample, do not surpass 20 µm. However, a greater quantity of powdery material was also identified. EDS analysis shows that it has a heterogeneous composition, similar to Green Earth in its main constituents, but with lower amounts of other elements. Notably, it presents higher amounts of Ca and S, and lower amount of Si. Finally, SEM imaging of Mars Yellow (Figure 37c) shows even smaller particles mixed with the powdery material; EDS results show a similar composition to Green Earth and Burnt Umber with the presence of elements like Ba, Ti or Cu. It is noteworthy that, even though those are iron-based pigments, the amount of this element detected in the samples was relatively low. Part of this can be attributed to the complex nature of some minerals containing iron, like glauconite and celadonite, but it is also due to the fact that commercial pigments can be made of a blend of several compounds [108]. It has been noted that the pigments' names provided by the suppliers are more related to the hue or colour, and not the mineral composition of the material [106]. Compounds like calcium sulphate, for instance, are added to pigments in order to give paintings a smoother, brighter finish [109], and other compounds can be added to create deeper hues [108].

Figure 37 - SEM micrographs of pigments: a) Green Earth, b) Burnt Umber and c) Mars Yellow.

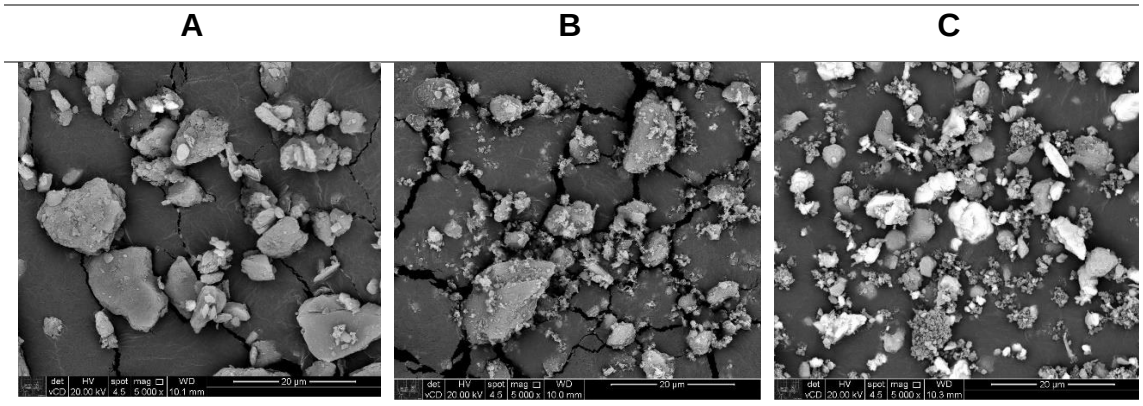

Source: The author.

Table 25 - EDS analyzes of pigments: Green Earth, Burnt Umber and Mars Yellow (wt. %).

Element	Green Earth (% wt.)	Burnt Umber (% wt.)	Mars Yellow (% wt.)
C	7.10	7.44	33.02
N	-	-	4.81
O	45.74	44.51	37.18
F	-	-	4.75
Na	1.76	-	-
Mg	2.21	1.11	1.47
Si	13.92	1.63	1.66
Al	6.20	1.39	0.96
S	5.54	19.27	-
K	0.34	-	-
Ca	13.73	22.33	8.08
Ba	-	-	3.12
Cu	-	-	0.83
Fe	3.48	2.33	4.11

Source: The author.

Raman analysis was performed to identify the composition of the Fe-based pigments, and the spectra can be seen in Figure 38. When analysing the Green Earth sample in the optical microscope, it is possible to observe particles mostly with two different colors: green and white. Raman spectra acquired for particles with each of these colors can be observed in Figure 38a. The spectrum obtained for the white particles shows a strong band at 1008 cm^{-1}, which together with bands at (414, 491, 668 and 1133) cm^{-1} suggests the presence of gypsum ($CaSO_4 \cdot 2H_2O$) [108,109], which is coherent with the Ca and S detected in the EDS analysis. The spectrum obtained for the green particles shows bands at (280, 710 and 1087) cm^{-1}, suggesting the presence of calcite ($CaCO_3$) [108], which could be associated with the compounds with C and Ca detected in the EDS analysis. The regions between 1200 and 1600 cm^{-1} for both green and white particles show similar profiles, which are close to what is reported for green earths in the literature [106,108,110], and they are basically the same as those present sometimes in the ferroceladonite spectra [104]. The peaks do not coincide with those reported in the literature for lower Raman shifts, which can be ascribed to an interference of the gypsum and calcite peaks.

Raman spectrum for Burnt Umber (Figure 38b) shows bands at (406 and 481) cm^{-1}, which can be attributed to iron oxides pigments such as burnt Sienna

[111]. The bands observed at (271, 708 and 1081) cm^{-1}, however, suggest the presence of ankerite [112], a mineral containing Fe, Ca and Mg.

The Raman spectrum obtained for Mars Yellow (Figure 38c) shows several peaks, which can be attributed to a mixture of different compounds (identified by letters a-f in the spectrum). Iron compounds like goethite (a) [8,113] and lepidocrocite (b) [8,113] can be found in the sample, as well as copper compounds like malachite (c) [114,115], dioptase (d) [115] and brochantite (e) [115]. Barium sulfate (f) was also identified [116].

Figure 38 - Raman spectra for pigments: a) Green Earth white and green particles, b) Burnt Umber and c) Mars Yellow. Peaks identified in c) are: goethite (a), lepidocrocite (b), malachite (c), dioptase (d), brochantite (e) and barium sulfate (f). Relevant peaks are indicated by the arrows in (a) and (b) and by letters in (c).

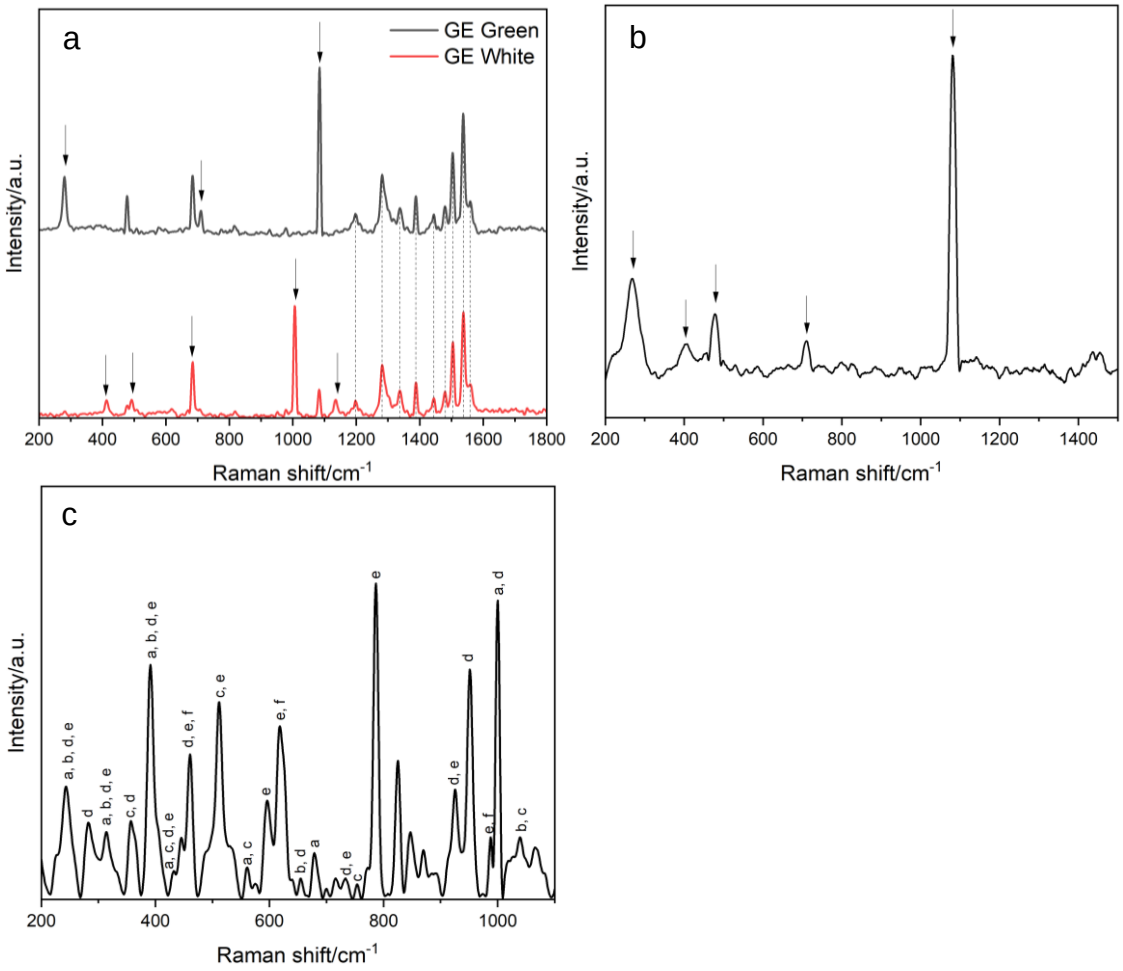

Source: The author.

For the voltammetric analysis the pigments were first reduced through a cathodic (negative going) scan from +1.7 V to -1.4 V. No cathodic peaks were

observed, which can be explained by the relatively low amount of Fe detected in the EDS analyzes. Also, considering the complexity of the samples, it is possible that more than one species is reduced at close potentials, which makes it difficult to observe specific cathodic processes. After the cathodic scan, the scan direction was immediately reversed until reaching the starting potential. The potential window displaying the relevant peaks of the anodic (positive going) scans for the three commercial pigments compared to the sample obtained from metallic iron is shown in Figure 39; peaks potentials are presented in Table 26. Peaks I and IV, characteristic peaks of iron oxidation and already discussed in previous sections, are observed in potentials close to those reported in the literature (-0.53 V and +0.32 V, respectively [86]). A third peak was observed for Mars Yellow (peak III*). Peak III* differs from peak III (present in the metallic iron sample) by 0.10 V, but it coincides exactly with the potential observed for the oxidative dissolution of metallic copper in this work. Considering that EDS and Raman spectroscopy showed the presence of copper in the sample, it is fair to assume that peak III* is actually related to the oxidation of copper, not iron. However, this is just a hypothesis and must be further investigate; as the Raman spectrum for Mars Yellow sample also identified several iron oxide compounds, this particular peak may also represent the oxidative dissolution of iron compounds, as previously discussed.

Figure 39 – Potential window displaying the relevant peaks for pigments Green Earth, Burnt Umber and Mars Yellow revealed in the anodic (positive going) scans. Cyclic voltammetry in 0.25 mol L^{-1} HAc/NaAc buffer. Scan rate: 100 mV s^{-1}. For comparison, the result of a scan for a sample collected from metallic iron is also presented.

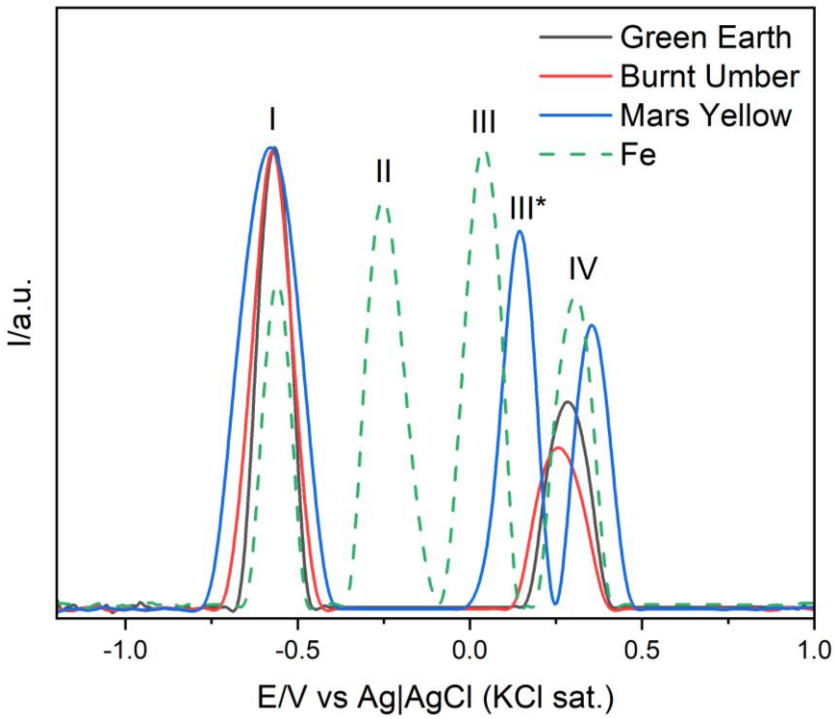

Source: The author.

Table 26 - Peaks potentials (*Ep*) identified in the anodic (positive going) scans for pigments Green Earth, Burnt Umber and Mars Yellow and for metallic iron. Cyclic voltammetry in 0.25 mol L^{-1} HAc/NaAc buffer. Scan rate: 100 mV s^{-1}.

Sample	E_p/V vs Ag|AgCl (KCl sat.)
Green Earth	-0.57 (I)
	+0.28 (IV)
Burnt Umber	-0.57 (I)
	+0.26 (IV)
Mars Yellow	-0.58 (I)
	+0.14 (III*)
	+0.35 (IV)
Fe	-0.56 (I)
	-0.25 (II)
	+0.04 (III)
	+0.31 (IV)

Source: The author.

5.5.2. Tin Pigments

One of the pigments (Pr11Pig03) from the *Pinacoteca* collection was composed mostly of cobalt and tin, a combination that forms a pigment known as cerulean blue. SEM imaging (Figure 40) of the sample shows some bigger geometrical particles (A), with dimensions close to 20 µm, and a lot of smaller powdery particles (B). EDS analysis (Table 27) shows that A is mainly composed of aluminum, carbon and oxygen, with tin and especially cobalt. B, however, is mainly composed of tin and cobalt.

Figure 40 - SEM micrograph of pigment Pr11Pig03. The two different particles analyzed by EDS are identified as A and B.

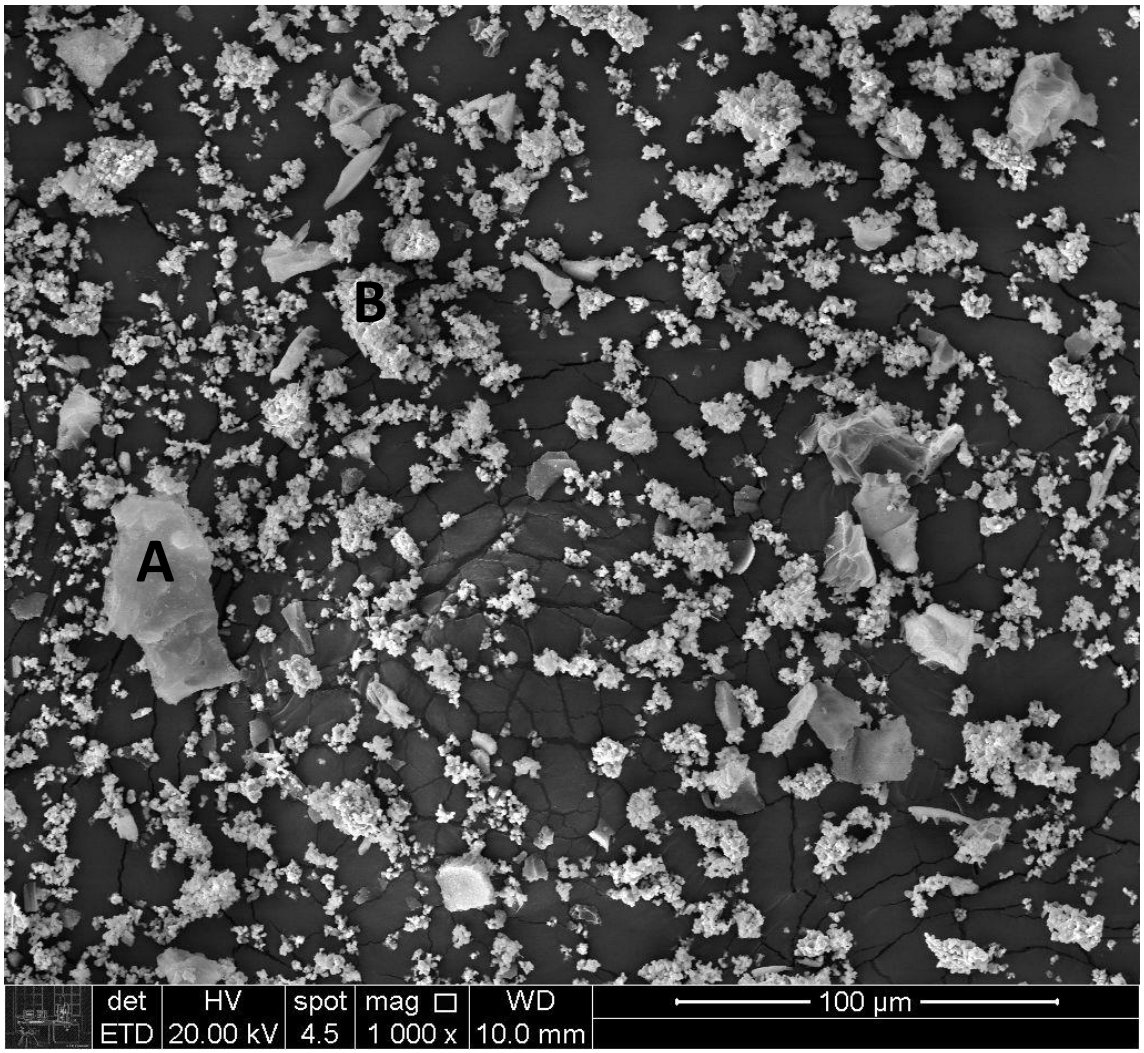

Source: The author.

Table 27 - EDS analysis of areas A and B, identified in Figure 40, for pigment Pr11Pig03 (wt. %).

Element	A (% wt.)	B (% wt.)
C	32.10	-
O	27.85	6.13
Mg	3.55	7.73
Al	18.10	0.72
Sn	2.61	63.80
Co	15.79	21.62

Source: The author.

Raman spectroscopy was then performed in order to identify the compounds present in the sample. The spectrum is shown in Figure 41, with the characteristic bands at (484, 522 and 660) cm^{-1} being attributed to cerulean blue ($CoO{\cdot}nSnO_2$) [117,118].

Figure 41 - Raman spectra for pigment Pr11Pig03. Relevant peaks are indicated by the arrows.

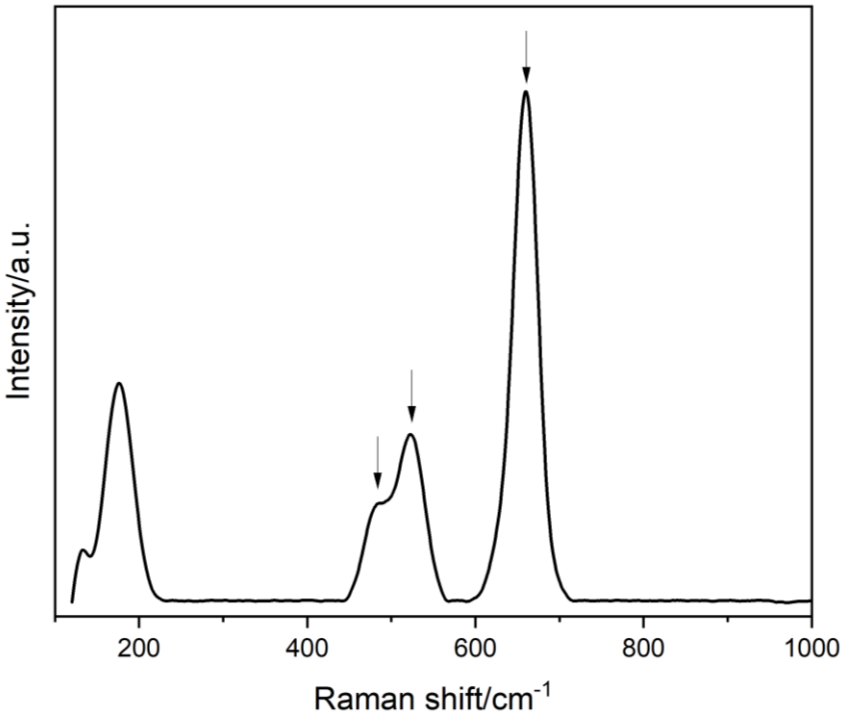

Source: The author.

Cerulean blue did not present any relevant peak when analyzed by cyclic voltammetry. Hence, square wave voltammetry was used as a more sensitive option. The window of the cathodic (negative going) scan performed with this latter technique with the relevant peaks is shown in Figure 42, and the peaks potentials presented in Table 28. Pr11Pig03 displays two reduction peaks: I at

-0.07 V and II at -0.58 V. They represent the reduction in two steps of Sn^{4+} to metallic tin, with the reaction attributed to peak I in Equation 17 and reaction attributed to peak II in Equation 18 [47].

$SnO_2 + 2\ H^+ + 2\ e^- \rightarrow x SnO + (1-x)Sn^{2+} + H_2O$ (peak I) Equation 17

$Sn^{2+} + 2\ e^- \rightarrow Sn$ (peak II) Equation 18

Peak I and II have been previously reported in the literature at -0.14 V and at -0.50 V [47], respectively.

Figure 42 – Potential window displaying the relevant peaks of pigment Pr11Pig03 revealed in the cathodic (negative going) scan. Square wave voltammetry in 0.25 mol L^{-1} HAc/NaAc buffer. Potential step increment 4 mV; square wave amplitude 25 mV; frequency 5 Hz.

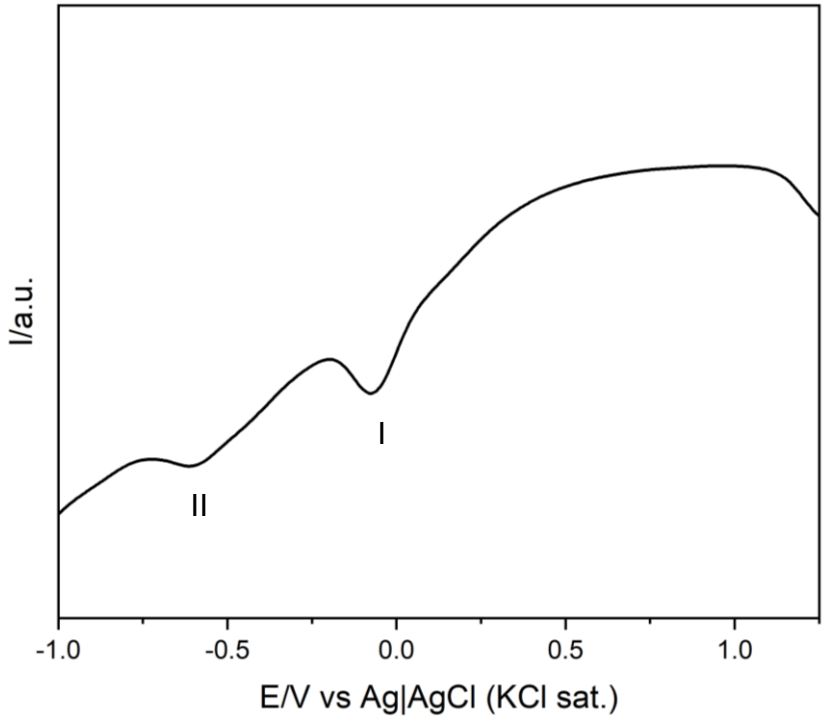

Source: The author.

Table 28 - Peak potentials (*Ep*) identified in the cathodic (negative going) scan for pigment Pr11Pig03. Square wave voltammetry in 0.25 mol L^{-1} HAc/NaAc buffer. Potential step increment 4 mV; square wave amplitude 25 mV; frequency 5 Hz.

Sample	E_p/V vs Ag|AgCl (KCl sat.)
Pr11Pig03	-0.07
	-0.58

Source: The author.

The potential window displaying the single relevant peak of the anodic (positive going) scan for pigment Pr11Pig03 compared to metallic tin is presented in Figure 43; peaks potentials are shown in Table 29. The observed peak corresponds to the oxidation of metallic tin to Sn^{2+} ions [47,67], which has been previously reported at -0.55 V [47] or -0.56 V [38]. Although cobalt pigments have been previously studied in phosphate buffer [119] and HCl + NaCl [120], neither in the cathodic nor in the anodic scan, peaks that could be ascribed to Co could be identified in the acetate buffer solution, independently of the employed voltammetric technique.

Figure 43 – Potential window displaying the relevant peak of pigment Pr11Pig03 revealed in the anodic (positive going) scan. Square wave voltammetry in 0.25 mol L^{-1} HAc/NaAc buffer. Potential step increment 4 mV; square wave amplitude 25 mV; frequency 5 Hz. For comparison, the result of a scan for a sample collected from metallic tin is also presented.

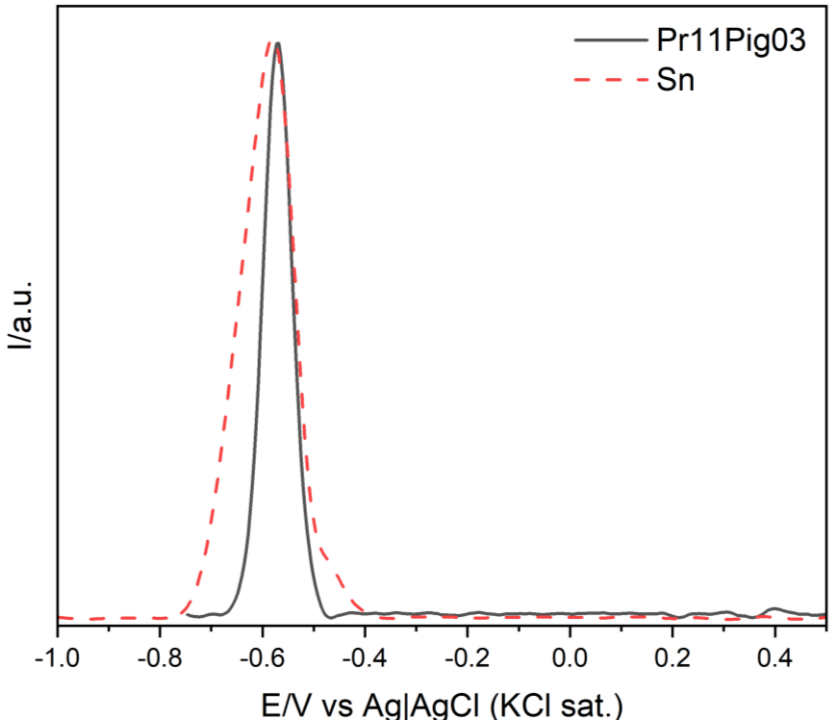

Source: The author.

Table 29 - Peaks potentials (*Ep*) identified in the anodic (positive going) scan of Pr11Pig03 and metallic tin. Square wave voltammetry in 0.25 mol L^{-1} HAc/NaAc buffer. Potential step increment 4 mV; square wave amplitude 25 mV; frequency 5 Hz.

Sample	E_p/V vs Ag|AgCl (KCl sat.)
Pr11Pig03	-0.57
Sn	-0.58

Source: The author.

5.5.3. Tungsten Pigment

Another of the pigments from the *Pinacoteca* collection (Pr09Pig15) is mainly composed of tungsten. In accordance with the previous investigation protocols, it was initially analyzed by SEM-EDS. SEM micrograph (Figure 44) shows particles with irregular shapes and sizes, but with dimensions lower than 100 µm. The EDS analyzes on different particles showed that the percentage of the elements may vary, but the pigment is mainly composed of tungsten with carbon and oxygen. The EDS for a representative particle is shown in Table 30.

Figure 44 - SEM micrograph of pigment Pr09Pig15.

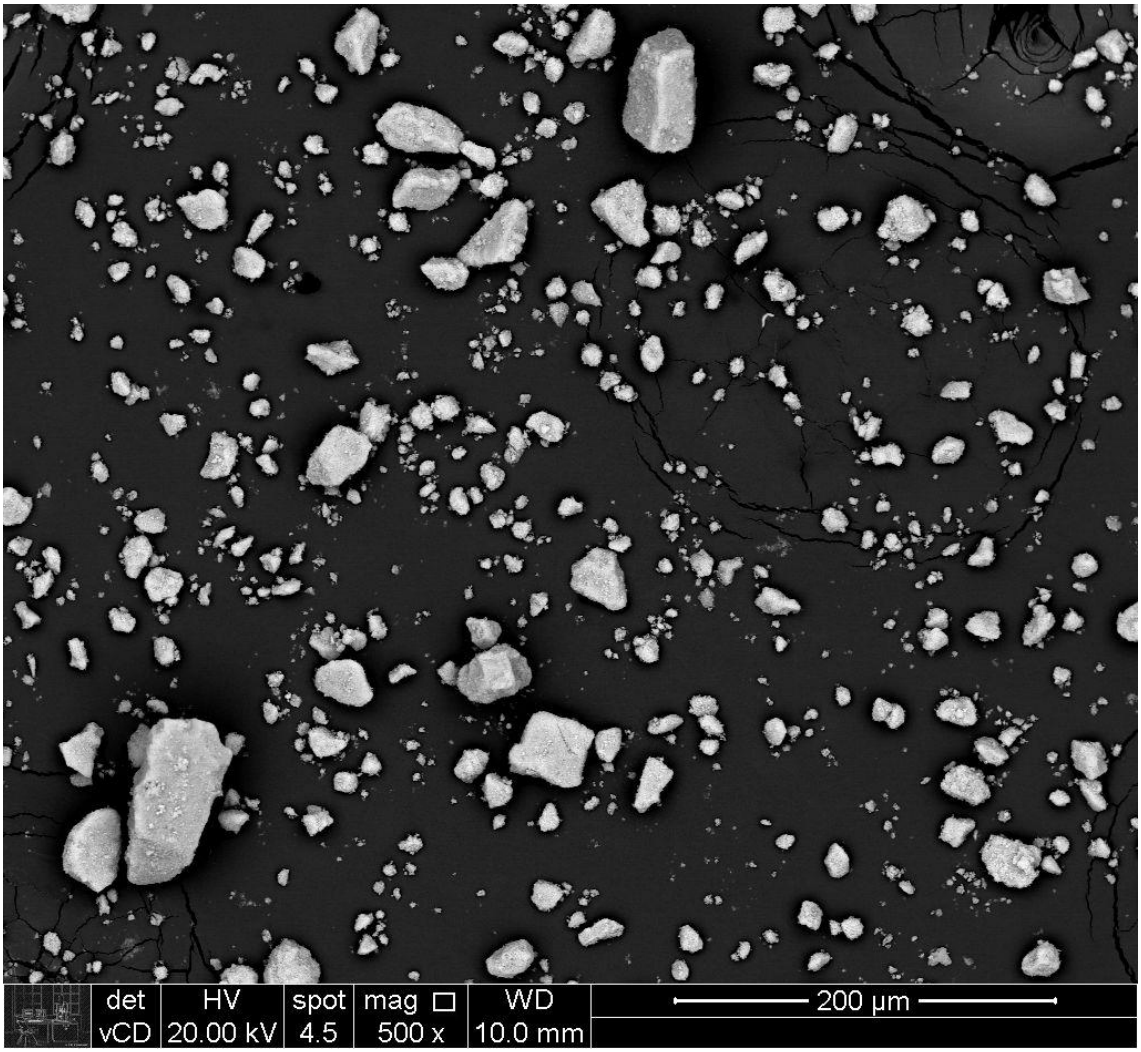

Source: The author.

Table 30 - EDS analysis of pigment Pr09Pig15 (wt. %).

Element	Pr09Pig15 (% wt.)
C	27.0
O	20.4
W	52.6

Source: The author.

Then, Raman spectroscopy was used for identifying the compounds present in the pigment. The spectrum is shown in Figure 45. The peaks observed in the region from (120 to 1000) cm^{-1} can be attributed to tungsten oxides. Peak at 124 cm^{-1} is related to lattice modes [121,122] or vibrational modes of $(W_2O_2)_n$ [123]. The peak at 224 cm^{-1} can be attributed to vibrational modes of W-O-W [121,122] or W-W [124], and the peak at 797 cm^{-1} is also related to vibrational

modes of W-O-W [124]. Vibration and deformation modes of O-W-O are associated to the peaks at 336 cm^{-1} [121–124], 623 cm^{-1} [122], 662 cm^{-1} [121], 697 cm^{-1} [121], 740 cm^{-1} [121,122], and 797 cm^{-1} [121,122]. The band in the (947 to 1026) cm^{-1} range can be attributed to vibrational modes of WO_2 and W=O [124]. Peaks at (425, 525, 623, 740 and 797) cm^{-1} can be related to the presence of WO_3 [123,125], and at (336, 837 and 908) cm^{-1} can be related to WO_4^{2-} [125]. The peak at 425 cm^{-1} has also been attributed to the deformation of W-O [124] or vibrational modes of $W\text{-}OH_2$ [121]. In the region above 1000 cm^{-1}, the peaks can be attributed to carbon interactions with other carbon atoms (like the peaks at (1073 and 1128) cm^{-1} [126]) or with oxygen (peaks between 1420 cm^{-1} and 1590 cm^{-1} attributed to COO^- vibrational modes [126], and peaks at (1073, 1358 and 1387) cm^{-1} attributed to CO_3^{2-} stretching [127]).

Figure 45 - Raman spectrum for pigment Pr09Pig15. Relevant peaks are indicated by the arrows.

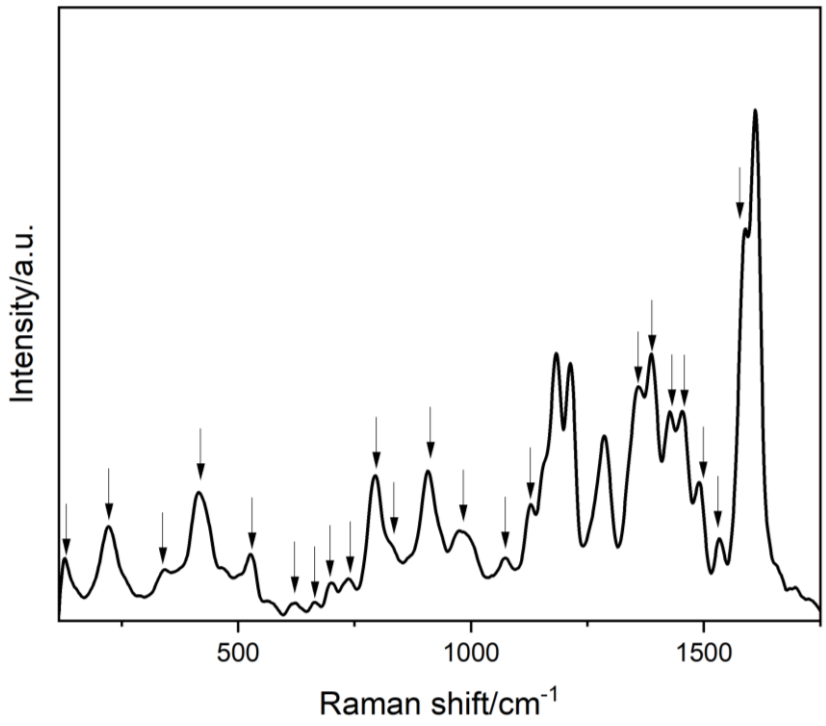

Source: The author.

Pigment Pr09Pig15 did not present any relevant peak when analyzed by cyclic voltammetry. Hence, square wave voltammetry was used as a more sensitive option. The window of the cathodic (negative going) scan with the relevant peaks is shown in Figure 46. The peaks potentials are presented in Table 31. Two reduction peaks are observed for pigment Pr09Pig15. Considering that

the electrochemistry of tungsten can be confusing due not only to the different types of oxides but also to the variety of compounds based on those oxides [89], there are different possibilities of reduction processes. The peak at -0.53 V can be attributed to the reduction of W_2O_5 to WO_2 or from WO_2 to metallic tungsten, previously reported at -0.59 V and -0.50 V [92]. According to Pourbaix diagram for tungsten [128], in pH values similar to that of the acetate buffer solution (4.5) the reduction of WO_4^{2-} to WO_2 and W_2O_5 occurs at -0.49 V, so it could also be related to the first reduction peak. Also according to Pourbaix diagram, the second reduction peak could be attributed to the reduction of WO_4^{2-} to metallic tungsten, which should happen at -1.0 V [128].

Figure 46 – Potential window displaying the relevant peaks of pigment Pr09Pig15 revealed in the cathodic (negative going) scan. Square wave voltammetry in 0.25 mol L^{-1} HAc/NaAc buffer. Potential step increment 4 mV; square wave amplitude 25 mV; frequency 5 Hz.

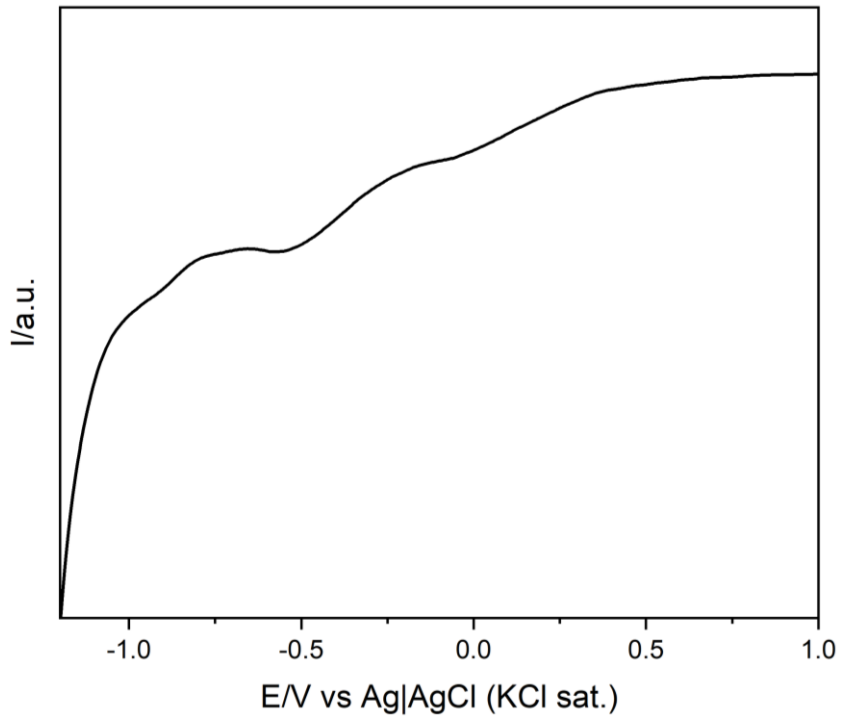

Source: The author.

Table 31 - Peaks potentials (*Ep*) identified in the cathodic (negative going) scan for pigment Pr09Pig15. Square wave voltammetry in 0.25 mol L^{-1} HAc/NaAc buffer. Potential step increment 4 mV; square wave amplitude 25 mV; frequency 5 Hz.

Sample	E_p/V vs Ag|AgCl (KCl sat.)
Pr09Pig15	-0.53
	-0.92

Source: The author.

The potential window of the anodic (positive going) scans displaying the relevant peaks of pigment Pr09Pig15 compared to metallic tungsten is shown in Figure 47, and peaks potentials are displayed in Table 32. The first peak, close to -0.60 V, could represent the oxidation of metallic tungsten to WO_2 and from WO_2 to W_2O_5, a reverse reaction from the first reduction peak. This last reaction, however, has also been reported at -0.40 V [91], and so it could be attributed to the second oxidation peak. The oxidation of WO_2 to WO_4^{2-} has also been observed previously at -0.27 V, and so it could also be a possibility for this second oxidation peak [92]. The next oxidation peaks, at (+0.27, +0.63 and +0.90) V, occur in a region where nonstoichiometric oxides are oxidized to WO_3 [89,91].

Figure 47 – Potential window displaying the relevant peaks for pigment Pr09Pig15 revealed in the anodic (positive going) scan. Square wave voltammetry in 0.25 mol L^{-1} HAc/NaAc buffer. Potential step increment 4 mV; square wave amplitude 25 mV; frequency 5 Hz. For comparison, the result of a scan for a sample collected from metallic tungsten is also presented.

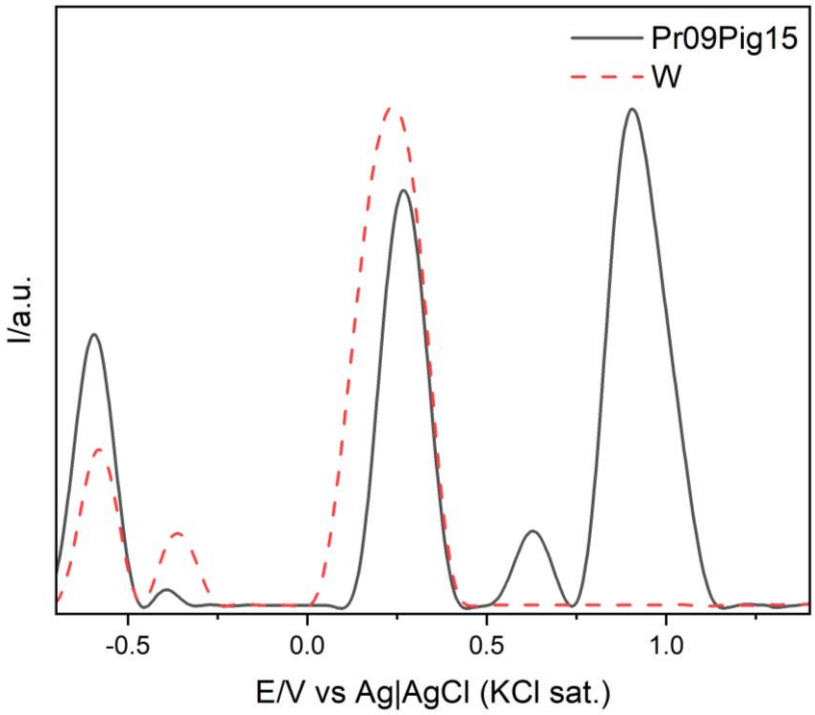

Source: The author.

Table 32 - Peaks potentials (*Ep*) identified in the anodic (positive going) scan for pigment of Pr09Pig15 and metallic tungsten. Square wave voltammetry in 0.25 mol L^{-1} HAc/NaAc buffer. Potential step increment 4 mV; square wave amplitude 25 mV; frequency 5 Hz.

Sample	E_p/V vs Ag|AgCl (KCl sat.)
Pr09Pig15	-0.59
	-0.39
	+0.27
	+0.63
	+0.90
W	-0.58
	-0.36
	+0.24

Source: The author.

5.5.4. Differentiation of pigments based on their metallic components

Considering that one of the aims of this work is to propose VMP as a micro-invasive technique that can be used to identify metallic elements present in pigments in artifacts, and to use this technique to diferentiate between them, a comparison between the position of the oxidation peaks obtained in the anodic (positive going) scans performed with samples collected both from metals and pigments is presented in Figure 48. Pr11Pig07 was selected as representative of copper pigment, and Burnt Umber of iron pigment. The chosen technique was square wave voltammetry, considering that only this technique allowed to investigate Sn and W-containing pigments. The Figure evidences that, even though the tungsten-containing pigment presents more oxidation peaks than the metallic sample, the anodic behavior of the pigments matches quite well those of their respective metals. Also, each metal (and their respective pigment) presents a different electrochemical response, and so VMP was successfully used to differentiate and identify pigments containing copper, iron, tin and tungsten. To facilitate visualization, Figure 49 shows the comparison between the voltammograms of each metal and its respective pigment in evidence.

Figure 48 - Comparison between the anodic behavior of metallic and pigment samples containing different metals verified in the VMP experimens. Square wave voltammetry in 0.25 mol L^{-1} HAc/NaAc buffer. Potential step increment 4 mV; square wave amplitude 25 mV; frequency 5 Hz.

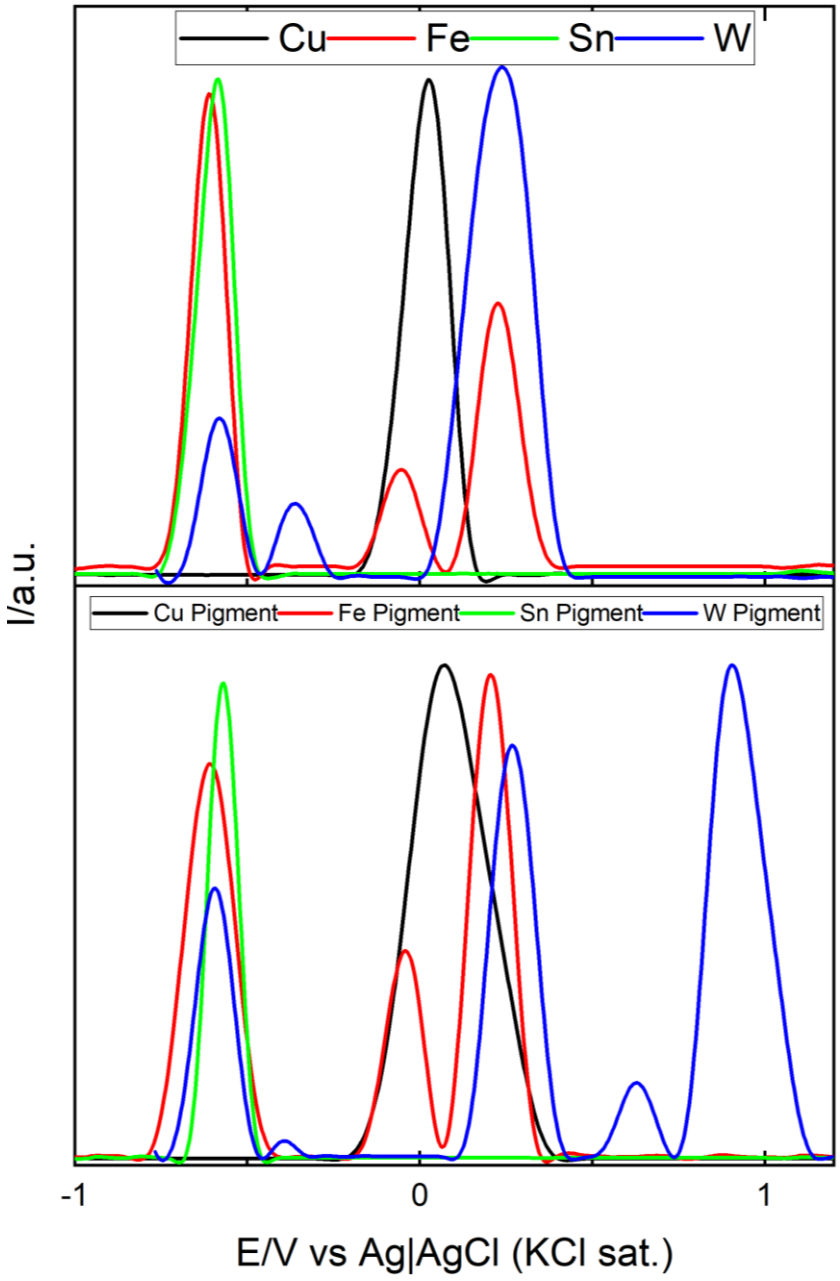

Source: The author.

Figure 49 - Comparison between the anodic behavior of metallic and pigment samples of each metal, highlighted, with: a) copper, b) iron, c) tin and d) tungsten. Square wave voltammetry in 0.25 mol L^{-1} HAc/NaAc buffer. Potential step increment 4 mV; square wave amplitude 25 mV; frequency 5 Hz.

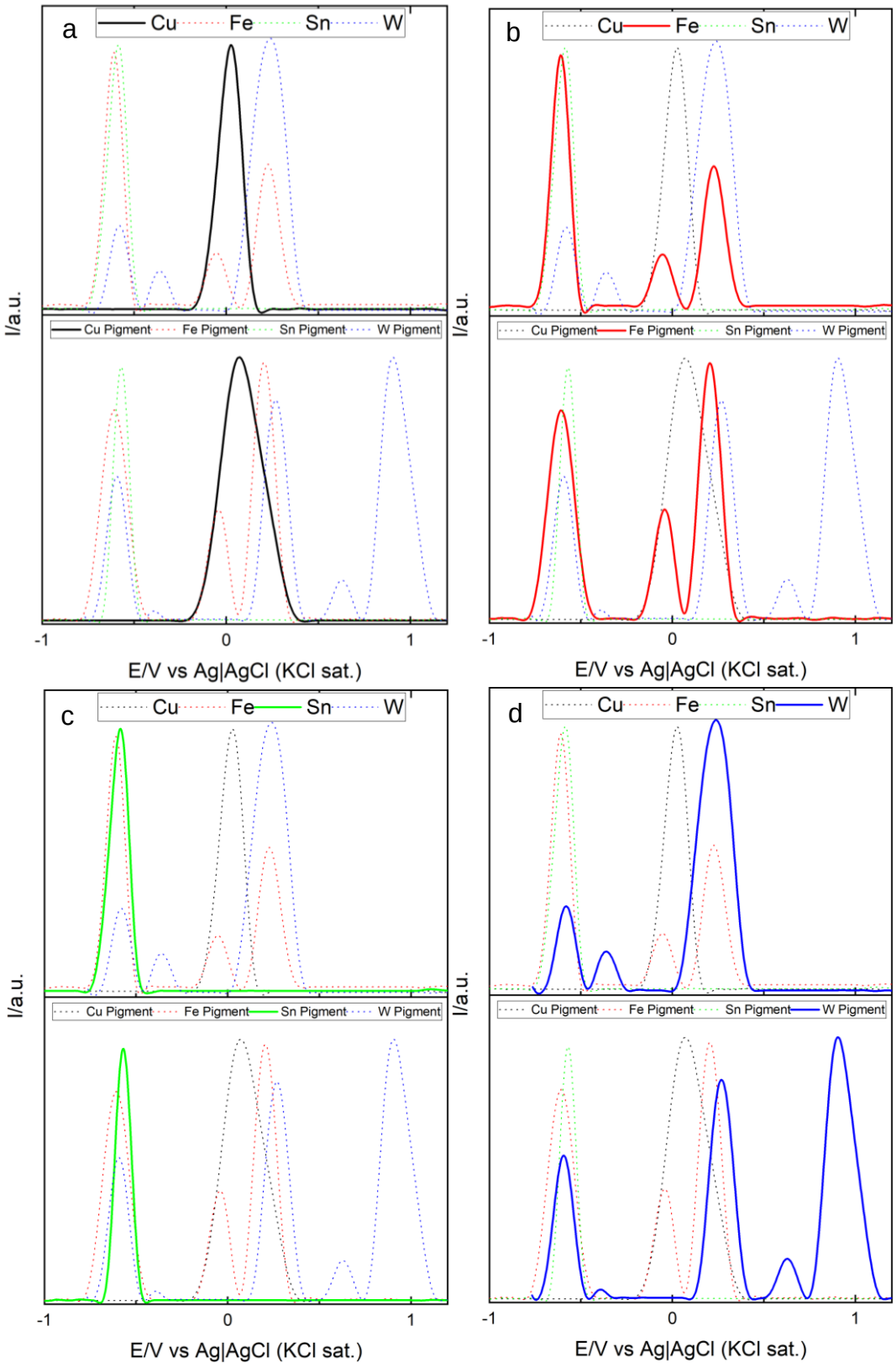

Source: The author.

6. CONCLUSIONS

In the present work VMP was used to create reference database for metals identification and then used to identify the presence of such elements in complex compounds like corrosion products and pigments. From the obtained results we can conclude that.

- Considering the set of selected metals (silver, copper, iron, tin, lead, zinc and tungsten) the sodium acetate buffer solution was the more universal electrolyte for the VMP experiments, allowing to determine specific oxidation peaks to all studied metals and also to differentiate between them by means of peaks potentials;
- Square wave voltammetry proved to be a more sensitive technique than cyclic voltammetry for identifying the diferente metallic elements and was systematically employed in cases where cyclic voltammetry was not effective;
- By means of VMP it was possible to identify the different metallic elements present in the composition of corrosion products and selected pigments obtained both from reference (Pinacoteca collection) and commercial (Sennelier) sources;
- The agreement between the positioning of the oxidation peaks for the corrosion produts and pigments samples and those determined for the reference metals proves the importance of creating a reference database as an effective tool to expand the use of VMP in the sciences of conservation and restoration of cultural heritage;
- The results also revealed that the use of tailormade conditions may help to enhance the results of the VMP experiments. In the present work, changing the scan rate and also the technique from cyclic to square wave voltammetry helped in the interpretation of the curves and also in the disclosure of oxidation peaks not present with the more standard experimental conditions adopted.

7. FUTURE PERSPECTIVES

VMP has shown its efficiency in identifying metallic pigments in powdered form. Some suggestions for future works in this area of research would be:

- evaluating the electrochemical response of pigments collected directly from works of art;
- analyzing the interference of binders, coatings and other additives used in the making of paintings;
- further studying the electrochemical processes in iron samples;
- expand the database creation for other metals and alloys not investigated in the present study;
- test the methodology in real cases studies, for instance, for differentiate inorganic pigments presenting the same or similar colors, which, nevertheless, are obtained from different metallic ions.

8. REFERENCES

[1] M.T.F. Guedes, L.M. Maio, Bem cultural, in: B. Grieco, L. Teixeira, A. Thompson (Eds.), Dicionário IPHAN Patrimônio Cult., Segunda ed, IPHAN/DAF/Copedoc, Rio de Janeiro, Brasília, 2016.

[2] A. Doménech-Carbó, Voltammetric methods applied to identification, speciation, and quantification of analytes from works of art: An overview, J. Solid State Electrochem. 14 (2010) 363–379. https://doi.org/10.1007/s10008-009-0858-6.

[3] E. Balliana, C. Barbante, Identification of copper alloys constituting cultural artefacts by electrochemical techniques, Università Ca' Foscari Venezia, 2006.

[4] D. Lauwers, A.G. Hutado, V. Tanevska, L. Moens, D. Bersani, P. Vandenabeele, Characterisation of a portable Raman spectrometer for in situ analysis of art objects, Spectrochim. Acta - Part A Mol. Biomol. Spectrosc. 118 (2014) 294–301. https://doi.org/10.1016/j.saa.2013.08.088.

[5] G.D. Smith, R.J.H. Clark, Raman microscopy in archaeological science, J. Archaeol. Sci. 31 (2004) 1137–1160. https://doi.org/10.1016/j.jas.2004.02.008.

[6] A. Kudelski, Analytical applications of Raman spectroscopy, Talanta. 76 (2008) 1–8. https://doi.org/10.1016/j.talanta.2008.02.042.

[7] G. Keresztury, Raman Spectroscopy: Theory, in: Peter Griffiths (Ed.), Handb. Vib. Spectrosc., John Wiley & Sons, INC., 2006. https://doi.org/10.1070/IM1976v010n04ABEH001810.

[8] L. Bellot-Gurlet, D. Neff, S. Réguer, J. Monnier, M. Saheb, P. Dillmann, Raman studies of corrosion layers formed on archaeological irons in various media, J. Nano Res. 8 (2009) 147–156. https://doi.org/10.4028/www.scientific.net/JNanoR.8.147.

[9] J. Buse, V. Otero, M.J. Melo, New Insights into Synthetic Copper Greens : The Search for Specific Signatures by Raman and Infrared Spectroscopy for Their

Characterization in Medieval Artworks, Heritage. 2 (2019) 1614–1629. https://doi.org/10.3390/heritage2020099.

[10] F. Schulte, K.-W. Brzezinka, K. Lutzenberger, H. Stege, U. Panne, Raman spectroscopy of synthetic organic pigments used in 20th century works of art, J. Raman Spectrosc. 39 (2008) 1455–1463. https://doi.org/10.1002/jrs.2021.

[11] A.J. Bard, L.R. Faulkner, Electrochemical Methods: Fundamentals and Applications, Second edi, John Wiley & Sons, INC., 2001. https://doi.org/10.1038/s41929-019-0277-8.

[12] F.J. Holler, D.A. Skoog, S.R. Crouch, Princípios de Análise Instrumental, Sexta ediç, Bookman, Porto Alegre, 2009.

[13] P. Patnaik, Dean's analytical chemistry handbook, Second Edi, McGraw-Hill Education, 2004. https://doi.org/10.5860/choice.42-1566.

[14] F. Scholz, B. Lange, Abrasive stripping voltammetry - an electrochemical solid state spectroscopy of wide applicability, Trends Anal. Chem. 11 (1992) 359–367. https://doi.org/10.1016/0165-9936(92)80025-2.

[15] A.J. Bard, Electroanalytical Chemistry: Volume 20-A Series of Advances, First edit, Marcel Dekker, INC., New York, 1998.

[16] A. Doménech-carbó, J. Labuda, F. Scholz, Electroanalytical chemistry for the analysis of solids : Characterization and classification (IUPAC Technical Report)*, Pure Appl. Chem. 85 (2013) 609–631. https://doi.org/10.1351/PAC-REP-11-11-13.

[17] T. Grygar, F. Marken, U. Schröder, F. Scholz, Electrochemical analysis of solids. A review, Collect. Czechoslov. Chem. Commun. 67 (2002) 163–208. https://doi.org/10.1135/cccc20020163.

[18] F. Scholz, L. Nitschke, G. Henrion, Identification of solid materials with a new electrochemical technique - the abrasive stripping analysis, Fresenius' Zeitschrift Für Anal. Chemie. 334 (1989) 56–58. https://doi.org/10.1007/BF00481974.

[19] R.G. Compton, C.E. Banks, Understanding voltammetry, Third edit, World Scientific Publishing Europe Ltd., New Jersey, 2018. https://doi.org/10.1142/9789812779809_0004.

[20] L.M. De Carvalho, M. Hilgemann, C. Spengler, P.C. Do Nascimento, D. Bohrer, Voltametria de Micropartículas Imobilizadas: Fundamentos e aplicações analíticas, Quim. Nova. 33 (2010) 1765–1772. https://doi.org/10.1590/s0100-40422010000800025.

[21] A. Doménech-Carbó, M.T. Doménech-Carbó, F.M. Valle-Algarra, J.V. Gimeno-Adelantado, L. Osete-Cortina, F. Bosch-Reig, On-line database of voltammetric data of immobilized particles for identifying pigments and minerals in archaeometry, conservation and restoration (ELCHER database), Anal. Chim. Acta. 927 (2016) 1–12. https://doi.org/10.1016/j.aca.2016.04.052.

[22] E. Ottenwelter, V. Costa, Evidence of metallic plating on archaeological artefacts by voltammetry of microparticles, Archaeometry. 57 (2015) 497–504. https://doi.org/10.1111/arcm.12091.

[23] F. Di Turo, N. Montoya, J. Piquero-Cilla, C. De Vito, F. Coletti, G. Favero, A. Doménech-Carbó, Archaeometric analysis of Roman bronze coins from the Magna Mater temple using solid-state voltammetry and electrochemical impedance spectroscopy, Anal. Chim. Acta. 955 (2017) 36–47. https://doi.org/10.1016/j.aca.2016.12.007.

[24] E.A. Vik, D.A. Carlson, A.S. Eikum, E.T. Gjessing, Electrocoagulation of potable water, Water Res. 18 (1984) 1355–1360. https://doi.org/10.1016/0043-1354(84)90003-4.

[25] G. Cepriá, O. Abadías, J. Pérez-Arantegui, J.R. Castillo, Electrochemical behavior of silver-copper alloys in voltammetry of microparticles: A simple method for screening purposes, Electroanalysis. 13 (2001) 477–483. https://doi.org/10.1002/1521-4109(200104)13:6<477::AID-ELAN477>3.0.CO;2-E.

[26] A. Hickling, D.J.G. Ives, The electrochemical behaviour of Iron oxides in dilute

sulphuric acid and the interpretation of the flade potential of iron, Electrochim. Acta. 20 (1975) 63–69. https://doi.org/10.1016/0013-4686(75)85046-8.

[27] K.Z. Brainina, M.B. Vydrevich, Stripping analysis of solids, J. Electroanal. Chem. 121 (1981) 1–28. https://doi.org/10.1016/S0022-0728(81)80565-7.

[28] P.D. Allen, N.A. Hampson, G.J. Bignold, The electrodissolution of magnetite – Part I. The electrochemistry of Fe3O4/C discs - Potentiodynamic experiments., J. Electroanal. Chem. 99 (1979) 299–309. https://doi.org/10.1016/S0022-0728(79)80094-7.

[29] P.D. Allen, N.A. Hampson, G.J. Bignold, The electrodissolution of magnetite – Part II. The oxidation of bulk magnetite., J. Electroanal. Chem. 111 (1980) 223–233. https://doi.org/10.1016/S0022-0728(80)80042-8.

[30] Y. Rico, J.C. Bidegain, C.I. Elsner, Synthetic and natural Iron oxide characterization through microparticle voltammetry, Geofísica Int. 48 (2009) 221–236.

[31] S. Waki, K. Dokko, T. Itoh, M. Nishizawa, T. Abe, I. Uchida, High-Speed voltammetry of Mn-doped LiCoO 2 using a microelectrode technique, J. Solid State Electrochem. 4 (2000) 205–209. https://doi.org/10.1007/s100080050196.

[32] F. Scholz, L. Nitschke, G. Henrion, H. Berlin, S. Chemic, B. Analytik, H. Strasse, D.-Berlin, Identification of solid materials with a new electrochemical technique - the abrasive stripping analysis, (1989) 56–58. https://doi.org/10.1007/BF00481974.

[33] G. Cepriá, C. Aranda, J. Pérez-Arantegui, F. Lacueva, J.R. Castillo, Voltammetry of immobilised microparticles: A powerful analytical technique to study the physical and chemical composition of brass, J. Electroanal. Chem. 513 (2001) 52–58. https://doi.org/10.1016/S0022-0728(01)00599-X.

[34] A. Elia, M. Dowsett, A. Adriaens, Electrochemical characterization of bronze historical objects using voltammetry of microparticles, Appl. Phys. A Mater. Sci. Process. 118 (2014) 449–455. https://doi.org/10.1007/s00339-014-8342-2.

[35] A. Doménech, M.T. Doménech-Carbó, T. Pasies, M. delCarmenBouzas, Modeling Corrosion of Archaeological Silver-Copper Coins Using the Voltammetry of Immobilized Particles, Electroanalysis. 24 (2012) 1945–1955. https://doi.org/10.1002/elan.201200252.

[36] A. Doménech-Carbó, M.T. Doménech-Carbó, M.A. Peiró-Ronda, "One-Touch" Voltammetry of Microparticles for the Identification of Corrosion Products in Archaeological Lead, Electroanalysis. 23 (2011) 1391–1400. https://doi.org/10.1002/elan.201000739.

[37] A. Doménech-Carbó, M.T. Doménech-Carbó, C. Álvarez-Romero, T. Pasíes, M. Buendía, Screening of Iberian Coinage in the 2th-1th BCE Period Using the Voltammetry of Immobilized Particles, Electroanalysis. 31 (2019) 1164–1173. https://doi.org/10.1002/elan.201900090.

[38] V. Costa, K. Leyssens, A. Adriaens, N. Richard, F. Scholz, Electrochemistry reveals archaeological materials, J. Solid State Electrochem. 14 (2010) 449–451. https://doi.org/10.1007/s10008-009-0864-8.

[39] L. Fabrizi, F. Di Turo, L. Medeghini, M. Di Fazio, F. Catalli, C. De Vito, The application of non-destructive techniques for the study of corrosion patinas of ten Roman silver coins: The case of the medieval Grosso Romanino, Microchem. J. 145 (2019) 419–427. https://doi.org/10.1016/j.microc.2018.10.056.

[40] M. Di Fazio, F. Di Turo, L. Medeghini, L. Fabrizi, F. Catalli, C. De Vito, New insights on medieval Provisini silver coins by a combination of non-destructive and micro-invasive techniques, Microchem. J. 144 (2019) 309–318. https://doi.org/10.1016/j.microc.2018.09.016.

[41] A. Doménech-Carbó, J. Bernabeu-Aubán, Correlation between lead isotope analysis and solid-state electrochemistry for determining the provenance of archaeological bronze, J. Solid State Electrochem. 23 (2019) 2803–2812. https://doi.org/10.1007/s10008-019-04378-3.

[42] A. Doménech-Carbó, J.M. del Hoyo-Meléndez, M.T. Doménech-Carbó, J. Piquero-Cilla, Electrochemical analysis of the first Polish coins using

voltammetry of immobilized particles, Microchem. J. 130 (2017) 47–55. https://doi.org/10.1016/j.microc.2016.07.020.

[43] M. Di Fazio, A.C. Felici, F. Catalli, M.T. Doménech-Carbó, C. De Vito, A. Doménech-Carbó, Solid-state electrochemical characterization of emissions and authorities producing Roman brass coins, Microchem. J. 152 (2020) 104306. https://doi.org/10.1016/j.microc.2019.104306.

[44] S. Madec, Rapport de microthèse: Caractérisation électrochimique des matériaux constitutifs des objets archéologiques en métal, Paris, 2006.

[45] A. Doménech, M.T. Doménech-Carbó, T. Pasies, M.C. Bouzas, Application of modified tafel analysis to the identification of corrosion products on archaeological metals using voltammetry of microparticles, Electroanalysis. 23 (2011) 2803–2812. https://doi.org/10.1002/elan.201100577.

[46] G. Cepriá, E. García-Gareta, J. Pérez-Arantegui, Cadmium yellow detection and quantification by voltammetry of immobilized microparticles, Electroanalysis. 17 (2005) 1078–1084. https://doi.org/10.1002/elan.200403217.

[47] A. Doménech-Carbó, M.T. Doménech-Carbó, Electrochemical characterization of archaeological tin-opacified lead-alkali glazes and their corrosion processes, Electroanalysis. 17 (2005) 1959–1969. https://doi.org/10.1002/elan.200503322.

[48] A. Doménech-Carbó, M.T. Doménech-Carbó, C. Álvarez-Romero, N. Montoya, T. Pasies-Oviedo, M. Buendía Ortuño, Electrochemical Characterization of Coinage Techniques the 17(th) Century: The maravedis Case., Electroanalysis. 29 (2018) 2008–2018. https://doi.org/10.1002/elan.201700326.

[49] F. Scholz, F. Rabi, W. -D Müller, The anodic dissolution of dental amalgams studied with abrasive stripping voltammetry, Electroanalysis. 4 (1992) 339–346. https://doi.org/10.1002/elan.1140040312.

[50] A.S. Ortiz-Miranda, A. Doménech-Carbó, M.T. Doménech-Carbó, L. Osete-Cortina, F. Bolívar-Galiano, I. Martín-Sánchez, Analyzing chemical changes in verdigris pictorial specimens upon bacteria and fungi biodeterioration using

voltammetry of microparticles, Herit. Sci. 5 (2017) 1–17. https://doi.org/10.1186/s40494-017-0121-x.

[51] A. Doménech-Carbó, M.Á. Villegas, F. Agua, S. Martínez-Ramírez, M.T. Doménech-Carbó, B. Martínez, Electrochemical Fingerprint of Archeological Lead Silicate Glasses Using the Voltammetry of Microparticles Approach, J. Am. Ceram. Soc. 99 (2016) 3915–3923. https://doi.org/10.1111/jace.14430.

[52] M.T. Di Turo, Francesca; Piquero-Cilla, J.; De Vito, C.; Coletti, F.; Favero, G.; Domenech Carbo, Dating Archaeological Strata in the Magna Mater Temple Using Solid- state Voltammetric Analysis of Leaded Bronze Coins, J. Chem. Inf. Model. 53 (2013) 1689–1699. https://doi.org/10.1017/CBO9781107415324.004.

[53] A. Doménech-Carbó, M.T. Doménech-Carbó, E. Montagna, C. Álvarez-Romero, Y. Lee, Electrochemical discrimination of mints: The last Chinese emperors Kuang Hsü and Hsüan T'ung monetary unification, Talanta. 169 (2017) 50–56. https://doi.org/10.1016/j.talanta.2017.03.025.

[54] A. Doménech-carbó, M.T. Doménech-Carbó, M.A. Peiró-Ronda, L. Osete-Cortina, Electrochemistry and authentication of archaelogical lead using voltammetry of microparticles: application to the Tossal de Sant Miquel iberian plate, Archaeometry. 6 (2011) 1193–1211. https://doi.org/10.1111/j.1475-4754.2011.00608.x.

[55] A. Domønech-carbó, M.T. Domønech-carbó, J. Redondo-marugµn, L. Osete-, Electrochemical Characterization of Corrosion Products in Leaded Bronze Sculptures Considering Ohmic Drop Effects on Tafel Analysis, Electroanalysis. 28 (2016) 833–845. https://doi.org/10.1002/elan.201500613.

[56] A.B.A. Sedano, M.L.T. García, M.D.V. Barbado, P.S. Batanero, Electrochemical study of copper and iron compounds in the solid state by using voltammetry of immobilized microparticles: Application to copper ferrite characterization, J. Electroanal. Chem. 566 (2004) 433–441. https://doi.org/10.1016/j.jelechem.2003.12.009.

[57] H. Aubriet, B. Humbert, M. Perdicakis, Voltammetry of Microparticles and in situ

microRaman measurements under potentiostatic conditions. I. Spectroelectrochemical behaviour of Prussian blue, PbO and Bi2O3, Electrochim. Acta. 257 (2017) 128–137. https://doi.org/10.1016/j.electacta.2017.10.009.

[58] A. Doménech, F. Rodríguez, L. Osete, Mapping of corrosion products of highly altered archeological iron using voltammetry of microparticles, Microchem. J. 106 (2013) 41–50. https://doi.org/10.1016/j.microc.2012.05.002.

[59] A. Doménech-carbó, M. Lastras, F. Rodríguez, E. Cano, J. Piquero-cilla, L. Osete-cortina, Monitoring stabilizing procedures of archaeological iron using electrochemical impedance spectroscopy, J. Solid State Electrochem. 18 (2014) 399–409. https://doi.org/10.1007/s10008-013-2232-y.

[60] G. Cepriá, A. Usón, J. Pérez-Arantegui, J.R. Castillo, Identification of iron(III) oxides and hydroxy-oxides by voltammetry of immobilised microparticles, Anal. Chim. Acta. 477 (2003) 157–168. https://doi.org/10.1016/S0003-2670(02)01371-5.

[61] A. Doménech-Carbó, M.T. Doménech-Carbó, J. Redondo-Marugán, L. Osete-Cortina, J. Barrio, A. Fuentes, M. V. Vivancos-Ramón, W. Al Sekhaneh, B. Martínez, I. Martínez-Lázaro, T. Pasíes, Electrochemical Characterization and Dating of Archaeological Leaded Bronze Objects Using the Voltammetry of Immobilized Particles, Archaeometry. 60 (2018) 308–324. https://doi.org/10.1111/arcm.12308.

[62] M. Perdicakis, H. Aubriet, A. Walcarius, Use of a commercially available wood-free resin pencil as convenient electrode for the “Voltammetry of Microparticles” technique, Electroanalysis. 16 (2004) 2042–2050. https://doi.org/10.1002/elan.200403056.

[63] B. Martínez, J. Piquero-Cilla, N. Montoya, M.T. Doménech-Carbó, A. Doménech-Carbó, Electrochemical analysis of gold embroidery threads from archeological textiles, J. Solid State Electrochem. 22 (2018) 2205–2215. https://doi.org/10.1007/s10008-018-3927-x.

[64] L. Fabrizi, L. Nigro, F. Cappella, F. Spagnoli, M. Guirguis, A.M. Niveau de Villedary y Mariñas, M.T. Doménech-Carbó, C. De Vito, A. Doménech-Carbó, Discrimination and Provenances of Phoenician Red Slip Ware Using both the Solid State Electrochemistry and Petrographic Analyses, Electroanalysis. 32 (2020) 258–270. https://doi.org/10.1002/elan.201900515.

[65] L. La-Torre-Riveros, A. Doménech-Carbó, C.R. Cabrera, M.T. Doménech-Carbó, W. Huahuasoncco-Condori, D. Quispe Guzmán, M. del C. Gutiérrez-Castillo, K. Carmona-Ochoa, A. Pérez-Trujillo, Solid-state electrochemical analysis of Inka pottery from Qotakalli archeological site in the Cusco (Perú) area, J. Solid State Electrochem. (2019) 1541–1552. https://doi.org/10.1007/s10008-019-04243-3.

[66] F. Di Turo, N. Montoya, J. Piquero-Cilla, C. De Vito, F. Coletti, I. De Luca, A. Doménech-Carbó, Electrochemical discrimination of manufacturing types of pottery from Magna Mater Temple and Fora of Nerva and Caesar (Rome, Italy), Appl. Clay Sci. 162 (2018) 305–310. https://doi.org/10.1016/j.clay.2018.06.024.

[67] A. Doménech, F.J. Torres, E. Ruiz De Sola, J. Alarcón, Electrochemical detection of high oxidation states of chromium(IV and V) in chromium-doped cassiterite and tin-sphene ceramic pigmenting systems, Eur. J. Inorg. Chem. (2006) 638–648. https://doi.org/10.1002/ejic.200500775.

[68] A. Doménech-carbó, M.T. Doménech-Carbó, A. Castelló-Palacios, V. Guerola-Blay, E. Pérez-Marín, Electrochemical identification of painters/workshops: The case of Valencian Renaissance-Baroque painters (ca. 1550- ca. 1670), Electrochim. Acta. 297 (2019) 685–695. https://doi.org/10.1016/j.electacta.2018.11.212.

[69] A. Costamagna, L'Adorazione del Mistero. Fra' Bartolomeo nel segno di Leonardo. Il restauro., Roma, 2004.

[70] T. Grygar, P. Bezdicka, D. Hradil, A. Doménech-carbó, F. Marken, L. Pikna, G. Cepriá, Voltammetric analysis of iron oxide pigments, Analyst. (2002) 1100–1107. https://doi.org/10.1039/b205199k.

[71] S. de Jesus Barradas Travassos, Estudo da evolução da camada de pátina em

chapas de aços patináveis ASTM A242 e obras de arte expostas à atmosfera de São Paulo, Universidade de São Paulo, 2020. https://doi.org/10.1088/1751-8113/44/8/085201.

[72] X. Ferragud, J. Piquero-Cilla, M.T. Doménech-Carbó, V.G. Blay, X. Company, A. Doménech-Carbó, Electrochemical analysis of gildings in Valencia altarpieces: a cross-age study since fifteenth until twentieth century, J. Solid State Electrochem. 21 (2017) 1477–1487. https://doi.org/10.1007/s10008-017-3512-8.

[73] D. V. Zhuzhelskii, E.G. Tolstopjatova, A.I. Volkov, S.N. Eliseeva, G.G. Láng, V. V. Kondratiev, Insights on the electrodeposition mechanism of tungsten oxide into conducting polymers: Potentiostatic vs. potentiodynamic deposition, Synth. Met. 267 (2020) 116469. https://doi.org/10.1016/j.synthmet.2020.116469.

[74] F. Scholz, B. Lange, A. Jaworski, J. Pelzer, Analysis of powder mixtures with the help of abrasive stripping voltammetry and coulometry, Fresenius. J. Anal. Chem. 340 (1991) 140–144. https://doi.org/10.1007/BF00324469.

[75] N. Zakharchuk, S. Meyer, B. Lange, F. Scholz, A Comparative Study of Lead Oxide Modified Graphite Paste Electrodes and Solid Graphite Electrodes with Mechanically Immobilized Lead Oxides, Croat. Chem. Acta. 73 (2000) 667–704.

[76] Y. Ben Amor, E. Sutter, H. Takenouti, B. Tribollet, M. Boinet, R. Faure, J. Balencie, G. Durieu, Electrochemical study of the tarnish layer of silver deposited on glass, Electrochim. Acta. 131 (2014) 89–95. https://doi.org/10.1016/j.electacta.2013.12.011.

[77] F. Arjmand, A. Adriaens, Quantification of tin and lead in binary alloys using voltammetry of immobilized microparticles, Electroanalysis. 23 (2011) 1941–1947. https://doi.org/10.1002/elan.1.

[78] B.J. Plowman, B. Sidhureddy, S. V. Sokolov, N.P. Young, A. Chen, R.G. Compton, Electrochemical Behavior of Gold–Silver Alloy Nanoparticles, ChemElectroChem. 3 (2016) 1039–1043. https://doi.org/10.1002/celc.201600212.

[79] Y. Zhao, C. Lin, Y. Li, R. Du, J. Wang, Electrochemical Corrosion Behavior of Copper Clad Laminate in NaCl Solution, Acta Phys. - Chim. Sin. 23 (2007) 1342–1346. https://doi.org/10.1016/S1872-1508(07)60070-9.

[80] S.S. Add El-Reuim, F.U. Assaf, A. El-Sayed, A.M. Zaky, Cyclic voltammetric behaviour of copper rich brasses in NaCi solution, Br. Corros. J. 30 (1995) 297–301. https://doi.org/10.1179/bcj.1995.30.4.297.

[81] G. Cepriá, E. Bolea, F. Laborda, J.R. Castillo, Quick, easy, and inexpensive way to detect small metallic particles in suspension using voltammetry of immobilized microparticles, Anal. Lett. 36 (2003) 923–931. https://doi.org/10.1081/AL-120019253.

[82] D. Šatović, S. Martinez, A. Bobrowski, Electrochemical identification of corrosion products on historical and archaeological bronzes using the voltammetry of micro-particles attached to a carbon paste electrode, Talanta. 81 (2010) 1760–1765. https://doi.org/10.1016/j.talanta.2010.03.037.

[83] J.A. Dean, Lange's handbook of chemistry, 15th ed., McGraw- Hill, Inc., New York, 1999. https://doi.org/10.5370/JEET.2015.10.6.2348.

[84] A. Doménech-carbó, Tracing, authenticating and dating archaeological metal using the voltammetry of microparticles, Anal. Methods. 3 (2011) 2181–2188. https://doi.org/10.1039/c1ay05416c.

[85] A. Doménech-Carbó, Electrochemical analysis of metallic heritage artefacts: Voltammetry of microparticles (VMP), in: Corros. Conserv. Cult. Herit. Met. Artefacts, 2013: pp. 165–189. https://doi.org/10.1533/9781782421573.2.165.

[86] A. Doménech-Carbó, S. Sánchez-Ramosa, M.T. Doménech-Carbó, J. V. Gimeno-Adelantado, F. Bosch-Reig, D.J. Yusá-Marco, M.C. Saurí-Peris, Electrochemical determination of the Fe(III)/Fe(II) ratio in archaeological ceramic materials using carbon paste and composite electrodes, Electroanalysis. 14 (2002) 685–696. https://doi.org/10.1002/1521-4109(200205)14:10<685::AID-ELAN685>3.0.CO;2-4.

[87] O. El Tall, N. Jaffrezic-Renault, M. Sigaud, O. Vittori, Anodic stripping voltammetry of heavy metals at nanocrystalline boron-doped diamond electrode, Electroanalysis. 19 (2007) 1152–1159. https://doi.org/10.1002/elan.200603834.

[88] E. Lassner, W.-D. Schubert, Tungsten: Properties, Chemistry, Technology of the Element, Alloys, and Chemical Compounds, Kluwer Academic / Plenum Publishers, New York, 1999.

[89] E.S. El Wakkad, H.A. Rizk, I.G. Ebaid, The electrochemical behavior of the tungsten electrode and the nature of the different oxides of the metal, J. Phys. Chem. 59 (1955) 1004–1008. https://doi.org/https://doi.org/10.1021/j150532a003.

[90] J.W. Johnson, C.L. Wu, The Anodic Dissolution of Tungsten, J. Electrochem. Soc. 118 (1971) 1909–1912. https://doi.org/10.1149/1.2407865.

[91] M. Anik, K. Osseo-Asare, Effect of pH on the Anodic Behavior of Tungsten, J. Electrochem. Soc.Journal Electrochem. Soc. 149 (2002) B224–B233. https://doi.org/10.1149/1.1471544.

[92] G.S. Kelsey, The Anodic Oxidation of Tungsten in Aqueous Base, J. Electrochem. Soc. 124 (1977) 814–819. https://doi.org/10.1149/1.2133418.

[93] R.L. Frost, Raman spectroscopy of selected copper minerals of significance in corrosion, Spectrochim. Acta Part A. 59 (2003) 1195–1204. https://doi.org/10.1016/S1386-1425(02)00315-3.

[94] R.L. Frost, W. Martens, J.T. Kloprogge, P.A. Williams, Raman spectroscopy of the basic copper chloride minerals atacamite and paratacamite: implications for the study of copper , brass and bronze objects of archaeological significance, J. Raman Spectrosc. (2002) 801–806. https://doi.org/10.1002/jrs.921.

[95] W. Martens, R.L. Frost, J.T. Kloprogge, P.A. Williams, Raman spectroscopic study of the basic copper sulphates — implications for copper corrosion and ‘ bronze disease ,’ J. Raman Spectrosc. (2003) 145–151. https://doi.org/10.1002/jrs.969.

[96] F. Di Turo, R. Parra, J. Piquero-Cilla, G. Favero, A. Doménech-Carbó, Crossing VIMP and EIS for studying heterogeneous sets of copper/bronze coins, J. Solid State Electrochem. 23 (2019) 771–781. https://doi.org/10.1007/s10008-018-04182-5.

[97] A. Doménech-Carbó, M.T. Doménech-Carbó, S. Capelo, T. Pasíes, I. Martínez-Lázaro, Dating Archaeological Copper/Bronze Artifacts by Using the Voltammetry of Microparticles, Angew. Commun. 53 (2014) 9262–9266. https://doi.org/10.1002/anie.201404522.

[98] A. Doménech-carbó, Capelo, Sofia, J. Piquero-Cilla, M.T. Doménech-Carbó, J. Barrio, A. Fuentes, W. Al Sekhaneh, Dating archaeological copper using electrochemical impedance spectroscopy. Comparison with voltammetry of microparticles dating: Dating archaeological copper by EIS, Mater. Corros. 67 (2016) 120–129. https://doi.org/10.1002/maco.201408048.

[99] A. Doménech-Carbó, M.T. Doménech-Carbó, J. V. Gimeno-Adelantado, F. Bosch-Reig, M.C. Saurí-Peris, S. Sánchez-Ramos, Electrochemistry of iron oxide pigments (earths) from pictorial microsamples attached to graphite - Polyester composite electrodes, Analyst. 126 (2001) 1764–1772. https://doi.org/10.1039/b100257k.

[100] J.M. de la Roja, V.G. Baonza, M. San Andrés, Application of Raman microscopy to the characterization of different verdigris variants obtained using recipes from old treatises, Spectrochim. Acta - Part A. 68 (2007) 1120–1125. https://doi.org/10.1016/j.saa.2007.06.053.

[101] C. Defeyt, P. Vandenabeele, B. Gilbert, J. Van Pevenage, R. Cloots, D. Strivay, Contribution to the identification of α-, β- And μ-copper phthalocyanine blue pigments in modern artists' paints by X-ray powder diffraction, attenuated total reflectance micro-fourier transform infrared spectroscopy and micro-Raman spectroscopy, J. Raman Spectrosc. 43 (2012) 1772–1780. https://doi.org/10.1002/jrs.4125.

[102] A.A. Esenpnar, A.R. Özkaya, M. Bulut, Synthesis and electrochemical properties

of crown ether functionalized coumarin substituted cobalt and copper phthalocyanines, J. Organomet. Chem. 696 (2011) 3873–3881. https://doi.org/10.1016/j.jorganchem.2011.08.045.

[103] S. Arslan, I. Yilmaz, Preparation, electrochemical, and spectroelectrochemical characterization of a new water-soluble copper phthalocyanine, Inorg. Chem. Commun. 10 (2007) 385–388. https://doi.org/10.1016/j.inoche.2006.12.004.

[104] F. Ospitali, D. Bersani, G. Di Lonardo, P.P. Lottici, “Green earths”: vibrational and elemental characterization of glauconites, celadonites and historical pigments, J. Raman Spectrosc. 39 (2008) 1066–1073. https://doi.org/10.1002/jrs.1983.

[105] V. Košařová, D. Hradil, I. Němec, P. Bezdička, V. Kanický, Microanalysis of clay-based pigments in painted artworks by the means of Raman spectroscopy, J. Raman Spectrosc. 44 (2013) 1570–1577. https://doi.org/10.1002/jrs.4381.

[106] A. Coccato, D. Bersani, A. Coudray, J. Sanyova, L. Moens, P. Vandenabeele, Raman spectroscopy of green minerals and reaction products with an application in Cultural Heritage research, J. Raman Spectrosc. 47 (2016) 1429–1443. https://doi.org/10.1002/jrs.4956.

[107] S.E. Jorge-Villar, H.G.M. Edwards, Green and blue pigments in Roman wall paintings: A challenge for Raman spectroscopy, J. Raman Spectrosc. 52 (2021) 2190–2203. https://doi.org/10.1002/jrs.6118.

[108] R. Bruder, V. Detalle, C. Coupry, An example of the complementarity of laser-induced breakdown spectroscopy and Raman microscopy for wall painting pigments analysis, J. Raman Spectrosc. 38 (2007) 909–915. https://doi.org/10.1002/jrs.1685.

[109] L.D. Mateos, D. Cosano, M. Mora, I. Muñiz, R. Carmona, C. Jiménez-Sanchidrián, J.R. Ruiz, Raman microspectroscopic analysis of decorative pigments from the Roman villa of El Ruedo (Almedinilla, Spain), Spectrochim. Acta - Part A Mol. Biomol. Spectrosc. 151 (2015) 16–21. https://doi.org/10.1016/j.saa.2015.06.091.

[110] N.C. Scherrer, Z. Stefan, D. Francoise, F. Annette, K. Renate, Synthetic organic pigments of the 20th and 21st century relevant to artist's paints: Raman spectra reference collection, Spectrochim. Acta - Part A Mol. Biomol. Spectrosc. 73 (2009) 505–524. https://doi.org/10.1016/j.saa.2008.11.029.

[111] K. Castro, P. Vandenabeele, M.D. Rodríguez-Laso, L. Moens, J.M. Madariaga, Micro-Raman analysis of coloured lithographs, Anal. Bioanal. Chem. 379 (2004) 674–683. https://doi.org/10.1007/s00216-004-2642-x.

[112] Y. Kim, M.C. Caumon, O. Barres, A. Sall, J. Cauzid, Identification and composition of carbonate minerals of the calcite structure by Raman and infrared spectroscopies using portable devices, Spectrochim. Acta - Part A Mol. Biomol. Spectrosc. 261 (2021) 119980. https://doi.org/10.1016/j.saa.2021.119980.

[113] F. Froment, A. Tournié, P. Colomban, Raman identification of natural red to yellow pigments : ochre and iron-containing ores, J. Raman Spectrosc. 39 (2008) 560–568. https://doi.org/10.1002/jrs.1858.

[114] I.M. Bell, R.J.H. Clark, P.J. Gibbs, Raman spectroscopic library of natural and synthetic pigments (Pre- ~ 1850 AD), Spectrochim. Acta - Part A. 53 (1997) 2159–2179. https://doi.org/10.1016/S1386-1425(97)00140-6.

[115] M. Bouchard, D.C. Smith, Catalogue of 45 reference Raman spectra of minerals concerning research in art history or archaeology, especially on corroded metals and coloured glass, Spectrochim. Acta - Part A Mol. Biomol. Spectrosc. 59 (2003) 2247–2266. https://doi.org/10.1016/S1386-1425(03)00069-6.

[116] V. Merk, J.K. Berg, C. Krywka, I. Burgert, Oriented crystallization of barium sulfate confined in hierarchical cellular structures, Cryst. Growth Des. 17 (2016) 677–684. https://doi.org/10.1021/acs.cgd.6b01517.

[117] S. Mosca, T. Frizzi, M. Pontone, R. Alberti, L. Bombelli, V. Capogrosso, A. Nevin, G. Valentini, D. Comelli, Identification of pigments in different layers of illuminated manuscripts by X-ray fluorescence mapping and Raman spectroscopy, Microchem. J. 124 (2016) 775–784. https://doi.org/10.1016/j.microc.2015.10.038.

[118] A.M. Cardeira, S. Longelin, S. Costa, A. Candeias, M.L. Carvalho, M. Manso, Analytical characterization of academic nude paintings by José Veloso Salgado, Spectrochim. Acta - Part A Mol. Biomol. Spectrosc. 153 (2016) 379–385. https://doi.org/10.1016/j.saa.2015.08.043.

[119] A. Doménech-carbó, M.T. Doménech-Carbó, H.G.M. Edwards, Quantitation from Tafel Analysis in Solid-State Voltammetry. Application to the Study of Cobalt and Copper Pigments in Severely Damaged Frescoes, Anal. Chem. 80 (2008) 2704–2716. https://doi.org/10.1021/ac7024333.

[120] A. Doménech-carbó, F.J. Torres, J. Alarcón, Electrochemical characterization of cobalt cordierites attached to paraffin-impregnated graphite electrodes, J. Solid State Electrochem. 8 (2004) 127–137. https://doi.org/10.1007/s10008-003-0443-3.

[121] M.F. Daniel, B. Desbat, J.C. Lassegues, Infrared and Raman study of WO3 tungsten trioxides and WO3, xH2O tungsten trioxide Hydrates, J. Solid State Chem. 67 (1987) 235–247. https://doi.org/0022-459618.

[122] B. Ingham, S. V. Chong, J.L. Tallon, Layered tungsten oxide-based organic - Inorganic hybrid materials: An infrared and raman study, J. Phys. Chem. B. 109 (2005) 4936–4940. https://doi.org/10.1021/jp045066l.

[123] G. Escalante, R. López, F.N. Demesa, G. Villa-Sánchez, V.H. Castrejón-Sánchez, I. Vivaldo de la Cruz, Correlation between Raman spectra and color of tungsten trioxide (WO3) thermally evaporated from a tungsten filament, AIP Adv. 11 (2021). https://doi.org/10.1063/5.0045190.

[124] H.-N. Cui, Preparation and characterization of optical multilayered coatings for smart windows applications, University of Minho, 2005. http://repositorium.sdum.uminho.pt/bitstream/1822/3341/1/All-CoverPages-Contents List.pdf.

[125] F.D. Hardcastle, I.E. Wachs, Determination of the molecular structures of tungstates by Raman spectroscopy, J. Raman Spectrosc. 26 (1995) 397–405. https://doi.org/10.1002/jrs.1250260603.

[126] V. Otero, D. Sanches, C. Montagner, M. Vilarigues, L. Carlyle, J.A. Lopes, M.J. Melo, Characterisation of metal carboxylates by Raman and infrared spectroscopy in works of art, J. Raman Spectrosc. 45 (2014) 1197–1206. https://doi.org/10.1002/jrs.4520.

[127] R.L. Frost, A. López, R. Scholz, Y. Xi, F.M. Belotti, Infrared and Raman spectroscopic characterization of the carbonate mineral huanghoite - And in comparison with selected rare earth carbonates, J. Mol. Struct. 1051 (2013) 221–225. https://doi.org/10.1016/j.molstruc.2013.07.051.

[128] M.J.N. Pourbaix, Atlas of electrochemical equilibria in aqueous solutions, Second Eng, National Association of Corrosion Engineers, Houston, Texas, 1974.

APPENDIX 1 – RSD VALUES

Voltammetric analysis of metals and alloys

Sample	Electrolyte	Method	1st scan	2nd scan	3rd scan	Mean	Standard deviation	RSD
Ag	NaOH	Cyclic voltammetry anodic	0,36	0,36	0,37	0,36	0,01	1,81
Cu			-0,27	-0,30	-0,30	-0,29	0,02	5,97
			-0,09	-0,09	-0,09	-0,09	0,00	0,00
PbSb			-0,58	-0,57	-0,57	-0,57	0,01	1,01
Ag	KCl	Cyclic voltammetry anodic	0,14	0,15	0,15	0,15	0,01	3,94
Cu			0,06	0,06	0,06	0,06	0,00	0,00
			0,40	0,40	0,38	0,39	0,01	2,94
PbSb		Square wave voltammetry anodic	-0,69	-0,67	-0,67	-0,68	0,01	1,71
			-0,39	-0,39	-0,41	-0,40	0,01	2,91
PbAl			-0,67	-0,67	-0,69	-0,68	0,01	1,71
				-0,38	-0,40	-0,39	0,01	3,63
Ag	OA	Cyclic voltammetry anodic	0,52	0,52	0,52	0,52	0,00	0,00
Cu			0,08	0,08	0,07	0,08	0,01	7,53
Sn			-0,43	-0,42	-0,43	-0,43	0,01	1,35
PbSb			-0,43	-0,43	-0,42	-0,43	0,01	1,35
PbAl			-0,41	-0,4	-0,42	-0,41	0,01	2,44
Ag	H_2SO_4	Cyclic voltammetry anodic	0,40	0,39	0,38	0,39	0,01	2,56
Cu			0,12	0,09	0,10	0,10	0,02	14,78
PbSb			-0,44	-0,44	-0,44	-0,44	0,00	0,00
			0,06	0,06	0,07	0,06	0,01	9,12
PbAl			-0,46	-0,45	-0,43	-0,45	0,02	3,42
Sn		Square wave voltammetry anodic	-0,50	-0,50	-0,50	-0,50	0,00	0,00
			-0,22	-0,22	-0,22	-0,22	0,00	0,00
PbSb			-0,44	-0,44	-0,44	-0,44	0,00	0,00
PbAl			-0,44	-0,43	-0,44	-0,44	0,01	1,32
Ag	HCl	Cyclic voltammetry anodic	0,12	0,11	0,10	0,11	0,01	9,09
Cu			0,03	0,04	0,03	0,03	0,01	17,32
			0,43	0,42	0,37	0,41	0,03	7,90
Sn			-0,37	-0,37	-0,38	-0,37	0,01	1,55
PbSb			-0,46	-0,45	-0,45	-0,45	0,01	1,27
			-0,36	-0,38	-0,36	-0,37	0,01	3,15
PbAl			-0,46	-0,45	-0,46	-0,46	0,01	1,26
			-0,37	-0,36	-0,36	-0,36	0,01	1,59
Ag	HAc/NaAc	Cyclic voltammetry anodic	0,61	0,60	0,60	0,60	0,01	0,96
Cu			0,12	0,16	0,16	0,15	0,02	15,75
Sn			-0,61	-0,6	-0,58	-0,60	0,02	2,56
PbSb			-0,45	-0,44	-0,46	-0,45	0,01	2,22
			-0,11	-0,10	-0,11	-0,11	0,01	5,41
PbAl			-0,48	-0,47	-0,47	-0,47	0,01	1,22
Zn		Square wave voltammetry anodic	-1,06	-1,05	-1,07	-1,06	0,01	0,94
W			-0,59	-0,57	-0,58	-0,58	0,01	1,72
			-0,36	-0,37	-0,36	-0,36	0,01	1,59
			0,23	0,22	0,23	0,23	0,01	2,55

Voltammetric analysis of corrosion products for the areas of the Green Sample indicated in Figure 8a

Sample	Method	1st scan	2nd scan	3rd scan	Mean	Standard deviation	RSD
Green 1	Cyclic voltammetry cathodic	-0,17	-0,18	-0,22	-0,19	0,03	13,70
		-0,75	-0,71	-0,78	-0,75	0,04	4,69
Green 2		-0,14	-0,14	-0,12	-0,14	0,01	7,52
		-0,78	-0,64	-0,68	-0,70	0,08	10,77
Green 3		-0,16	-0,19	-0,17	-0,17	0,02	9,83
		-0,64	-0,72	-0,69	-0,68	0,04	6,08
Green 4		-0,17	-0,14	-0,19	-0,17	0,02	13,65
		-0,67	-0,69	-0,71	-0,69	0,02	3,19
Green 5		-0,16	-0,13	-0,14	-0,14	0,02	12,21
Green 1	Cyclic voltammetry anodic	0,12	0,10	0,10	0,11	0,01	10,83
Green 2		0,07	0,08	0,07	0,07	0,01	7,87
Green 3		0,12	0,12	0,14	0,13	0,01	9,12
Green 4		0,11	0,12	0,11	0,11	0,01	5,09
Green 5		0,14	0,14	0,14	0,14	0,00	0,00

Voltammetric analysis of corrosion products for the areas of the Brown Sample indicated in Figure 8b

Sample	Method	1st scan	2nd scan	3rd scan	Mean	Standard deviation	RSD
Brown 1	Cyclic voltammetry cathodic	-0,93	-0,92	-0,89	-0,91	0,02	2,41
Brown 2		-0,90	-0,91	-0,96	-0,92	0,03	3,53
Brown 3		-0,9	-0,89	-0,90	-0,89	0,01	0,91
Brown 1	Cyclic voltammetry anodic	-0,52	-0,53	-0,53	-0,53	0,01	1,10
		0,11	0,07	0,13	0,10	0,03	29,57
		0,35	0,35	0,34	0,35	0,01	1,67
Brown 2		-0,53	-0,54	-0,54	-0,54	0,01	1,08
		0,08	0,09	0,13	0,10	0,03	26,46
		0,27	0,26	0,30	0,28	0,02	7,52
Brown 3		-0,52	-0,52	-0,54	-0,53	0,01	2,19
		0,10		0,08	0,09	0,01	15,71
		0,35		0,33	0,34	0,01	4,16

Voltammetric analysis of pigments – Peaks reproducibility (each experiment was performed with a different sample)

Sample	Method	1st scan	2nd scan	3rd scan	Mean	Standard deviation	RSD
Pr09Pig03	Cyclic voltammetry cathodic	-0,2	-0,14	-0,14	-0,16	0,03	21,65
		-0,32	-0,32	-0,29	-0,31	0,02	5,59
Pr11Pig07		-0,47	-0,45	-0,43	-0,45	0,02	4,44
Pr11Pig11		-0,34	-0,34	-0,38	-0,35	0,02	6,54
Pr09Pig03	Cyclic voltammetry anodic	0,16	0,14	0,13	0,14	0,02	10,66
Pr11Pig07		0,09	0,13	0,11	0,11	0,02	18,18
Pr11Pig11		0,07	0,06	0,08	0,07	0,01	14,29
Green Earth	Cyclic voltammetry anodic	-0,55	-0,58	-0,56	-0,56	0,02	2,71
		0,31		0,33	0,32	0,01	4,42
Burnt Umber		-0,55	-0,55	-0,56	-0,55	0,01	1,04
		0,33	0,31	0,30	0,31	0,02	4,88
Mars Yellow		-0,53	-0,56	-0,58	-0,56	0,03	4,52
		0,13		0,15	0,14	0,01	10,10
		0,37		0,37	0,37	0,00	0,00
Pr11Pig03	Square wave voltammetry cathodic	-0,07	-0,07	-0,07	-0,07	0,00	0,00
		-0,58	-0,58	-0,6	-0,59	0,01	1,97
	Square wave voltammetry anodic	-0,57	-0,57	-0,58	-0,57	0,01	1,01
Pr09Pig15	Square wave voltammetry cathodic	-0,52	-0,52	-0,53	-0,52	0,01	1,10
			-0,94	-0,89	-0,92	0,04	3,86
	Square wave voltammetry anodic	-0,59	-0,60	-0,59	-0,59	0,01	0,97
		-0,38	-0,34	-0,36	-0,36	0,02	5,56
		0,28	0,25	0,23	0,25	0,03	9,93
		0,64	0,66	0,62	0,64	0,02	3,13
		0,89	0,93	0,90	0,91	0,02	2,30